

**Pyrolysis-assisted Catalytic Hydrogenolysis of Lignin in
Solvents for Aromatic Monomer Preparation**

Jiaqi WANG

Table of contents

Chapter 1 Introduction

1.1 Global energy and environmental issues caused by the use of fossil resources.....	1
1.2 The role of biomass as alternative to fossil resources.....	2
1.3 Lignocellulosic biomass.....	4
1.4 Chemical constituents of cell walls of lignocellulosic biomass.....	7
1.4.1 Cellulose.....	7
1.4.2 Hemicellulose.....	8
1.4.3 Lignin.....	10
1.4.4 Architecture of cell wall.....	13
1.5 Isolation of lignin.....	15
1.6 Technically available lignin.....	16
1.6.1 Kraft lignin.....	17
1.6.2 Organosolv lignin.....	18
1.6.3 Other technical lignins.....	18
1.6.4 Potential market of technical lignins.....	19
1.7 Chemical approaches for lignin depolymerization.....	20
1.7.1 Pyrolysis.....	21
1.7.1.1 Homolysis and heterolysis.....	21
1.7.1.2 Pyrolytic depolymerization of lignin.....	23
1.7.1.3 Side-chain and OCH ₃ transformation.....	23
1.7.1.4 Re-condensation.....	24
1.7.2 Thermal depolymerization in solvents.....	24
1.7.3 Reductive catalytic depolymerization.....	26
1.8 Objectives of this thesis.....	27

Chapter 2 Stable oligomer formation from lignin by pyrolysis of softwood in an aprotic solvent with a hydrogen donor

2.1 Introduction.....	29
2.2 Experimental.....	31
2.2.1 Materials.....	31

2.2.2 Pyrolysis and product fractionation	31
2.2.3 Product analysis	33
2.3 Results and discussion	35
2.3.1 Characterization of separated fractions	35
2.3.2 Effect of temperature on formation behavior	37
2.3.3 Molecular weight distribution of lignin-derived products	39
2.3.4 NMR analysis of lignin-derived oligomer	42
2.3.5 Cell wall effect	49
2.4 Conclusions	52

Chapter 3 Pyrolysis-assisted catalytic hydrogenolysis of softwood lignin at elevated temperatures for the high yield production of monomers

3.1 Introduction	53
3.2 Experimental	55
3.2.1 Materials	55
3.2.2 Pyrolysis-assisted catalytic hydrogenolysis	56
3.2.3 Product analysis	57
3.2.4 Gas phase catalytic reaction of guaiacol	58
3.3 Results and discussion	59
3.3.1 Monomer formation from Japanese cedar MWL	59
3.3.2 Dimer production from Japanese cedar MWL	66
3.3.3 Model compound study	68
3.3.4 Japanese cedar organosolv lignin	73
3.4 Conclusions	76

Chapter 4 Pyrolysis-assisted catalytic hydrogenolysis of pinoresinol

4.1 Introduction	77
4.2 Experimental	78
4.2.1 Materials	78
4.2.2 Catalytic reaction	78
4.2.3 Product analysis	79
4.3 Results and discussion	79
4.4 Conclusions	86

Chapter 5 Role of pyrolysis in pyrolysis-assisted catalytic hydrogenolysis of lignin and mechanistic insights into catalytic conversion

5.1 Introduction.....	87
5.2 Experimental.....	88
5.2.1 Materials	88
5.2.2 Catalytic reaction	89
5.2.3 Product analysis	89
5.3 Results and discussion	90
5.3.1 Coniferyl alcohol and dihydroconiferyl alcohol	90
5.3.2 Other pyrolysis intermediates and conversion pathway from lignin.....	93
5.3.3 Role of side-chain functional group in catalytic conversion.....	98
5.4 Conclusions.....	101

Chapter 6 Solvent effects on monomer formation in pyrolysis-assisted catalytic hydrogenolysis of softwood lignin

6.1 Introduction.....	103
6.2 Experimental.....	105
6.2.1 Materials	105
6.2.2 Thermal reaction	105
6.2.3 Product analysis	105
6.3 Results and discussion	106
6.3.1 Pyrolysis of coniferyl alcohol (CA).....	106
6.3.2 Catalytic hydrogenolysis of coniferyl alcohol (CA)	111
6.3.3 Monomer formation from milled wood lignin (MWL).....	115
6.4 conclusion	119

Chapter 7 Concluding remarks

7.1 Conclusions.....	120
7.2 Prospects for the future research.....	121

References

Acknowledgments.....	132
List of publications.....	134

List of figures

Fig. 1-1	A simple taxonomy of plant	5
Fig. 1-2	Anatomical structure of wood trunk.....	5
Fig. 1-3	Three-dimensional structure of the cell wall of a tracheid cell	6
Fig. 1-4	Chemical structure of cellulose	7
Fig. 1-5	Crystalline and paracrystalline regions in cellulose microfibril	8
Fig. 1-6	Chemical structures of typical hemicelluloses	9
Fig. 1-7	Typical Linkages between phenylpropane units in lignin	11
Fig. 1-8	A proposed chemical structure of softwood lignin.....	12
Fig. 1-9	Potential applications of technical lignins.....	20
Fig. 1-10	Theoretical calculation results of bond dissociation energies for C-C/C-O linkages in lignin model compounds.	22
Fig. 2-1	Aromatic solvent and H donor used in this study.....	31
Fig. 2-2	Experimental setup for pyrolysis.....	32
Fig. 2-3	Separation process of wood pyrolyzate.....	33
Fig. 2-4	¹ H-NMR spectra of a) water-soluble, b) hexane-soluble, and c) purified EtOAc-soluble portions obtained from wood pyrolysis in the presence of aromatic solvent and H-donor at 350 °C for 5 min. d) acetylated derivatives of purified EtOAc-soluble portion; e) milled wood lignin from Japanese cedar wood	36
Fig. 2-5	GC/MS chromatograms of monomeric lignins in hexane-soluble portion obtained at 350 °C/ 5 min (signals of dimers, aprotic solvent and H-donor are not shown)	37
Fig. 2-6	The yield of a) solid residue, and b) purified EtOAc-soluble and c) water-soluble portions from wood pyrolysis in the presence of DPB and H donor at 270–380 °C. wood (50 mg), DPB (200 mg), H donor (50 mg)	38
Fig. 2-7	GPC chromatograms of purified EtOAc-soluble fractions obtained from Japanese cedar wood. (a) solid line: neat pyrolysis at 350 °C for 5 min under nitrogen, (b) dotted and dashed line: pyrolysis in an aromatic solvent (diphenoxybenzene, DPB), and (c) dash line: pyrolysis in DPB with a hydrogen donor (1,2,3,10b-tetrahydrofluoranthene)	40
Fig. 2-8	GPC chromatograms of the purified EtOAc-soluble fractions obtained from Japanese cedar wood after treatment at various temperatures and for different times. the results are grouped by the yield of lignin-derived oligomer.....	41

Fig. 2-9	^1H - ^1H COSY NMR spectra of (a) the purified EtOAc-soluble fraction obtained after treatment at 350 °C for 5 min (NMR solvent: acetone- d_6) and (b) its acetylated derivatives (NMR solvent: CDCl_3)	43
Fig. 2-10	^1H -NMR spectra of acetylated purified EtOAc-soluble fractions obtained after treatment at 350 °C for various times.....	44
Fig. 2-11	^1H -NMR spectra of acetylated purified EtOAc-soluble portions obtained under various pyrolysis conditions where the yield of lignin-derived oligomer was maximum at about 80 wt% excluding conditions (270 °C/ 5 min, around 20 wt%).....	45
Fig. 2-12	HSQC NMR spectra of (a) Japanese cedar MWL (Solvent: $\text{DMSO-}d_6$), and purified EtOAc-soluble portions obtained at 350 °C for (b) 5 min and (c) 10 min	46
Fig. 2-13	HSQC NMR spectrum of purified EtOAc-soluble portion obtained at 270 °C/ 60 min	47
Fig. 2-14	Chemical structures identified by the HSQC NMR spectra	47
Fig. 2-15	Correlation between (a) yield of lignin-derived oligomer and (b) yields of hydrolysable sugars in solid residues (350 °C at various treatment times	50
Fig. 2-16	HSQC NMR spectrum of purified EtOAc-soluble portion obtained at 350 °C/ 5 min in the absence of H donor	51
Fig. 2-17	Temperature effect on the production of oligomers from lignin in cell wall during pyrolysis of Japanese cedar wood in aromatic solvent and H donor.....	52
Fig. 3-1	A diagram of the closed batch-type reaction system.....	56
Fig. 3-2	A photograph and diagram of the tandem micro-reactor GC/MS system.....	59
Fig. 3-3	Gel permeation chromatograms of the reaction mixtures obtained from the pyrolysis-assisted catalytic hydrogenolysis of Japanese cedar MWL in anisole at 200–350 °C (MWL: 10 mg, Pd/C: 10 mg, anisole: 2 mL, H_2 : 3 mL at 0.1 MPa). GPC column exclusion limit: 1500 Da at 9.5 min	60
Fig. 3-4	The yields of monomers obtained from the pyrolysis-assisted catalytic hydrogenolysis of Japanese cedar MWL at varying temperatures and for different durations (MWL: 10 mg, Pd/C: 10 mg, anisole: 2 mL, H_2 : 3 mL at 0.1 MPa). PO: propiovanillone, AO: acetovanillone, DHCA: dihydroconiferyl alcohol, PG: propyl guaiacol, EG: ethyl guaiacol, MG: methyl guaiacol, G: guaiacol, PP: propyl phenol, EP: ethyl phenol, MP: methyl phenol, EC: ethyl catechol, C: catechol.....	61
Fig. 3-5	The yields of monomers obtained from the pyrolysis-assisted catalytic hydrogenolysis of Japanese cedar MWL at 350 °C for 10 min with varying amounts of Pd/C and H_2 (MWL: 10 mg, anisole: 2 mL, H_2 : 3 mL at 0.1 or 1.0 MPa). VA: vanillic acid, IE (<i>cis</i>): isoeugenol (<i>cis</i>), IE (<i>trans</i>): isoeugenol (<i>trans</i>), E: eugenol, VG: vinyl guaiacol, CALD: coniferyl aldehyde, VO: vanillin, PO: propiovanillone, AO: acetovanillone, DHCA: dihydroconiferyl alcohol, PG: propyl guaiacol, EG: ethyl guaiacol, MG: methyl guaiacol, G: guaiacol, PP: propyl phenol, EP: ethyl phenol, EC: ethyl catechol. * H_2 pressure at room temperature prior to the reaction. a value of 0 MPa indicates that N_2 was used instead of H_2	63

Fig. 3-6	Gel permeation chromatograms of the reaction mixtures obtained from the pyrolysis-assisted catalytic hydrogenolysis of Japanese cedar MWL in anisole at 350 °C for 10 min with varying amounts of Pd/C and H ₂ (MWL: 10 mg, anisole: 2 mL, H ₂ : 3 mL at 0.1 or 1.0 MPa). GPC column exclusion limit: 1500 Da at 9.5 min.*H ₂ pressure at room temperature prior to the reaction.....	64
Fig. 3-7	Proposed reaction pathways for monomer production via the catalytic hydrogenolysis of lignin with pyrolysis, Pd/C and H ₂ at 250–350 °C	65
Fig. 3-8	The dimer regions of GC/MS total ion chromatograms acquired from the trimethylsilyl (TMS) derivatives of products obtained from the pyrolysis-assisted catalytic hydrogenolysis of Japanese cedar MWL in anisole at 300 or 350 °C (MWL: 10 mg, Pd/C: 10 mg, anisole: 2 mL, H ₂ : 3 mL at 0.1 MPa)	67
Fig. 3-9	Gel permeation chromatograms of the reaction mixtures obtained from the pyrolysis-assisted catalytic hydrogenolysis of the model dimers a (having 4- <i>O</i> -5 bonds; 1), b (having α -aryl bonds; 2) and c (having 5-5 bonds; 3) at 200–350 °C for 60 min in anisole (model: 10 mg, Pd/C: 10 mg, anisole: 2 mL, H ₂ : 3 mL at 0.1 MPa). the numerical value attached to each signal indicates the recovery or yield (mol%, based on aromatic rings). GPC column exclusion limit: 1500 Da at 9.5 min	68
Fig. 3-10	The GC/MS total ion chromatograms of the TMS-derivatives of reaction mixtures obtained from the pyrolysis-assisted catalytic hydrogenolysis of the 4- <i>O</i> -5 model compound (1) in anisole at 200–350 °C for 60 min.....	69
Fig. 3-11	The GC/MS total ion chromatograms of the TMS-derivatives of reaction mixtures obtained from the pyrolysis-assisted catalytic hydrogenolysis of the α -aryl model compound (2) in anisole at 200–350 °C for 60 min (compound 2 : 10 mg, Pd/C: 10 mg, anisole: 2 mL, H ₂ : 3 mL at 0.1 MPa)	69
Fig. 3-12	The GC/MS total ion chromatograms of the TMS-derivatives of reaction mixtures obtained from the pyrolysis-assisted catalytic hydrogenolysis of the 5-5 model compound (3) in anisole at 250–350 °C for 60 min (compound 3 : 10 mg, Pd/C: 10 mg, anisole: 2 mL, H ₂ : 3 mL at 0.1 MPa). *treatment time: 10 min	70
Fig. 3-13	Diagrams showing the proposed interactions of biphenyl (3)- and diarylmethane (1)-type dimers on a Pd surface determining reaction selectivity	71
Fig. 3-14	The GC/MS total ion chromatograms obtained from reactions mixtures following the catalytic hydrogenolysis of gas phase guaiacol over Pd/C at different temperatures in a micro-reactor with H ₂ as the carrier gas	72
Fig. 3-15	The HSQC NMR spectrum of Japanese cedar organosolv lignin, acquired in acetone- <i>d</i> ₆ (structure A, B, C refer to Fig. 2-14).....	73
Fig. 3-16	Gel permeation chromatograms of the reaction mixtures obtained from the pyrolysis-assisted catalytic hydrogenolysis of Japanese cedar organosolv lignin in anisole at 200–350 °C for 60 min. chromatograms obtained from MWL are also included as dashed gray curves for comparison (organosolv lignin: 10 mg, Pd/C: 10 mg, anisole: 2 mL, H ₂ : 3 mL at 0.1 MPa). GPC column exclusion limit: 1500 Da at 9.5 min.....	74
Fig. 3-17	The yields of monomers obtained from the pyrolysis-assisted catalytic hydrogenolysis of Japanese cedar organosolv lignin in anisole at 200–350 °C for 60 min (organosolv	

	lignin: 10 mg, Pd/C: 10 mg, anisole: 2 mL, H ₂ : 3 mL at 0.1 MPa). DHCA: dihydroconiferyl alcohol, PG: propyl guaiacol, EG: ethyl guaiacol, MG: methyl guaiacol, G: guaiacol, PP: propyl phenol, EP: ethyl phenol, MP: methyl phenol.....	75
Fig. 4-1	Gel-permeation chromatography of products recoveries from β - β model. (holding times are 1 h).....	80
Fig. 4-2	The GC/MS total ion chromatograms (monomer region) of the TMS-derivatives of reaction mixtures obtained from the thermocatalytic hydrogenolysis of the pinoresinol model compound (10) in anisole at 200–350 °C for 60 min. (enlarged by 20 times) asterisk mark is from impurities	81
Fig. 4-3	The GC/MS total ion chromatograms (dimer region) of the TMS-derivatives of reaction mixtures obtained from the thermocatalytic hydrogenolysis of the pinoresinol model compound (10) in anisole at 200–350 °C for 60 min	82
Fig. 4-4	The GC/MS total ion chromatograms of the TMS-derivatives of reaction mixtures obtained from the thermocatalytic hydrogenolysis of the pinoresinol model compound (10) in anisole at 350 °C for 60 min	82
Fig. 4-5	3D configuration of β - β model.....	82
Fig. 4-6	The mass spectra of various dimers corresponding to the compounds shown in Fig. 4-2, Fig. 4-3	83
Fig. 4-7	Proposed pathways for the products from pinoresinol	84
Fig. 4-8	¹ H NMR spectra of TLC-purified products obtained from pinoresinol pyrolysis in the presence of an aromatic solvent and a hydrogen donor at 350°C for 10 min. asterisk mark is from pinoresinol	85
Fig. 4-9	The GC/MS total ion chromatograms of the reaction mixtures obtained from the pyrolysis-assisted catalytic hydrogenolysis of kraft lignin in anisole at 350 °C for 10 min.....	86
Fig. 5-1	Gel-permeation chromatograms of the reaction mixtures obtained from the catalytic hydrogenolysis of coniferyl alcohol (CA, left) and dihydroconiferyl alcohol (DHCA, right) in anisole at 200–350 °C for 60 min. Solid line: Pd/C, H ₂ ; dashed line: Pd/C, N ₂ ; dotted line: no catalyst, N ₂ ; asterisk: retention time of CA, DHCA, coniferyl aldehyde, isoeugenol (<i>cis/trans</i>), eugenol; double asterisk: retention time of ethyl guaiacol; triple asterisk: retention time of guaiacol, methyl guaiacol.....	90
Fig. 5-2	Recovery and yield of monomers obtained by catalytic hydrogenolysis of coniferyl alcohol (top) and dihydroconiferyl alcohol (bottom) in anisole at 200–350 °C for 60 min.....	91
Fig. 5-3	Recovery and yields of monomers obtained by catalytic hydrogenolysis of 4-substituted guaiacols (H-, methyl-, ethyl-, and propyl-) in anisole at 300 and 350 °C for 60 min. asterisk: percentage recovery of original side-chain structure in identified monomers	93
Fig. 5-4	Yields of monomers obtained by catalytic hydrogenolysis of various monomers produced during lignin pyrolysis in anisole at 300 °C for 60 min. a: H ₂ used as carrier	

	gas in GC–MS analysis (others used He); b: reaction time 2 min; c: conducted at 350 °C; d: conducted in N ₂	94
Fig. 5-5	Side-chain composition of monomers obtained by catalytic hydrogenolysis of various monomers produced during lignin pyrolysis in anisole at 300 °C for 60 min.....	95
Fig. 5-6	Proposed pathways for various types of monomers produced by pyrolysis of lignin during pyrolysis-assisted catalytic hydrogenolysis using Pd/C and H ₂ in anisole at 300 and 350 °C.....	96
Fig. 5-7	Proposed roles of lignin pyrolysis in pyrolysis-assisted catalytic hydrogenation of lignin	97
Fig. 5-8	Proposed effects of side-chain functional groups of 4-substituted guaiacols on their ability to adsorb onto the Pd surface, governing reactivity and reaction pathways	98
Fig. 5-9	Successive transformations proposed for catalytic hydrogenolysis of coniferyl alcohol with strong adsorption on the Pd surface	101
Fig. 6-1	A proposed scheme for the production of monomers from lignin polymers under pyrolysis-assisted catalytic hydrogenolysis conditions	103
Fig. 6-2	Gel-permeation chromatograms of the reaction mixtures obtained from coniferyl alcohol (CA) after treatment at 350 °C for 1 h in different solvents. dotted and dash black line: N ₂ ; dash blue line: Pd/C, N ₂ ; solid red line: Pd/C, H ₂	107
Fig. 6-3	Total monomer yield from coniferyl alcohol after treatment at 350 °C for 1 h in different solvents. black column: N ₂ ; dark grey column: Pd/C, N ₂ ; light grey column: Pd/C, H ₂	107
Fig. 6-4	Monomer composition in the products obtained from coniferyl alcohol after treatment at 350 °C for 1 h in different solvents. (a): N ₂ ; (b): Pd/C, N ₂ ; (c): Pd/C, H ₂ . see Table 1 for full names of all legends	108
Fig. 6-5	Proposed conversion pathways of CA depended by the properties of the solvent at 350 °C.....	109
Fig. 6-6	Proposed solvent effects on the redox reactions of coniferyl alcohol in pyrolysis	110
Fig. 6-7	Monomers obtained from pyrolysis assisted catalytic hydrogenolysis of guaiacol and catechol in water at 350 °C for 60 min. (reaction compound: 10 mg, Pd/C: 10 mg; water: 2 mL; H ₂ : 3mL/0.1 MPa).....	113
Fig. 6-8	Proposed effect of hexane on the adsorption manner of monomer products in pyrolysis-assisted hydrogenolysis process	113
Fig. 6-9	GPC chromatograms of products obtained from pyrolysis-assisted catalytic hydrogenolysis of MWL after treatment at 350 °C for 30 min in benzene and dioxane.....	114
Fig. 6-10	Proposed association manners of DHCA, methanol, and dioxane on Pd surface during pyrolysis-assisted hydrogenolysis process	114
Fig. 6-11	Monomers obtained from pyrolysis-assisted catalytic hydrogenolysis of Japanese cedar MWL in different solvents at 350 °C. (MWL: 10 mg, Pd/C: 10 mg; solvent: 2 mL; H ₂ : 3mL/0.1 MPa). percentage in parenthesis is the total monomer yield at 30 min as compared with that at 60 min	115

Fig. 6-12	Side reactions as expected to occur during pyrolysis-assisted catalytic hydrogenolysis of coniferyl alcohol	116
Fig. 6-13	GC/MS total ion chromatograms of the TMS-derivatives of reaction mixtures obtained from coniferyl alcohol through thermal treatment in (a) water, (b) methanol, (c) anisole, (d) toluene, (e) hexane at 350 °C after treatment with 60 min.....	117

List of tables

Table 1-1	Composition of three types of phenylpropane-units in softwood, hardwood, and herbaceous plant.....	10
Table 1-2	Contents of typical linkages in softwood and hardwood.....	12
Table 1-3	Lignin distribution in loblolly pine tracheids as determined by bromination technique with SEM-EDXA system	14
Table 1-4	Lignin distribution in Douglas-fir tracheids as determined by SEM-EDXA technique.....	14
Table 1-5	Properties of various types of technical lignins as compared with MWL	16
Table 2-1	Experimental conditions used for pyrolysis of Japanese cedar wood flour (50 mg)	34
Table 3-1	Molecular structures and abbreviations for the various monomeric products	62
Table 5-1	Chemical structures of monomeric products and their abbreviations.....	92
Table 5-2	Influences of environment (N ₂ or H ₂) on the side-chain composition of the guaiacols produced by catalytic hydrogenolysis of coniferyl alcohol and dihydroconiferyl alcohol at 350 °C for 60 min	100
Table 6-1	Chemical structures and abbreviations for various monomeric products.....	109

Chapter 1

Introduction

1.1 Global energy and environmental issues caused by the use of fossil resources

Coal, crude oil, and natural gas are three main fossil resources, formed from anaerobic decomposition of dead plants and animals buried millions of years ago. The uses of fossil resources started to flourish during the industrial revolution: steam engines replaced windmills and watermills for mechanical work, gasoline engines and diesel engines replaced horses for transportation and commuting, coal and natural gas replaced wood and peat for household heating demand, kerosene replaced whale oil for lighting. In addition to the energy demand, the chemicals produced by petroleum refinery, known as petrochemicals, are the fundamental materials underpinning modern society. For example, compared to traditional natural fiber, such as wool, cotton, and linen, the synthetic fibers, such as polyester, spandex, and acrylic fibers, are commonly added in clothing to endow various functions, such as anti-wrinkle, quicker drying, better durability and elasticity. Also, commodity plastics, including polyethylene, polypropylene, and polystyrene are widely used for food packaging, bags, chairs and so on. Therefore, fossil resources-based fuel and chemical materials are an integral part of modern society.

However, with the improvement of living quality and economic growth, the global energy consumption had increased substantially from 6.098 billion tonnes in 1973 to 14.406 billion tonnes in 2019, and is estimated to increase to 15.755 billion tonnes in 2030, measured in crude oil equivalent (IEA, 2020). It was also reported that, by the end of 2019, the total technically recoverable resources of petroleum, natural gas, and coal in world were 6.208 trillion barrels, 810 trillion m³, and 20.78 trillion tonnes, respectively, while their economically exploitable reserves were only 1.702 trillion barrels, 229 trillion m³, and 1.070 trillion tonnes, respectively. The depletion of fossil fuel becomes a foreseeable dilemma for the next generations, because the reserves-to-production (R/P) ratios of petroleum, natural gas, and coal are only 49.9, 49.8, and 132 years, respectively (B.P. statistical review, 2020). Therefore, a depression in economics growth and a stagnation of society development would happen by the end of 21 century, unless

more advanced technologies are developed for fossil resources exploit, or alternatives are found to substitute fossil resources.

On the other hand, the CO₂ emission from fossil resources has been attracting the attention of research groups and institutes around the world, because it has become a common sense that anthropogenic CO₂ emission causes the 1.07 °C rise in average surface temperature since 18th century (IPCC, 2021). The rising temperature has caused a host of environmental problems that negatively impact ecosystem. The geographical distributions of some organisms are changing slowly (Parmesan, 2006). Species tend to migrate towards poleward and upward regions, leading to the inter-species competition and the destruction of ecosystems. Likewise, pests and parasites have migrated to the high latitudes, affecting human disease incidence in some Europe countries. The melting pole ice and glacier caused the rise in sea level by 21 cm from 1880 to 2009 (Church and White, 2011). Maintained this rising rate, many coastal cities will be submerged in the near future. Increased night temperature enhances the plant maintenance respiration (Peng et al., 2004), and lead to the reduction of annual crop yields. Without any countermeasure applied, the warming climate will force the global economy depressed more than 20% by 2100 (Burke et al., 2015).

1.2 The role of biomass as alternative to fossil resources

To solve the above problems, the primary energy dependences of many countries has begun to shift from fossil resources to renewables, and from single to diversified. Nuclear and renewable energy, thereby, are adopted to serve as alternatives to fossil resources, and their utilization is even incorporated into laws and government goals by most developed and some developing countries.

The consumption of fossil resources is predominantly concentrated in 4 sections: power generation, heat supply, transportation fuels, and industrial chemicals (IEA, 2020). In terms of power generation, hydro-, wind-, and solar power are developing fast, because not only can they achieve carbon neutrality for the factory construction in a short time, but also their marginal cost of power generation is almost zero. By contrast, biomass to electricity is a less competitive option. Nevertheless, bio-electricity has less impact on power grid shock, because the bio-electricity can be produced steadily and is not affected the weather.

In terms of heat supply, air conditioning is sufficient for residential heat demand, while the heat pump is likely the potential solution to alleviate the demand for fossil fuel in some industries. However, renewable thermal energy mainly comes from the combustion of biomass. Modern use of solid biomass in household and industry accounts for around 40% of global renewable energy demand (IEA, 2020). Compared to fossil fuel, biomass has lower sulfur content, and thereby releases fewer pollutants during combustion. In addition, in remote areas, biomass can meet the heat demand of human daily activities.

Bio-engine fuels were once considered the most likely alternative to fossil engine fuels. To meet the mandate of government policies, engine-based automotive companies are beginning to blend petro-gasoline/diesel with the renewable bio-gasoline/diesel to reduce CO₂ emission. However, as electricity becomes the dominant form of energy utilization, the engine-driven motors in transportation vehicles are being replaced by the electric-driven motors. Currently, Tesla, BYD, Toyota, and other electric vehicle companies are performing well, and they have begun to seize the share of engine vehicles in the automotive market. Nevertheless, in the cases of the long-distance heavy transport vehicle, aviation, and aerospace, the engine motors cannot be replaced by electronic motors, because only liquid fuels can provide the stronger power and longer range durability. Thus, the development of the biofuel technologies has attracted the attention of researchers for decades.

There are three generations of bio-fuel. The 1st generation biofuel is the food-based bio-ethanol and bio-diesel produced by fermentation of edible crops and by chemical transesterification of vegetable oils, respectively. These mature technologies give 1st bio-fuel a fair competitiveness in price to fossil fuel, but such price is strongly influenced by food crop prices. The 2nd generation bio-fuel is the bio-ethanol produced from lignocellulose, such as non-edible crops and woody biomass, which are much cheaper than food crops. However, the higher cost and lower efficiency of cellulases, used in lignocellulosic biomass hydrolysis process, make the 2nd generation bio-ethanol less competitive with fossil fuel. But still, the 2nd generation is promising because its popularity will not cause a food crisis that happened in the 2000s brought by the use of 1st generation biofuels. The 3rd generation bio-fuel is the bio-diesel produced from algae, yet is thought unsustainable because a significant fertilizer and energy input are required.

Fine chemicals, and polymers are highly dependent on the bulk chemicals produced by steam cracking of fossil resources, especially the petroleum. Annually, 14 % primary petroleum,

and 8 % natural gas are consumed for chemical production (IEA, 2018). Four types of primary bulk chemicals, ammonia, methanol, light olefins (ethylene, propylene), BTX aromatics (benzene, toluene, and xylenes), are the most fundamental building blocks in chemical production section, and their global production are approximately 185 Mt/yr, 100 Mt/yr, 255 Mt/yr, 110 Mt/yr, respectively. The only alternative to produce these carbon-containing petrochemicals is biomass. Pyrolysis, gasification, and torrefaction of biomass could provide bio-oil, natural gas, and bio-char, respectively, as the alternatives to crude oil, natural gas, and coal. With the analogous process to the petroleum refinery, biomass can be further converted to methanol, light olefins, and BTX. The integration of these biomass conversion technologies provides a process known as biorefinery. Because the use of biomass as feedstock can reduce the reliance on fossil resources and can mitigate the impacts on environment, biomass conversion researchers have reached a preliminary consensus that bio-refinery products could serve as the “drop in” alternatives to petro-refinery chemicals.

1.3 Lignocellulosic biomass

Continents and oceans are two ecosystems on Earth for biomass production. The net primary biomass in open ocean is about 41.5 billion dry tons, but the turnover time is 42. Accordingly, such rapid-circulating marine biomass is impractical for harvesting. By contrast, continental biomass, such as trees, bushes, grass, agriculture and forestry waste, is easier to harvest. Although these lignocellulosic biomass are diverse, 92.3% of them, totaling 1.7 trillion dry tons, are present in forest ecosystems (Lieth et al., 2012).

In order to make the best use of these diverse biomass in biorefinery, it is essential to understand their chemical composition. The chemical compositions in various biomass species are related to their origins, forms and complexity. Based on the taxonomy in Fig. 1-1, most of lignocellulosic biomass can be simply classified into softwood, hardwood, and grass (Rabemanolontsoa and Saka, 2013; Takada et al., 2017).

Secondary growth of seeds plants, especially for softwood and hardwood, accumulate large amounts of organic materials in cell walls. Fig. 1-2 shows the anatomical structure of wood trunk. From inside to outside, the tree is made of pith, xylem (heartwood and sapwood), vascular cambium (the undifferentiated cells layer), and phloem (live bark and dead bark). The ray

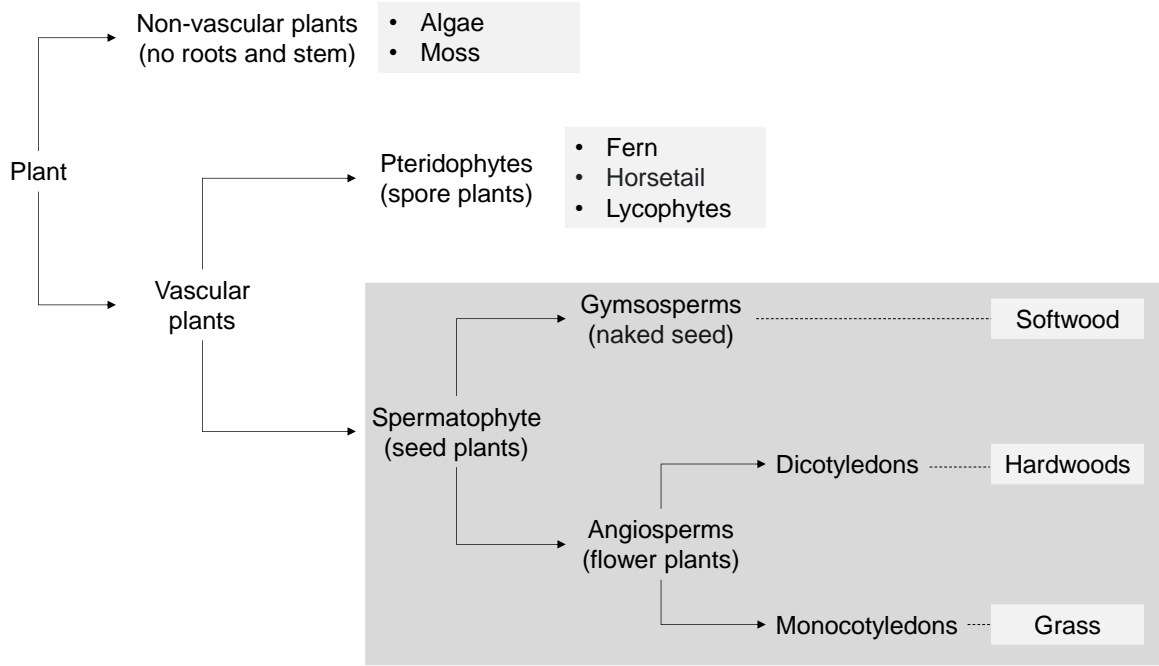


Fig. 1-1 A simple taxonomy of plant.

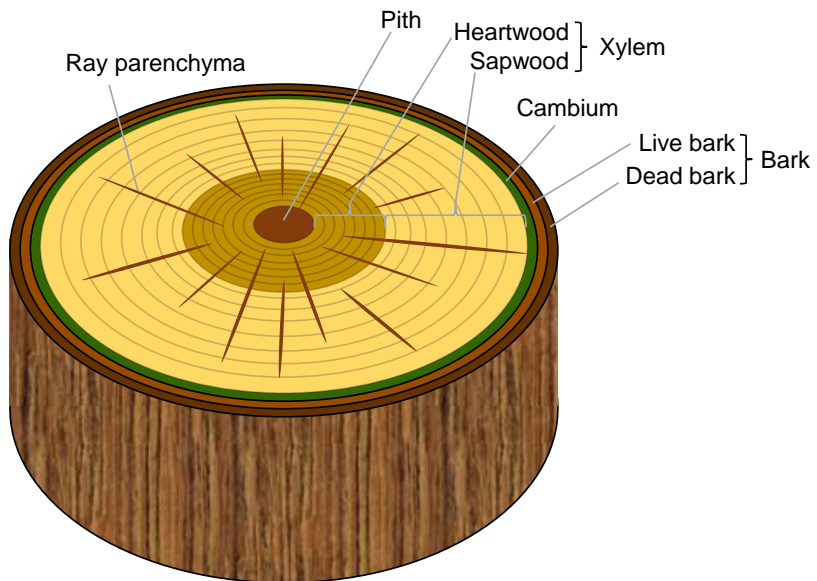


Fig. 1-2 Anatomical structure of wood trunk.

parenchyma connects the heartwood and sapwood, transporting some of nutrients and functional chemicals stored in the former to the latter to fight against pests. In the secondary growth period, the undifferentiated cells in vascular cambium layer differentiate outward into living phloem and inward into living xylem, and energy and materials are stored in the newly-formed cell wall. As a result, the stem of trees is thickened to give the staunch trunk. The growth of wood cells is affected by temperature, moisture and light, so the high-density latewood is formed during growing season, and the historical regional climate variability was recorded in growth rings.

Cell wall remains after the vascular cambium cell dividing, growing, differentiating, and dying. When the cell is growing, a thin and extensible layer, named primary wall, was formed outside the cell membrane. When the cell is fully grown to vessel and fiber in hardwood and tracheid in softwood, a thick layer forms inside the primary wall (Fig. 1-3) (Plomion et al., 2001). Such thick layer, named as secondary wall, is made up of three distinct layers (S1, S2, and S3) in which the orientation of cellulose microfibrils varies between the layers. The warty layer consisted of a condensed lignin begins to form between S3 layer and the plasma membrane when the cell is in the final lignification stage. When the cell dies, the protoplasm is depleted, and the lumen is formed. The space between two adjacent cell wall is called as middle lamella (ML), and the joint corner between multiple cell walls is called as cell corner region (MLcc). As a matter of fact, the utilization of lignocellulosic biomass is actually the utilization of materials and energy stored in cell walls.

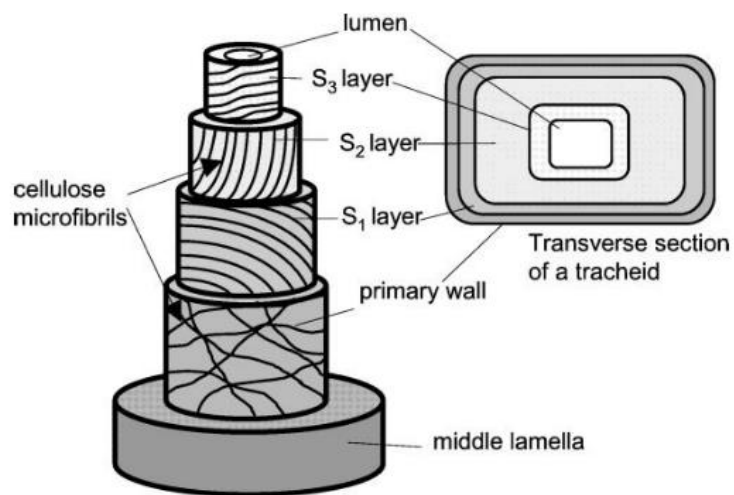


Fig. 1-3 Three-dimensional structure of the cell wall of a tracheid cell.

1.4 Chemical constituents of cell walls of lignocellulosic biomass

It is reported that the cellulose, hemicellulose, lignin, protein, extract and ash contents of Japanese cedar (a softwood) are of 38%, 23%, 33%, 0.5%, 3.4%, and 3%, respectively, while that of Japanese beech (a hardwood) are of 44%, 28%, 24%, 0.6%, 2%, 0.6%, respectively (Rabemanolontsoa and Saka, 2013). Accordingly, the cell wall of woody biomass is composed predominantly by cellulose, hemicellulose and lignin, while the protein, extractives, and inorganic compounds are trace elements.

1.4.1 Cellulose

Cellulose is the most abundant carbon resource in the nature. It is the prime building block of cell wall, and endows the tension strength of cell wall. Cellulose molecule is a linear and hydrophilic polysaccharide composed of tens of thousands of D-glucose units linked by β (1 \rightarrow 4) glycosidic bonds in a manner shown in Fig. 1-4. The hydrogen bond between hydroxyl group and oxygen on glucose residues will not only form in intrachain, but also in interchain. The intrachain hydrogen bond, as the auxiliary linkage, firms the connection between adjoining glucose residue, and prevents cellulose molecule from coiling and branching like starch. The interchain hydrogen bonds and van der waals force combine to stack the adjacent cellulose molecules in parallel to form the basic elementary fibrils, which further aggregated to microfibrils with a diameter of 3 nm (Mellerowicz and Sundberg, 2008), then macrofibrils with a diameter of 12 nm (Terashima et al., 2009).

During the biosynthesis of cellulose microfibril, the terminal enzyme complex arranged closely in linear or rosette, providing the chance for the self-assembly of cellulose chains. The region having highly ordered cellulose in microfibril is called as crystalline region, while the

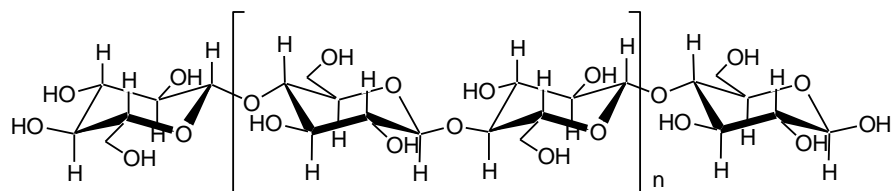


Fig. 1-4 Chemical structure of cellulose.

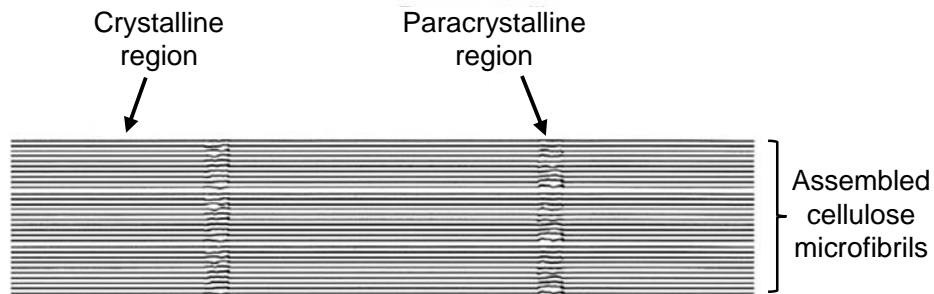


Fig. 1-5 Crystalline and paracrystalline regions in cellulose microfibril (Matsuoka et al., 2014).

disordered region is called as amorphous or paracrystalline region (Fig. 1-5). The morphology and crystalline structure of cellulose are very similar in softwood and hardwood, because cellulose I β dominates in higher plant cell wall. In the contrast, the I α structure dominates in algae, but can be converted to I β hydrothermally. Both I α and I β celluloses are thermodynamically metastable, and can be naturally produced in plants. However, the cellulose I cannot be rearranged to other polymorphs in natural environment, and hence, cellulose fiber is a relatively stable fiber.

The most widespread use of cellulose is the paper produced from pulping industry. Current technologies can also alter the morphology and crystalline nature of cellulose. Regeneration and mercerization of cellulose I yields the more stable cellulose II, which can be used to produce Rayon and TencelTM for clothing materials, and cellophane for films (Moon et al., 2011).

1.4.2 Hemicellulose

Hemicellulose is an amorphous polysaccharide connecting cellulose and lignin. Unlike cellulose, hemicellulose is a heterogeneous and branched polysaccharides with a degree of polymerization of around 200 (Zhou et al., 2017) and is soluble in alkali. Hemicellulose was used to be defined as the extractable polysaccharides in cell wall. However, such definition cannot discriminate hemicellulose from pectin, a heterogenous polysaccharide that is constructed by galacturonic acid backbones and exists in primary wall and ML. In comparison to pectin, the building blocks of hemicellulose include glucose, mannose, galactose, and rhamnose (hexoses), xylose and arabinose (pentoses), and some uronic acid, such as 4-*O*-methyl-D-glucuronic acid.

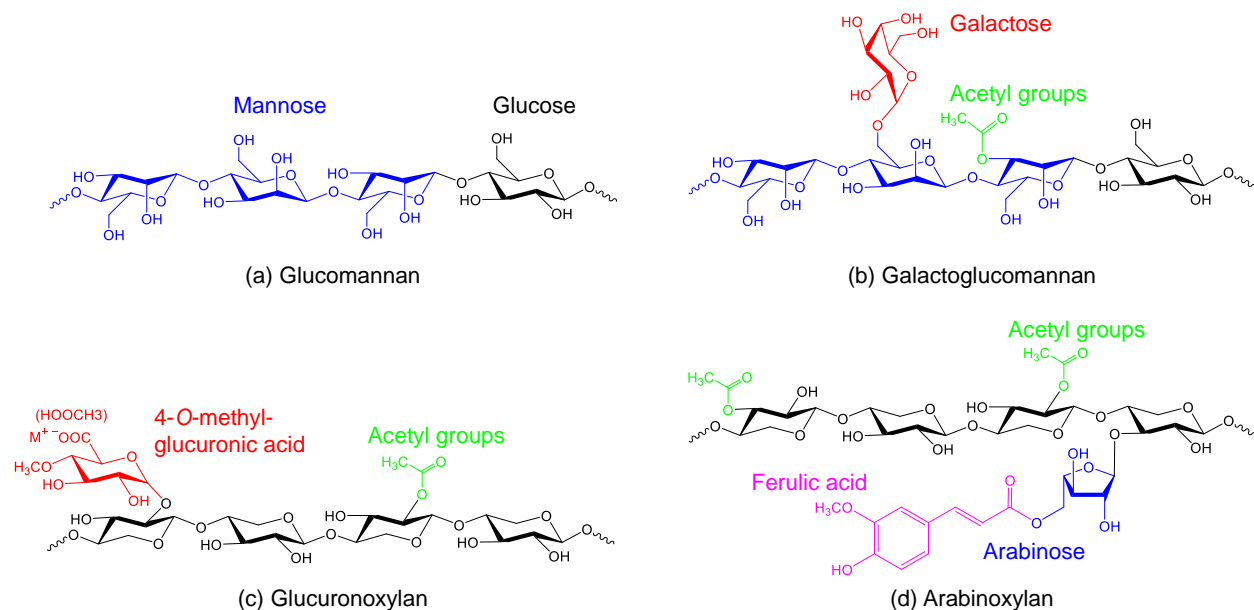


Fig. 1-6 Chemical structures of typical hemicelluloses (Wang, 2021).

Xylan, glucomannan, and galactoglucomannan are the typical hemicelluloses (Fig. 1-6). Xylan has the backbone made of xylose monomers via β -1,4-linkage, with the acetyl groups attached on the xylose residue. When some functional groups, such as 4-O-methyl-D-glucuronic acid group, and arabinose, are attached on such backbone, such xylan becomes to glucuronoxylan, and arabinoxylan, respectively. In comparison, glucomannan has the backbone made of mannose and glucose monomers via β -1,4-linkage with the acetyl groups attached on the mannose residue. When plenty of α -1,6-linked D-galactopyranose attaches on the mannose residues, such glucomannan become to galactoglucomannan.

The composition of hemicellulose varies depending on wood species. In softwood, glucomannan, galactoglucomannan and xylan constitute the hemicellulose, which accounts for 14-25% of the dry wood (Zhou et al., 2017). It was reported that typical ratios of mannose/glucose/galactose residues in softwood is of 3:1:1 (Timell and Syracuse, 1967). In hardwood, glucuronoxylan is the predominant hemicellulose, which accounts for 15-30 wt% of the dry wood. In comparison, glucomannan only accounts for 3-5 wt% in hardwood, and its ratio of mannose/glucose is typically 2:1. In herbaceous biomass, arabinoxylan is the predominant hemicellulose. The presence of arabinose as the side-chain can link with ferulic acid, which is the building block of lignin.

1.4.3 Lignin

Lignin is the most abundant aromatic resource in the nature. When lignin first evolved in plants 350 million years ago, there were no microorganisms able to digest it. As a result, carbon was stored in plants and buried in earth. Since the carbon had not returned to atmosphere for millions of years, the oxygen level was rising and earth was cooling, and here came to the carboniferous period. Nowadays, most terrestrial plants have the lignin, because the stiffness of lignin enables plants to growth upwards against gravity, and the aromatic property of lignin helps plant resist microbial degradation. Due to the hydrophobicity, the diffusion of water and swelling of lignin-contained cell wall is prevented, and hence, the water conduction in xylem became more efficient. As the result, trees can grow up to a hundred meters.

The proto-lignin in cell wall is a polymer consisted of phenylpropane units including coniferyl alcohol (G type), sinapyl alcohol (S type), and *p*-coumaryl alcohol (H type). Contents of the three basic aromatic units vary depending on the plant species. Generally, softwood contains G type exclusively, while hardwood consists of S and G type. H type is negligible in both softwood and hardwood, but is included in herbaceous plants (Table 1-1).

Table 1-1 Composition of three types of phenylpropane-units in softwood, hardwood, and herbaceous plant.(Belgacem and Gandini, 2008)

Phenylpropane-units	Softwood (%)	Hardwood (%)	Herbaceous plant (%)
G	>95	25-50	35-80
S	0	45-75	20-55
H	<5	0-8	5-35

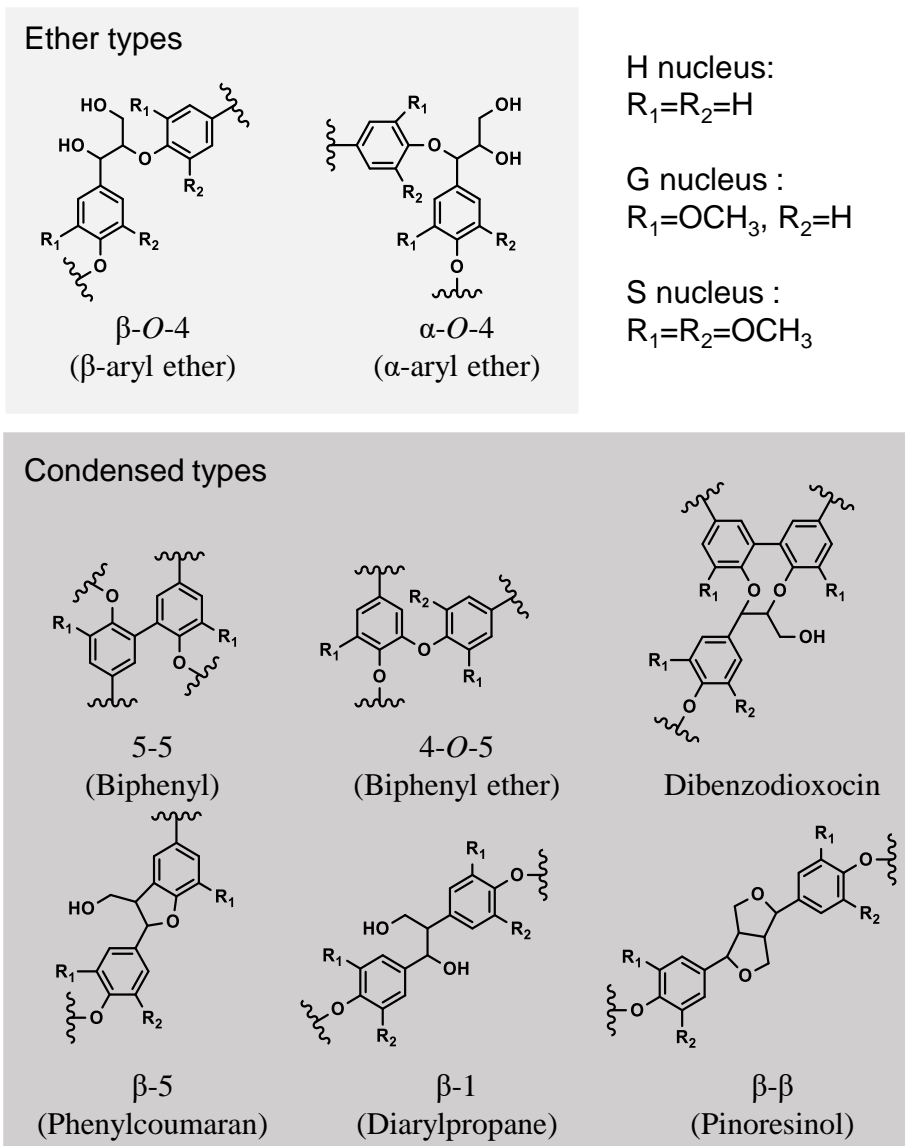


Fig. 1-7 Typical Linkages between phenylpropane units in lignin.

In lignin biosynthesis, the three types of cinnamyl alcohols precursor are converted to radical intermediates by oxidation with peroxidase and laccase enzymes. Then, intermediates polymerize through various linkages (Fig. 1-7). The linkages are classified into ether types, including β -O-4 and α -O-4, and condensed types, including 4-O-5, β -1, β -5, β - β , and 5-5. Fig. 1-8 shows a structural model of spruce lignin, wherein the blue lines represent ether linkages, and the red lines represent C-C condensed linkages. These various types of linkages make lignin a quite heterogenous polymer with a complex structure.

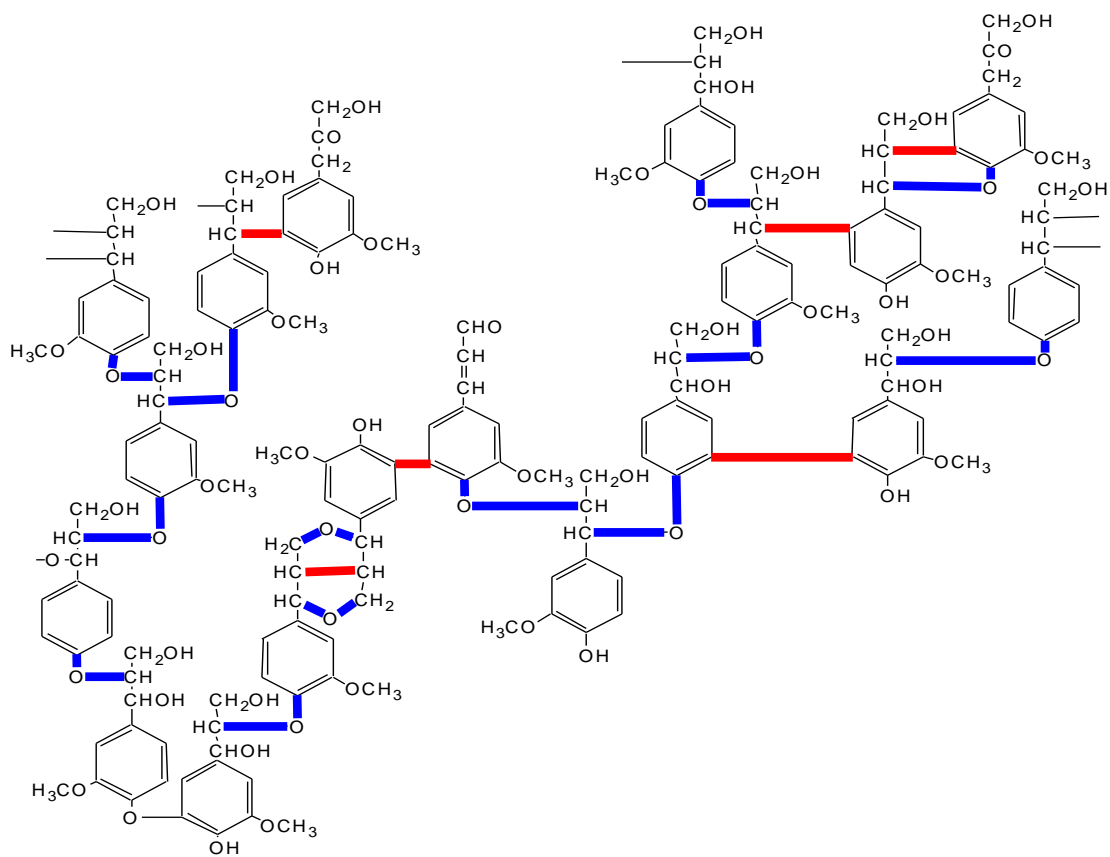


Fig. 1-8 A proposed chemical structure of softwood lignin (Pepper, 1972).

Table 1-2 Contents of typical linkages in softwood and hardwood (Zakzeski et al., 2010).

Linkage type	Contents (%)	
	Softwood	Hardwood
α -O-4	6-8	6-8
β -O-4	45-50	60-65
β -5	9-12	6
β -1	7-10	15
β - β	3	3-7.5
4-O-5	4-8	1.5-6.5
5-5	18-25	2.3-4.5

The contents of these linkages per 100 C9 units in softwood and hardwood are compiled in Table 1-2. β -O-4 is the most important and abundant linkages in both softwood and hardwood. Hardwood lignin generally contains smaller amounts of condensed linkages (the 4-O-5, β -5, and 5-5) than softwood lignin, because the -OCH₃ groups attached on the C5 of S type nucleus prevent the radical coupling at C5 during biosynthesis process. Contrary to this, the side-chain of phenylpropanoid in hardwood lignin has more coupling chance to form β -O-4, β -1, and β - β linkages. Thus, β -ether content in hardwood lignin is higher than that in softwood lignin. These various linkages in lignin exhibit quite different pyrolysis reactivity and decomposition behavior.

1.4.4 Architecture of cell wall

As Fig. 1-3 shows, there are three regions in cell wall: middle lamella, primary wall, and secondary wall. They show up in different lignification steps when cells grow up, and hence, the chemical constituents are different in these three regions.

Middle lamella is primarily composed of pectic polysaccharides with small amounts of protein, whereas cellulose and hemicellulose are absent. The primary wall is consisted of cellulose, xyloglucan, and pectin, and xyloglucan-bound cellulose microfibrils is embedded in pectin matrix (Mellerowicz et al., 2001). However, in most case, primary wall is very thin, around 100-350 nm thick, to be distinguished from middle lamella (Plomion et al., 2001). So, the middle lamella and the two adjoined primary cell wall are combined to be called as compound middle lamella (CML). It was reported that, the CML of softwood was measured to be 200-400 nm (Gao et al., 2014).

Secondary wall is the most important region for cell wall, because its thickness of 1-10 μ m accounts for 75-85% cell wall (Plomion et al., 2001). The ultrastructure of secondary wall is built up by bundle cellulose microfibrils embedded in lignin-hemicellulose matrix, and pectin is not contained in this region.

Lignin is unevenly distributed in the cell walls of softwoods and hardwoods. In general, lignin concentration in ML, especially of MLcc, is higher than that in secondary wall. For example, in softwood, lignin concentration (g/g) is greater than 50% in CML, but only up to around 20% in secondary wall (Fergus et al., 1969). The lignin concentrations in different fractions of loblolly pine cell (softwood) are shown in Table 1-3 (Saka et al., 1982). Since the secondary wall has much greater thickness, i.e., greater volume and mass, most of the lignin is

distributed in the secondary wall rather than in CML. Thus, the results in Table 1-4 from scanning electron microscopy coupled with energy dispersive X-ray analysis (SEM-EDX) of Douglas-fir tracheid (softwood cell) suggest that 66.2-80% of lignin is distributed in secondary wall, while only 20-33.8% is distributed in CML and MLcc (Krashen, 1982). Nevertheless, lignin in CML has higher content of condensed type linkages compared to that in secondary wall (Terashima et al., 1986). Therefore, it is suggested that milled wood lignin (MWL), discussed below, is highly related to the lignin in middle lamella and cell corner (Holtman et al., 2004), whereas cellulolytic enzyme lignin (CEL) is more like the proto-lignin in secondary wall.

Table 1-3 Lignin distribution in loblolly pine tracheids as determined by bromination technique with SEM-EDXA system (Saka et al., 1982).

Wood	Morphological differentiation	Fractional volume (%)	Lignin (% of total)	Lignin concentration (g/g)
Earlywood	S ₁	13	11.8	0.25
	S ₂	60	43.7	0.2
	S ₃	9	9.2	0.28
	ML	12	21.4	0.49
	ML _{cc}	6	14	0.64
Latewood	S ₁	6	6.2	0.23
	S ₂	80	64.2	0.18
	S ₃	5	5.6	0.25
	ML	6	13.6	0.51
	ML _{cc}	3	10.4	0.78

Table 1-4 Lignin distribution in Douglas-fir tracheids as determined by SEM-EDXA technique (Krashen, 1982).

Wood	Morphological regions	Lignin concentration ratio	Proportion of lignin (% of total lignin)
Earlywood	MLcc	3.57	11.3
	CML	2.38	22.5
	Secondary wall	1	66.2
Latewood	MLcc	3.57	9.9
	CML	2.72	10.1
	Secondary wall	0.93	80

1.5 Isolation of lignin

Early researchers had tried the isolation of lignin from polysaccharides in wood. Klason (1908) used concentrated sulfuric acid to remove polysaccharides from wood, leaving a brown-colored residue so called as Klason lignin. Hibbert conducted the ethanololysis of softwood with 2% HCl in ethanol, to isolate 10% low-molecular-weight lignin (Cramer et al., 1939). Freudenberg et al. (1940) used the permanganate degradation for spruce wood with 70% aqueous potassium hydroxide at elevated temperatures. Though the phenolic-OH released from ether cleavage was subsequently methylated, only 8 % lignin was converted to veratric acid. Also, they tried to use nitrobenzene oxidation of spruce wood in hot alkali, and 25 % lignin was converted to vanillin. Harris et al. (1938) tried to conduct hydrogenolysis of softwood and hardwood with copper-chromium oxide at 240-280 °C in dioxane, but the products were propylcyclohexane derivatives.

All the isolation methods mentioned above utilize chemical treatment processes, in which lignin in wood is degraded. To avoid such degradation, Brauns (1935) extracted lignin by alcohol at room temperature for several days. This process gave a light cream-colored powder known as Brauns lignin. However, recent researchers concluded that this low molecular mass lignin is lignan. The breakthrough of pure lignin isolation was made by Björkman (1956), who had the fine wood milled in a vibratory ball mill with toluene, followed by the extraction by the neutral dioxane-water mixture. A pale tan powder was obtained, and known as MWL. This lignin only accounts for 16.8% of total lignin, but contains limited carbohydrates. Pew (1957) removed the polysaccharide fraction in milled wood by commercial glycosidase. This method was improved by Chang et al. (1975), who used the cellulase to hydrolyze the milled wood. Such process gave a higher yields of lignin fractions and known as cellulolytic enzyme lignin (CEL). The yield reached ~60% but CEL contained a higher content of carbohydrates than MWL. The MWL and CEL are thought to be the representative of proto-lignin in wood. Elemental analysis of MWL suggests that the formulas of softwood and hardwood lignin are $C_9H_{8.3}O_{2.7}(OCH_3)_{0.97}$ and $C_9H_{8.7}O_{2.9}(OCH_3)_{1.58}$, respectively (Lin and Dence, 1992).

New lignin-isolation methods were recently investigated. Yamasaki et al. (2006) liquified Japanese beech in subcritical (270 °C) and supercritical (350 °C) alcohols. The results suggested that subcritical short-chain alcohols give a good degree of delignification. Li et al. (2009) used

the steam explosion of lignocellulosic biomass at 205-225 °C for 5-10 min, followed by the lignin isolation with alkaline extraction. The results showed that, for spruce, 10-27% of lignin becomes alkali-soluble, and the Mw of soluble fraction was 4,000-7,000 Da. The β -O-4 linkage in this lignin accounts for only 1.5-5.3%, which is much lower than that of MWL. During the steam explosion, acetyl group on hemicellulose would be released as acetic acid for auto-acidolysis of carbohydrates. Mishra and Saka (2011) investigated the liquefaction behavior of Japanese beech wood in subcritical phenol, and reported that delignification at 270 °C reached 99%. Brandts et al. (2011) treated lignocellulosic biomass in ionic liquids at 120 °C for hours to remove lignin and hemicellulose. Although 80-93% lignin was removed from Miscanthus, an herbaceous plant, the maximum yield of lignin accounts for only approximately 50%, based on Klason lignin.

1.6 Technically available lignin

Utilization of polysaccharides in lignocellulosic biomass has been the prime objective for hundreds of years. One typical and common technique is pulping, a process removes lignin and leaves cellulose, hemicellulose fibers for paper preparation. Acid, and alkaline conditions are utilized for this purpose. The resulting fibers from wood biomass are stronger than from herbaceous biomass.

Table 1-5 Properties of various types of technical lignins as compared with MWL (Ludmila et al., 2015).

	Lignosulfonate	Kraft lignin	Soda lignin	Organosolv lignin	Enzymatic hydrolysis lignin	MWL
Ash,%	4.0-8.0	0.5-3.0	0.7-2.3	1.7	1.0-3.0	1.5
Moisture,%	5.8	3.0-6.0	2.5-5.0	7.5	4.0-9.0	-
Carbohydrate,%	-	1.0-2.3	1.5-3.0	1.0-3.0	10.0-22.4	1.5-8.7
Nitrogen,%	0.02	0.05	0.2-1.0	0-0.3	0.5-1.4	-
Sulphur,%	3.5-8	1.0-3.0	0	0	0-1.0	0
Molecular weight, kDa	1.0-50.0 (up to 150)	1.5-5.0 (up to 25)	1.0-3.0 (up to 15)	0.5-5.0	5.0-10.0	5.5-20
Polydispersity	4.2-7.0	2.5-3.5	2.5-3.5	1.5	4.0-11.0	1.8-2.7
Annual production, (000 tonnes)	1000	75	20	3	-	-

In traditional pulping kraft process, lignin is burnt for recovering energy. Such Polysaccharides-first processes are known as 1st generation biorefinery in biomass conversion community. Nonetheless, some pulping plants purify the lignin fractions, and utilize lignin as a commodity. The properties of typical technical lignins including MWL are summarized in Table 1-5.

1.6.1 Kraft lignin

Kraft process is widely used in pulping industry because it brings a strong pulp fiber. In this process, lignin in wood is degraded and solubilized in white liquor (an alkaline solution consisted of NaOH and Na₂S), forming a solution called black liquid. Alkaline condition helps the cleavage of C_α-OH and C_α-O-aryl, leaving an electrophilic C_α to be substituted by bisulfide ion (HS⁻). The introduced HS⁻ then facilitates the cleavage of β-O-4 bond, resulting in the extensive depolymerization of lignin in wood. As β-ether is extensively cleaved, this lignin has relatively lower molecular weight and high content of phenolic-OH. On the other hand, OH⁻ ionizes phenols, thereby promoting the dissolution of lignin in water.

Kraft lignin can be isolated from black liquor by water dilution or acid precipitation. The acid precipitation process can reduce the ash content in kraft lignin. Isolated kraft lignins have very different properties depending on the original wood species, and contain more condensed structure compared to the protolignin in wood. This is not only because of the cleavage of β-O-4 bond and remaining of condensed type linkages, but also re-condensation during cooking. Quinone methides are the key intermediates for this re-condensation, forming diarylmethane type linkages.

Commercially available kraft lignin was supplied in 265 kt/year in 2018, with the price of 260-500 \$/t (Dessbesell et al., 2020). However, the production of kraft lignin is growing rapidly and is expected to surpass lignosulfonate within a few decades, because the purification approaches become more efficient. Kraft lignin is of medium-high purity, and is used for fertilizers, pesticides, carbon fiber, and also the production of some fine chemicals, such as vanillin. However, kraft lignin is not a suitable source for catalytic conversion, because the sulfur it contains poisons the catalyst.

1.6.2 Organosolv lignin

Organosolv process is a more environmentally benign alternative to kraft process, because the organic solvent is easy to recycle. In the organosolv pulping process, the wood chip is typically treated in ethanol/water mixture at around 200 °C with small amount of acid to catalyze the hydrolysis of lignin and hemicellulose. Cleavage of α -ether plays the major role for lignin depolymerization in organosolv process (Microscopy et al., 2002), and the re-condensation is restricted at such a weak acidic condition. Fragments released from lignin are simply solvated in organic solvent, instead of being ionized and dissolved in a same manner in kraft process.

Alcell lignin used to be a commercially available in large amount. Current annual production of this lignin is very limited and nearly all from pilot plants. Although organosolv plant does not need much capital investment on boiler, the high costs of solvent and pressurization equipment reduce the competitiveness of organosolv process. However, the development of 2nd generation biofuel might be the cradle of organosolv process, as sulfur-free and ash-free environment is more benign to give an enzymatic hydrolysable pulp. Thus, the organosolv lignin, as the by-products, is the future commercially available technical lignin.

Organosolv lignin is a relatively low-molecular-weight lignin with limited ash content. Because pulping conditions are of less drastic, organosolv lignin is less modified and more homogeneous than other three technical lignins mentioned above. The high quality of this lignin enables it to be used as raw material for high-value added products, such as phenolic resin, activated carbon, carbon fiber. The price of organosolv lignin is reported to be 280-520 US\$/ton (Ludmila et al., 2015). Because it is sulfur-free and not expensive, organosolv lignin is an ideal source for the catalytic conversion for aromatic production.

1.6.3 Other technical lignins

Sulfite pulping gives lignosulfonate as a by-product. In this process, wood chip is treated with solutions containing sulfite (SO_3^{2-}) and bisulfite (HSO_3^-) ions. The acidic conditions help to remove the -OH and -OAr_{yl} on C_α , leaving the carbocations readily substituted by HSO_3^- (Matsushita, 2015). As lignin is degraded and sulphonated, lignosulfonate becomes a water-soluble anionic spherical microgel with high ash content. However, the acid condition can cause the condensation of positive charged C_α cation with negative charged aromatic nucleus to give the diarylmethane structures, resulting in the high-molecular-weight property of lignosulphonates.

the price of lignosulfonate is around 200 US\$/t in 2022. Although the annual production of lignosulphonates is around 1.3 million tons (Dessbesell et al., 2020), the chemical and structural properties of this lignin only enable it to work as dispersing agents, and cement additives.

Soda lignin comes from soda pulping of herbaceous biomass, and in some cases hardwood. Soda lignins are sulphur free and contain smaller amount of ash contents than kraft lignins. The alkaline conditions also endows soda lignin a relatively lower molecular weight and higher content of phenolic-OH content. Thus, soda lignin could be used for the production of phenolic resins.

An emerging technical available lignin is the enzymatic hydrolysis lignin that comes from cellulosic ethanol industry combined with steam-explosion technology. Cellulase is used to hydrolyze polysaccharides in steam-exploded biomass in a manner similar to CEL preparation, giving a residue containing mainly lignin. The carbohydrate content of this residue is very high, while ash, sulphur, and nitrogen contents are decided by the contents of inorganic component and proteins in the original biomass. As the by-product from the 2nd generation bio-fuel, enzymatic hydrolysis lignin and organosolv lignin are the potential lignin sources in the future. By removing carbohydrates, the enzymatic hydrolysis lignin becomes high-purity lignin that might be used for the production of high-value added products. However, the high content of condensed structures in such lignin may hinder the production of aromatic monomers.

1.6.4 Potential market of technical lignins

Currently, most of lignin is just burnt for energy recovery, which wastes the aromatic property of lignin. Valorization of lignin can improve biorefinery productivity and profitability. Fig. 1-9 summarizes the potential applications of technical lignins. Ludmila et al. (2015) compared the prices of various possibly downstream products produced from lignin. The BTXs are 700-1,500 USD/ton, phenols are 1,000-2,000 USD/ton, activated carbon is 500-2,500 USD/ton, phenolic resin is 1,100-2,300 USD/ton, carbon fiber is 7,000-1,1000 USD/ton, and vanillin is 12, 000 USD/ton. However, due to the small market volume, the estimated market values of vanillin and carbon fibre were only 0.1 and 1.6 billion USD, respectively. In contrast, the market sizes of BTX and phenol are approximately 121.8 Mt, and 11.4 Mt, respectively, in

2021 (“statista,” 2022). Accordingly, the market values of BTX and phenols are 85-183 billion USD and 11.4-22.8 billion USD, respectively.

As lignin is the most abundant aromatic polymer in nature, the aromatics obtained from lignin depolymerization could serve as a drop-in alternative to the petro-based bulk chemicals and fine chemicals, each with a potential downstream market of millions to billions of dollars. However, the purity and properties of technical lignins limit their utilization. For example, lignosulfonate is only suitable uses as low value-added production, such as cement additive and dispersants, whereas soda lignin/organosolv lignin can be modified for the production of high value-added commodities, such as phenolic resin and activated carbon. Although high-quality lignins are limited in annual production (Table 1-5), their potential values of downstream market are quite high. Accordingly, organosolv lignin and soda lignin is the good sources for aromatic chemicals preparation.

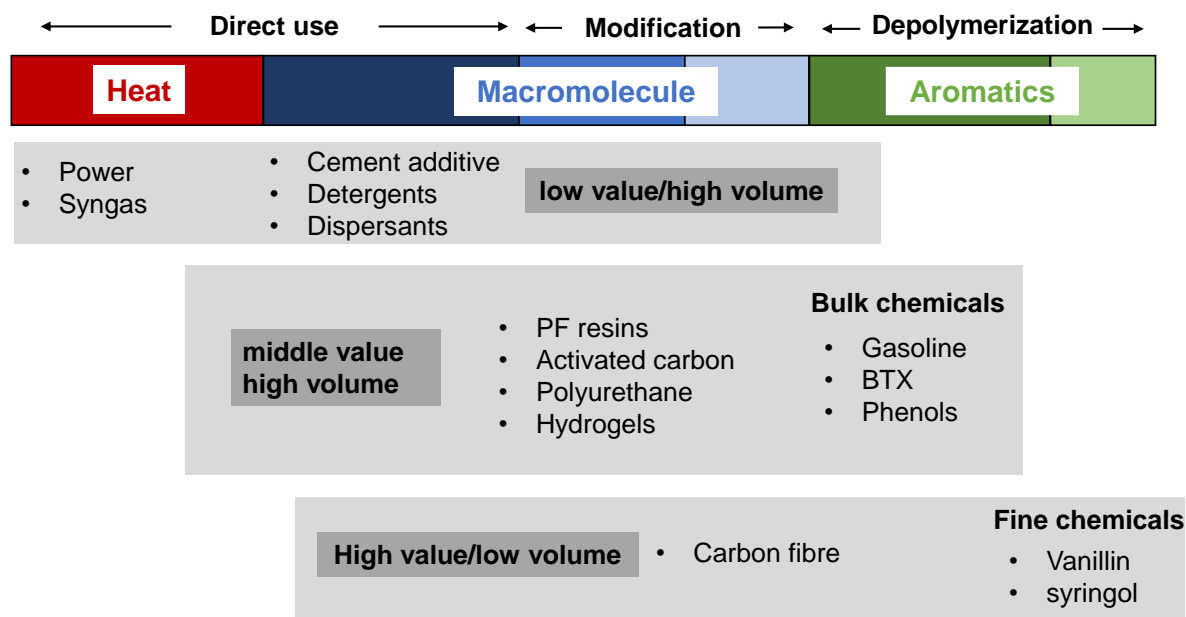


Fig. 1-9 Potential applications of technical lignins.

1.7 Chemical approaches for lignin depolymerization

The preparation of aromatic monomers from lignin requires cleavage of the C-O/C-C bonds. To make lignin-based aromatics preparation economically feasible, lignin

depolymerization approaches need to achieve in practical high monomer yields, preferably with a good product selectivity. In most methods, α/β ether cleavages are easier than the cleavage of condensed C-C bonds. Acidic and alkaline conditions are efficient for α/β -ether cleavage, and hence, they are applied in pulping industry for delignification (section 1.6). However, the recondensation behaviors of lignin would form the diarylmethane linkages, suppressing the monomer recovery and increasing the molecular weight for lignin products. The oxidative depolymerization is also very effective, and is already widely employed for bleaching pulp. Although the oxidation condition can achieve the cleavage of C-C linkages, the over-oxidation would degrade the aromatic-rings. Also, the radicals formed by oxidants would cause the recondensation, reducing the product selectivity (Ma et al., 2015). These approaches are commonly conducted at temperature of 100-250 °C.

1.7.1 Pyrolysis

Lignin degrades thermochemically in the wide-temperature range of 200-800 °C (Asmadi et al., 2011a). Thus, thermal degradation of lignin would play a role when the temperature is elevated in any lignin depolymerization approaches. Based on lignin pyrolysis behavior, 200-400 °C is classified as the primary pyrolysis stage where depolymerization of lignin occurs through cleavage of α - and β - ether bonds. On the other hand, degradation at > 400 °C is classified as the secondary pyrolysis stage, where primary pyrolysis products degrade further.

1.7.1.1 Homolysis and heterolysis

The acid/alkaline-assisted lignin depolymerization mentioned above are dominated by the heterolytic reaction, whereas the oxidation depolymerization predominantly proceeds in homolytic reaction. In contrast, the depolymerization behavior of lignin under pyrolysis conditions include both homolytic and heterolytic mechanisms.

When C-C and C-O bonds in lignin are cleaved homolytically, a pair of radicals is generated. The difficulty to break a chemical bond homolytically is reflected by the bond dissociation energy (BDE). Fig. 1-10 compares the BDEs for various lignin related linkages. These data suggest that the α -ether is the weakest linkage in lignin, followed by β -ether, whereas 5-5 is the strongest linkage in lignin, followed by 4-O-5, resinol, and β -aryl bonds.

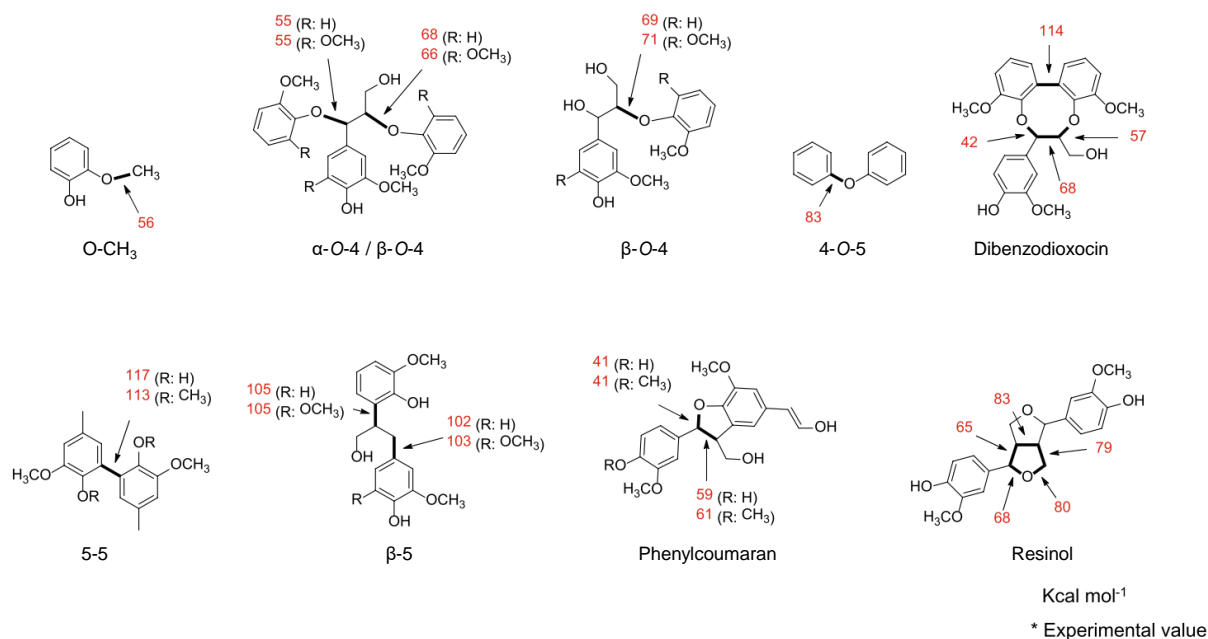


Fig. 1-10 Theoretical calculation results of bond dissociation energies for C-C/C-O linkages in lignin model compounds (Kawamoto, 2017).

When β -ether in lignin is cleaved heterolytically, the six-member ring is formed in the side-chain, and C-O linkages are more likely cleaved by the retro-ene reactions (Klein and Virk, 1981).

Kawamoto et al (2008a) clearly demonstrated the ether cleavage mechanisms (homolysis vs. heterolysis) by using α - and β - ether types dimers and trimers, in which various substituents introduced at the para positions of the C-O linkages. When ether linkage is cleaved in heterolysis, the cleavage reactivity must be directly correlated with the Hammett's σ_p parameter, whereas opposite trend must be observed for homolysis. Heterolysis reactivity increase by the electron-withdrawing substituent, whereas homolysis reactivity increases by the electron-donating substituent. As a result, they clarified that the α -ether in phenolic unit is cleaved heterolytically, whereas other linkages [α -ether (non-phenolic) and β -ether (phenolic and non-phenolic)] cleave in the homolysis mechanism. These results indicate that the cleavage of α - and β -ether linkages mostly occur homolytically to produce large amounts of radical species. This information is very important for considering the control of lignin pyrolysis reactions.

1.7.1.2 Pyrolytic depolymerization of lignin

Studies on lignin-related dimer models at primary pyrolysis stage indicated that lignin depolymerization is achieved by the cleavage of α - and β - ether bonds, but the condensed linkages are stable (Nakamura et al., 2008). Phenolic α -ether and phenolic β -ether start to cleave at 200 °C and 250 °C, respectively, while the cleavage temperature of their nonphenolic types were much higher at 350 °C and 400 °C, respectively. The main product from nonphenolic β -ether dimer is vinyl ether. In contrast, β -aryl dimers were stable in depolymerization and predominantly converted to stilbenes. It is also proposed that the formation of quinone methide intermediates from phenolic β -O-4 type linkages significantly reduces the BDE of the C-O bonds to 44.1 kcal/mol (Kawamoto, 2017). Accordingly, lignin depolymerization preferably starts from the phenolic end if quinone methide is formed. But, quinone methide formation is significantly influenced by the pyrolysis conditions. Under pyrolysis conditions (no solvent conditions), quinone methide is not effectively formed due to the limitation of proton-transfer. For example, even in the phenolic form, the reactivity of C γ -deoxy-type β -ether dimer is similar to the nonphenolic form, due to the difficulty in quinone methide formation by cleaving the C α -OH group. The vinyl ether formed from nonphenolic β -O-4 through C γ -elimination can be easily hydrolyzed at 350 °C, giving homovanillin as typical pyrolysis products (Miyamoto and Kawamoto, 2019).

The cleavage of the β -ether in the α/β -diether type trimer is reported to depend on the reactivity of the α -ether linkages (Kawamoto et al., 2008a). In the phenolic form, α -ether is cleaved in the heterolysis mechanism even at 250 °C to form a quinone methide intermediate, in which the β -ether is automatically cleaved. Higher temperature (350 °C) is required for the cleavage of β -ether of the nonphenolic form, because homolysis of α -ether occurs at 350 °C. The resulting C γ -radical is fragmented through the β -scission type C β -O cleavage to form a phenoxy radical.

1.7.1.3 Side-chain and OCH₃ transformation

Guaiacyl-type model dimer studies suggested that coniferyl alcohol is the primary pyrolysis product from the cleavage of β -ether cleavage. However, coniferyl alcohol is unstable along with the polymerization, because the side-chain is easily modified by radical and quinone methide mechanisms, leading to the formation of coniferyl aldehyde, vinylguaiacol, and isoeugenol (Kotake et al., 2013).

By increasing the temperature to $> 450\text{ }^{\circ}\text{C}$, the O-CH₃ bonds are initiated to be cleaved to produce catechols from guaiacols (Asmadi et al., 2011b, 2012). This is coupled with the ipso rearrangement of the OCH₃ group to CH₃ (transformation of guaiacols to o-cresols). The latter pathway is initiated from the phenoxy radicals, which abstract hydrogen from the O-CH₃ group to form OĊH₂. This radical adds to the double bond of benzene ring, and the rearranged from the C-OCH₃ bond to C-CH₂OH bond. The subsequent reactions form coke and polyaromatic hydrocarbons via the o-quinone methide intermediate.

1.7.1.4 Re-condensation

Since ether bond content in lignin accounts for 50-70 % of the linkage in lignin, lignin is expected to be significantly depolymerized at $350\text{ }^{\circ}\text{C}$ where α - and β - ether linkages are mostly cleaved. However, the monomer yield from lignin pyrolysis is much lower than expected, and solid char is rather the main product due to the re-condensation of the pyrolysis products (Biswas et al., 2016; Nakamura et al., 2008).

Two types of recondensation mechanisms are proposed, radical coupling and quinone methide mechanisms. As discussed above, most of the α - and β - ether linkages are pyrolytically cleaved in the homolytical mechanisms to produce radical species, which condense through the radical coupling mechanism (Nakamura et al., 2007). This type of recondensation can be suppressed by using H-donors.

Primary pyrolysis products from lignin contain phenolic OH group formed by the cleavage of the other linkages, along with the conjugated C=C side chains (ex: coniferyl alcohol, coniferyl aldehyde, isoeugenol, vinyl guaiacol from G-lignin). From these structures, quinone methide intermediates are easily formed, followed by recondensation, Use of aprotic solvents has been proposed to inhibit this recondensation, since solvation inhibits the proton transfer process required for the quinone methide formation.

1.7.2 Thermal depolymerization in solvents

Lignin depolymerization behaviors in various solvents are widely studied in hydrothermal and solvolysis processes. When solvents are used for lignin thermal depolymerization, a better heat and mass transfer could be achieved, thereby benefiting primary products dispersing from large lignin molecule and giving a higher yield of liquid products (23 -85 wt%) (Feng et al., 2018; Labidi, 2016; Singh et al., 2014; Yang et al., 2021). Hydrothermal treatment of biomass is a

cheap, catalyst-free and environmental benign approach for lignin depolymerization. Tanahashi (1990) treated guaiacylglycerol- β -guaiacyl ether (a β -O-4 dimer) under steam explosion conditions at 230 °C, and obtained not only guaiacol, vanillin, coniferyl alcohol, but also stilbene, phenylcoumaran and resinol. Okuda et al. (2004) and Sasaki and Goto (2008) studied the organosolv lignin degradation behavior in phenol-water mixture at 400 °C. They reported that phenol binded to the reactive sites on lignin, suppressing repolymerization.

Organic solvents have better dissolution capability for lignin, and hence, solvothermal treatment has a better mass transfer for lignin depolymerization. Yamazaki et al. (2006) studied beech wood degradation behavior in various alcohols at 270, and 350 °C. They found that propanol is the best solvent for lignin liquification, while decanol is the worst. Tsujino et al. (2003), and Minami et al. (2003) used dimer models to investigate the degradation behaviors of typical lignin linkages in supercritical methanol. Their results indicated that degradation behaviors of β -ether and β -aryl are quite similar to those under dry pyrolysis conditions discussed in section 1.7.1, and re-condensed structure such as diarylmethylene formed in organic solvent. Shuai et al. (2016) and Lan et al. (2018) involved various aldehyde to cap the reactive sites of lignin during solvothermal treatment. Their works suggested that chemical protection strategies are very effective in suppressing the irreversible re-condensation, because the monomer yields were significantly increased.

Fundamental studies on lignin depolymerization behavior in aprotic solvent are limited, especially in nonpolar solvent. Nevertheless, Kotake et al. (2013, 2014, 2015) studied the pyrolysis behavior of coniferyl alcohol, MWL, and wood in aprotic solvent with the emphasis on the monomer production. They pointed out that aprotic solvent suppresses the intermolecular proton transfer, and hence, inhibiting the formation of quinone methide intermediates from pyrolysis products. Consequently, the monomer yields increased significantly compared to that under the dry pyrolysis conditions. In addition, they suggested that syringyl type monomers are more susceptible to the radical reactions than guaiacyl type. However, the use of H-donor can help to stabilize the radicals to give a noticeable yield of on S-type monomers.

1.7.3 Reductive catalytic depolymerization

Historically, Harris et al. (1938) and Cooke et al. (1941) treated the solvolysis lignin with copper chromite (CuCr) catalyst under the drastic conditions (temperature: 250–260 °C, initial H₂ pressure: 22-23 MPa), and got three types of propylcyclohexanols as the main monomeric products in a 13.2-44 % yield. Godard et al. (1941) hydrogenated wood at 280 °C (initial H₂ pressure: 24 MPa) with CuCr, and also got propylcyclohexane derivatives with a yield of 36 %, based on lignin. Latter, Pepper et al. (1948) studied hydrogenation of maple wood under milder conditions (temperature: 173 °C, initial H₂ pressure: 20.4 MPa) with Ni, to get aromatic monomers in a 27.3 wt% yield.

In the last decades, hydrogenolysis of lignin were extensively studied under mild conditions. This reductive catalytic depolymerization approach is very effective to produce a high yield of monolignols from wood. For example, decomposition of birch wood (hardwood) in methanol without catalyst at 250 °C gave monomeric products in only 8% yield, but the total monomer yield rase to 52 % with the existence of Ru/C and hydrogen (Van Den Bosch et al., 2015). Nevertheless, the maximum monomer yield is still restrained by the condensed linkages in lignin. For example, yield of monomers by catalytic hydrogenolysis of Masson pine (softwood) at 220 °C is limited to 29 wt% due to the higher contents of condensed C-C linkages in softwood lignins (Luo et al., 2022). Song et al. (2013) and Ouyang et al. (2019) used methanol as a solvent for hydrogenolysis and found that no external hydrogen gas was needed as methanol worked as hydrogen source. Schutyser et al. (2015) and Héroguel et al. (2019) studied the influences of solvent and catalyst for lignin hydrogenolysis process. Sun et al. (2018) compared the hydrogenolysis of different wood species using various reactors (batch and flow-type).

More recently, lignin-first concept combines the chemical protection strategy and hydrogenolysis approach to attain the high monomer yield. Shuai et al. (2016) used formaldehyde to form acetal in lignin side-chain during acid delignification process, and the extracted lignin was treated by hydrogenolysis to give a monomer yield closed to the amount when all ether linkages were cleaved Lan et al. (2018) further studied the α,γ -diol acetalization with other aldehydes. Deuss et al. (2015, 2017) used ethylene glycol as an acetal reagent. These combinations emphasize the importance of capping effect for stabilization of lignin fragments against re-condensation during the delignification process. However, the monomer yields from

their studies are still limited by the ether content in lignin, because the condensed C-C linkages are stable.

1.8 Objectives of this thesis

Japanese cedar wood (*Cryptomeria japonica*) used in this study is a softwood, and its lignin is consisted of guaiacyl nucleus. Accordingly, monomer composition from softwood lignin is expected to be simpler than from hardwood lignin containing syringyl units along with guaiacyl type. Nevertheless, the content of condensed structures is higher in softwood lignin and the recondensation possibility is greater. Thus, even though softwoods are cheaper and growing faster than hardwood, plantation of softwood for aromatic production is not technically favorable at the present technology level. The main objective of this dissertation is to exploit the efficient aromatic monomer production method from softwood lignin by elucidating the degradation mechanisms of softwood lignin under pyrolysis and catalytic hydrogenolysis conditions.

In *chapter 2*, Japanese cedar wood was pyrolyzed in diphenoxybenzene (an aprotic solvent) and a hydrogen donor in the temperature range of 270-380 °C. The temperature effects on the formation behavior of oligomer are discussed, and the chemical characteristics of obtained oligomer is elucidated. With the understanding of the linkages presented in pyrolysis-derived oligomer, efficient depolymerization from oligomer has been studied under the catalytic condition.

In *chapter 3*, catalytic hydrogenolysis of MWL and organosolv lignin with Pd/C in anisole are investigated in the temperature range of 250-350 °C. In addition, hydrogenolysis trials using model dimers were concluded to assess the cleavage reactivity of 4-*O*-5, 5-5, and α -5 type linkages. Finally, we proposed an efficient method that enable us to produce monomers from Japanese cedar wood lignin in > 60% yield.

In *chapter 4*, catalytic hydrogenolysis of pinoresinol in anisole are investigated in the temperature range of 250-350 °C. The new compounds obtained were deduced based on mass spectra, and the possible formation pathways are discussed.

In *chapter 5*, typical lignin pyrolysis monomer products were performed under pyrolysis-assisted catalytical hydrogenolysis with Pd/C in anisole in the temperature range of 200–350 °C.

The conversion pathways of these monomer models and the role of pyrolysis on products selectivity from pyrolysis-assisted catalytic hydrogenolysis of lignin were discussed.

In *chapter 6*, the pyrolysis-assisted catalytic hydrogenolysis is conducted in various solvents including water, methanol, 1,4-dioxane, acetone, toluene, benzene, hexane and anisole to understand the solvents effects on the pyrolytic and catalytic conversion steps. The characteristic features of the solvents are discussed at the molecular level, particularly focusing on undesirable side reaction.

Finally, *Chapter 7* summarized the monomer production behaviors of softwood lignin by pyrolysis-assisted catalytic hydrogenolysis, with the emphasis on 1) pyrolytic depolymerization, 2) dispersion and reactions in solvent, and 3) adsorption and catalytic reaction on Pd/C. Prospects for potential application and the future studies to fulfill this research were further proposed as conclusions.

Chapter 2

Stable oligomer formation from lignin by pyrolysis of softwood in an aprotic solvent with a hydrogen donor

2.1 Introduction

Lignin is an amorphous aromatic polymer composed of phenylpropane units linked via ether (C–O) and condensed (C–C) bonds. There are three types of aromatic nuclei in phenylpropane units: *p*-hydroxyphenyl (H), guaiacyl (G), and syringyl (S). The proportions of these units vary with the plant species. Japanese cedar (*Cryptomeria japonica*), a softwood, contains almost only G-type units. Because lignin accounts for 20–35% of lignocellulosic biomass, it could be used as a renewable resource for the production of aromatic chemicals. However, it is difficult to do this because of the lack of an efficient conversion process for lignin. Pyrolysis is a promising way to convert lignin.

Ether bonds, such as α -O-4 and β -O-4, are cleaved easily at approximately 350 °C, where efficient devolatilization of lignin occurs. By contrast, condensed bonds, such as β -aryl, β - β , and 5-5', are stable against depolymerization of lignin macromolecules (Kawamoto et al., 2007a; Nakamura et al., 2008). Because the content of ether bonds is generally greater than that of condensed bonds, lignin is expected to be largely depolymerized at 350 °C. However, the yield of depolymerization products from lignin pyrolysis is generally much lower than expected, and solid char is the main product (Biswas et al., 2016; Cho et al., 2012). This can be explained by the high re-condensation reactivity of the pyrolysis products.

Investigations using lignin model compounds are effective for clarifying the molecular mechanisms of the cleavage of lignin ether bonds and subsequent re-condensation. The effects of aromatic substituents introduced at the para position of the ether oxygen of model dimers and trimers, clearly indicate heterolysis and homolysis mechanisms for α -O-4 types in phenolic terminal and non-phenolic intermediate units, respectively (Kawamoto et al., 2008a). The β -O-4 type linkages cleave homolytically, but the reactivity depends on the chemical structure of the

model dimer (Kawamoto et al., 2008b). Reactivity differences have been explained with a quinone methide pathway (Watanabe et al., 2015) and radical chain (Watanabe et al., 2015, 2009) mechanisms as proposed for the homolytic cleavage of the β -ether bonds. The resulting radical species polymerize by the radical coupling mechanism.

With the abstraction of hydrogen, radical species resulting from the cleavage of the ether bonds are stabilized as phenols such as coniferyl alcohol [3-(4-hydroxy-3-methoxyphenyl)-2-propen-1-ol]. However, coniferyl alcohol is unstable above 250 °C, where it efficiently recondenses and eventually converts to char (Kotake et al., 2013). Therefore, the yield of coniferyl alcohol is low in lignin pyrolysis. A quinone methide mechanism has been proposed for condensation (Nakamura et al., 2007). Compounds with a conjugated C=C double bond at the para position to phenolic OH tend to condense by a similar mechanism. Along with the condensation, the side chain of coniferyl alcohol is converted to produce various compounds such as coniferyl aldehyde, dihydroconiferyl alcohol, isoeugenol, and vinyl guaiacol (Kotake et al., 2013).

As a method of suppressing the two polymerization mechanisms, Kotake et al. proposed pyrolysis with aprotic solvents and hydrogen (H) donors (Kotake et al., 2015, 2014). Quinone methide formation would be suppressed in the aprotic solvent, while the H donor would stabilize radical species formed by pyrolysis. They also indicated that coexisting wood polysaccharides would act as H donors for stabilization of lignin-derived radicals. Under these conditions, the monomer yield increased from 2–3 wt% to 16 wt% (lignin basis), with the main monomers being dihydroconiferyl alcohol and isoeugenol. Nevertheless, most of the products were oligomers that have not yet been characterized. Characterization of this fraction is important to improve the proposed pyrolysis conditions.

In this study, the formation of oligomers during pyrolysis of Japanese cedar wood was investigated using 1,3-diphenoxybenzene (DPB) as the aprotic solvent and 1,2,3,10b-tetrahydrofluoranthene as the H donor at 270–380 °C. The chemical characteristics of the oligomers were determined and the role of wood polysaccharides in the cell wall was evaluated. The pyrolysis conditions are similar to those used in Kotake's research (Kotake et al., 2014).

2.2 Experimental

2.2.1 Materials

Japanese cedar wood (cellulose: 38.3 wt%, hemicellulose: 24.5 wt%, lignin: 33.3 wt%, and extractives: 3.4 wt%) (Rabemanolontsoa et al., 2011) was ground into flour and sieved (< 150 μm), and then extracted with ethanol/benzene (2:1, v/v) to remove the extractives. Milled wood lignin (MWL) was prepared from Japanese cedar wood flour in accordance with an established method (Björkman A, 1956). The contents of hydrolyzable sugars in this MWL were glucose 0.6 wt%, xylose 0.7 wt%, mannose 0.3 wt%, and arabinose, 0.2 wt%. These sugars were derived from the carbohydrates remaining in the MWL (Hosoya et al., 2007).

DPB, which has a melting point of 60.0 °C (Sax et al., 1960) and estimated boiling point of 374.2 \pm 25.0 °C (Scifinder, 2019), was used as the aromatic solvent. 1,2,3,10b-Tetrahydrofluoranthene which has a melting point of 72–73 °C (Eliot Steinberg, 1954) and estimated boiling point of 353.5 \pm 17.0 °C (Scifinder, 2019) was used as the H donor. These compounds (Fig. 2-1) were purchased from Tokyo Chemical Co., Ltd. (Tokyo, Japan) and were of guaranteed grade and used without purification.

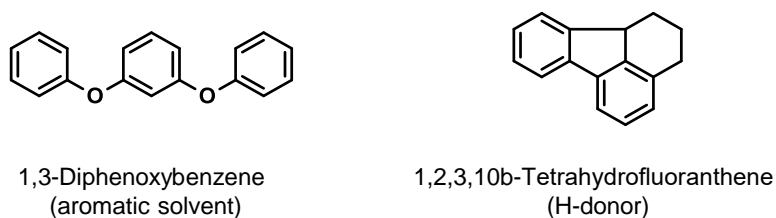


Fig. 2-1 Aromatic solvent and H donor used in this study.

2.2.2 Pyrolysis and product fractionation

Oven-dried extractive-free cedar wood flour (50 mg), DPB (200 mg), and H donor (50 mg) were placed in the bottom of a Pyrex tube reactor (internal diameter: 8.0 mm, glass thickness: 1.0 mm, length: approximately 300 mm) (Fig. 2-2). The amount of DPB (200 mg) was the minimum amount sufficient to solvate the wood flour. The amount of the H-donor (50 mg) was also sufficient to influence the lignin pyrolysis reactions, which was determined by the preliminary

experiments using different loading levels of H-donor. The inside air was replaced with N₂ through a three-way cock connected to an aspirator and a N₂ balloon. The tube reactor was preheated to around 100 °C until the DPB and H donor melted. Then, through a small hole in the upper wall, the lower two-thirds of the reactor was inserted into a muffle furnace preheated to a set temperature between 270 °C and 380 °C. After the specified treatment time at normal pressure, the reactor was removed from the furnace and cooled immediately under airflow for 1 min and then in flowing cold water for 1 min.

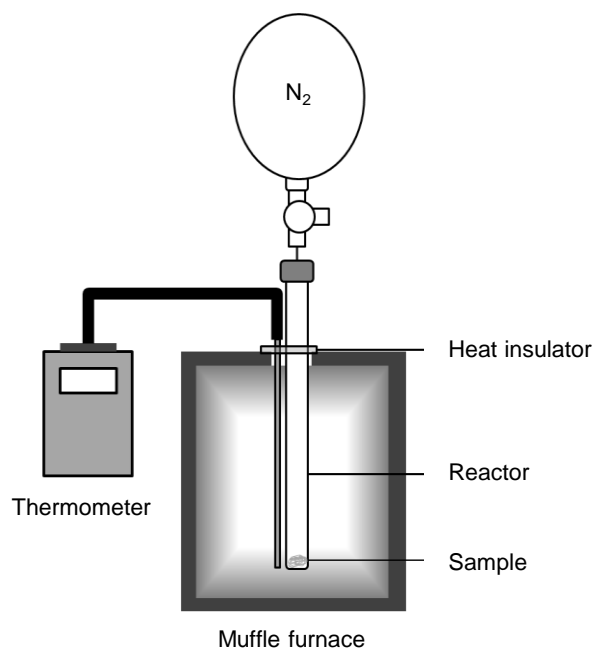


Fig. 2-2 Experimental setup for pyrolysis.

The pyrolysis products were separated into four fractions by extraction with binary solvent systems (Fig. 2-3). In the first extraction step using ethyl acetate (EtOAc) and water (1:1, v/v), relatively polar carbohydrate-derived products were extracted into water. The EtOAc layer contained hydrophobic lignin-derived products, DPB, and the H donor. Char and unreacted wood were separated as solid residue. The water layer was evaporated *in vacuo*. The EtOAc layer was evaporated *in vacuo* after dehydration over anhydrous Na₂SO₄. The EtOAc-soluble (lignin) fraction was further purified by washing with *n*-hexane. Each dried fraction was weighed on an electronic balance. Some samples were acetylated in acetic anhydride and pyridine at room temperature, followed by removal of the solvent and reagent through evaporation *in vacuo*.

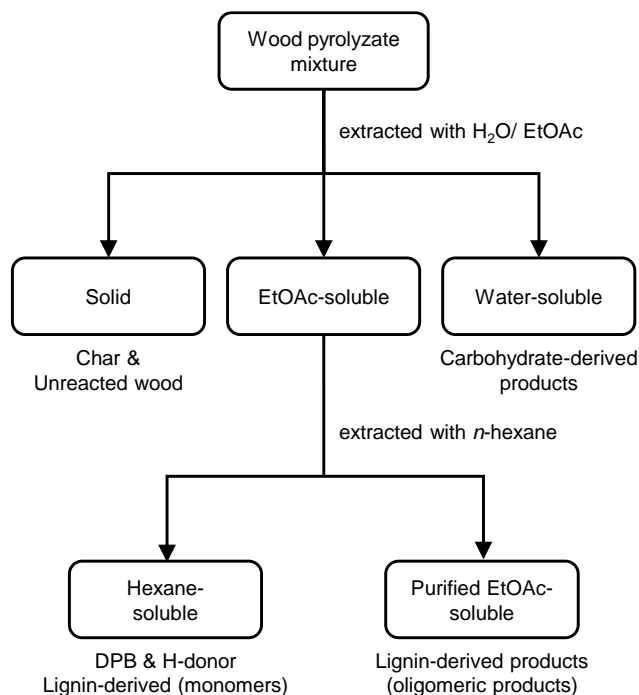


Fig. 2-3 Separation process of wood pyrolyzate.

2.2.3 Product analysis

GPC was conducted to analyze the molecular weight distribution of the purified EtOAc-soluble (lignin) fraction using a Shimadzu LC-10A system with a Shodex KF-801 column (exclusion limit molecular weight: 1,500 Da, polystyrene standard) at a flow rate of 0.6 mL/min and a temperature of 40 °C. Tetrahydrofuran was used as the eluent with a UV detector at 280 nm. The NMR spectra were measured by a Varian AC-400 (400 MHz) spectrometer (Varian, CA, USA). The chemical shifts and coupling constants (J) are reported in δ (ppm) and Hz, respectively.

The hydrolyzable sugars in the solid residue were obtained by an acid hydrolysis process as described in our previous work (Nomura et al., 2017). After neutralization with an OnGuard II/A ion exchange column (Dionex, Sunnyvale, USA), the hydrolyzates were quantified by high-performance anion-exchange chromatography (Prominence, Shimadzu Corp., Kyoto, Japan) with an electrochemical detector (DECADE Elite, Antec Scientific, Zoeterwoude, Netherlands). The column was CarboPac PA1 (4 × 250 mm, Dionex) with a column temperature of 35 °C. The eluent was 0.2 M NaOH in ion-exchanged water at a flow rate of 1.0 mL/min, and the carrier gas was N₂.

Gas chromatography/mass spectrometry was performed to analyse the lignin-derived monomers in hexane-soluble portion by using Shimadzu 2010 Plus gas chromatograph (Shimadzu Corporation, Kyoto, Japan) coupled with a Shimadzu QP 2010 Ultra mass spectrometer (Shimadzu Corporation, Kyoto, Japan). The instrumental conditions consisted of: column, Agilent CPSil 8CB (length: 30 m, diameter: 0.25 mm); injector temperature, 250 °C; split ratio, 10; column temperature, 50 °C (1 min), 5 °C /min to 120 °C, 10 °C /min to 330 °C, 330 °C (5 min); carrier gas, helium; flow rate, 1.22 mL/min. The mass spectrometric scan parameters included a scan range of 35–500 m/z and a scan interval of 0.3 s.

Table 2-1 Experimental conditions used for pyrolysis of Japanese cedar wood flour (50 mg).

Reaction conditions				Data presented		
Temperature (°C)	Time (min)	DPB (mg)	H-donor (mg)	GPC	1H-NMR	2D-HSQC
270	5	200	50	✓		
	10	200	50	✓		
	30	200	50	✓		
	60	200	50	✓	✓	✓
300	5	200	50	✓		
	10	200	50	✓		
	30	200	50	✓		
	60	200	50	✓	✓	
	90	200	50	✓		
320	3	200	50	✓		
	5	200	50	✓		
	7	200	50	✓		
	10	200	50	✓		
	15	200	50	✓		
	30	200	50	✓	✓	
	50	200	50	✓		
350	3	200	50	✓	✓	
	5	200	50	✓	✓	✓
	5	200	0	✓		✓
	5	0	0	✓		
	7	200	50	✓		
	10	200	50	✓	✓	✓
	15	200	50	✓	✓	
380	3	200	50	✓		
	5	200	50	✓		
	7	200	50	✓		
	10	200	50	✓	✓	
	15	200	50	✓		

Table 2-1 summarizes the experimental conditions used in this study and the analysis data presented in this article. Pyrolysis experiments at 350 °C were repeated twice to confirm the reproducibility, although the data presented in this paper were not treated statistically. The yields reported in this article are mean values.

2.3 Results and discussion

2.3.1 Characterization of separated fractions

¹H-NMR spectra were measured for water-soluble (Fig. 2-4a), hexane-soluble (Fig. 2-4b), and purified EtOAc-soluble (Fig. 2-4c) fractions obtained at 350 °C with a 5 min treatment time. Spectra were also measured for acetate derivatives of the purified EtOAc-soluble fraction (Fig. 2-4d) and MWL isolated from Japanese cedar (Fig. 2-4e).

In the spectrum of the water-soluble fraction (Fig. 2-4a), many signals were observed between 1.5–3 ppm and 3.5–4.5 ppm. These peaks were assigned to saturated alkyl protons and RO-CH₂, respectively. The signals observed in the low magnetic field region above 6 ppm, which is where signals for aromatic and other double bond protons are located, were relatively small. Two signals at 5.40 and 5.46 ppm were assigned to the C1-protons of levomannosan (1,6-anhydro-β-D-mannopyranose) and levoglucosan (1,6-anhydro-β-D-glucopyranose), both of which are typical pyrolysis products from wood polysaccharides in softwoods. Saturated alkyl groups may be contained in the polar components, such as sugar-related products, because they are soluble in water.

The signals mentioned in Fig. 2-4a were not observed in the spectrum of the purified EtOAc-soluble fraction (Fig. 2-4c). In this spectrum, methoxyl and aromatic protons were observed as broad signals at 3.5–4 ppm and 6.5–8 ppm, respectively. These broad signals indicated that the main component of this fraction was the lignin-derived oligomer. This was also demonstrated by gel-permeation chromatography (GPC) analysis (Fig. 2-6). Therefore, the carbohydrate-derived products were efficiently removed from wood pyrolysis products by extraction with a binary mixture of EtOAc/H₂O. The signals at 1–3 ppm originated from the saturated alkyl described below.

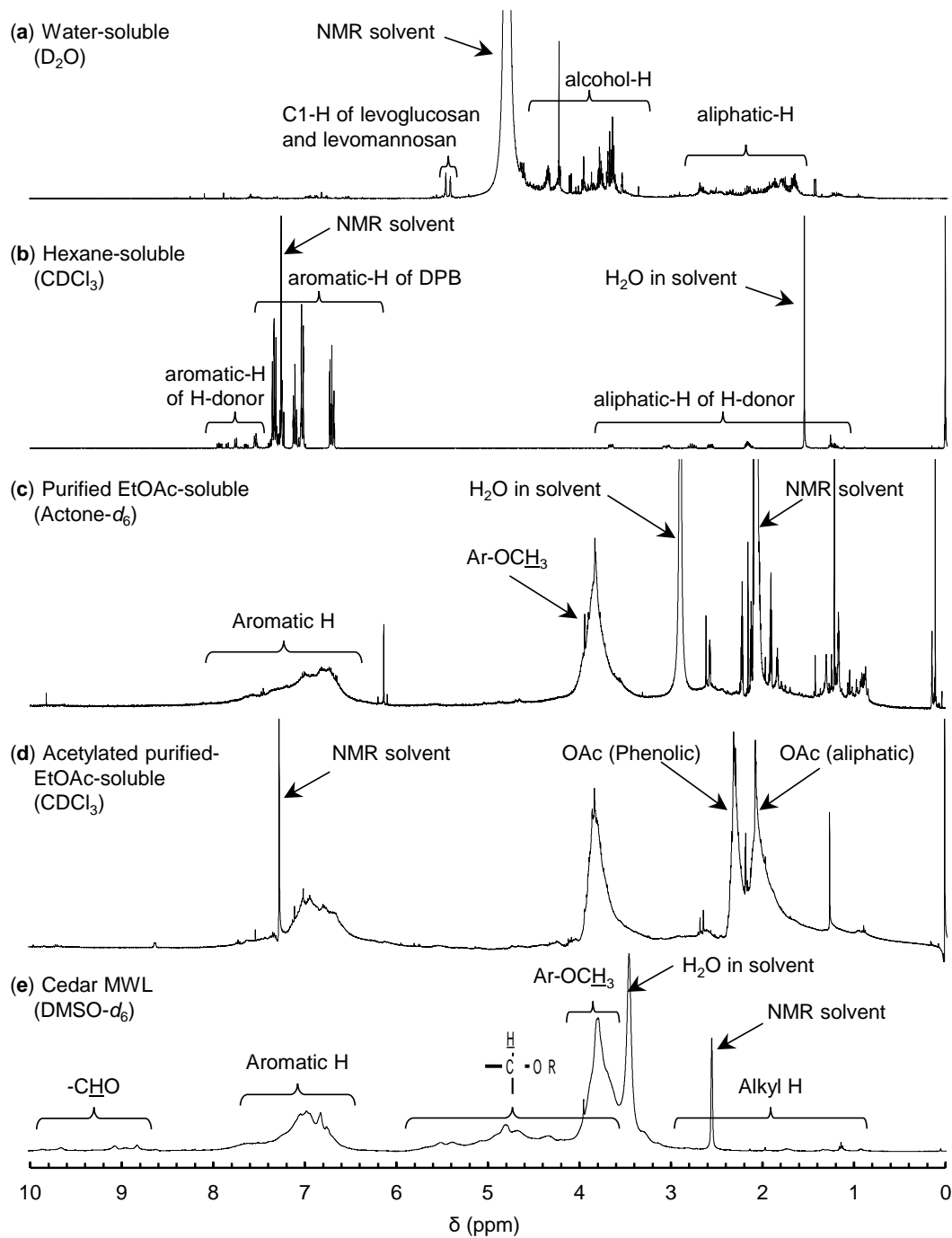


Fig. 2-4 1H -NMR spectra of a) water-soluble, b) hexane-soluble, and c) purified EtOAc-soluble portions obtained from wood pyrolysis in the presence of aromatic solvent and H-donor at 350 °C for 5 min. d) acetylated derivatives of purified EtOAc-soluble portion; e) milled wood lignin from Japanese cedar wood.

The major components of the hexane-soluble fraction were DPB and the H donor used for the pyrolysis (Fig. 2-4b). These signals were not observed in the spectrum of the purified EtOAc-soluble fraction (Fig. 2-4c), which indicated that washing with hexane effectively removed DPB and the H donor. No signals other than those for DPB and H donor were observed in the spectrum for the hexane-soluble fraction (Fig. 2-4c), but gas chromatography mass spectrometry analysis of this fraction indicated that lignin-derived monomers were present in this fraction (Fig. 2-5). Van den Bosch also reported that hexane extraction could separate monomers from lignin-derived pyrolysis products to leave oligomers as residue (Van Den Bosch et al., 2015).

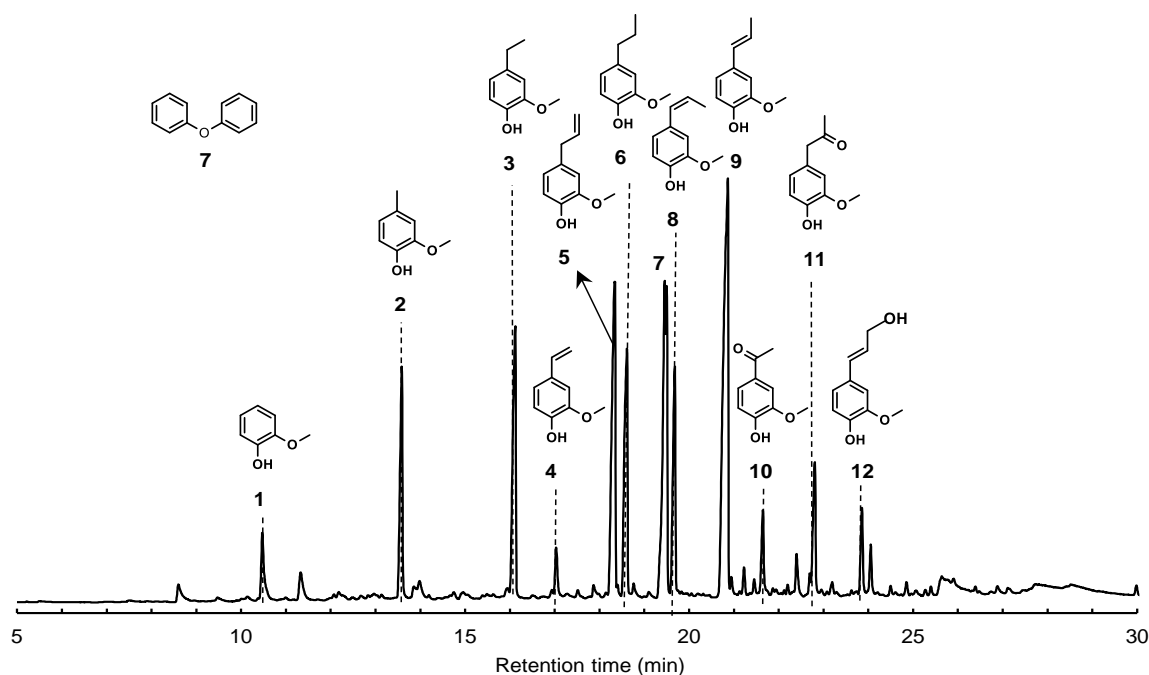


Fig. 2-5 GC/MS chromatograms of monomeric lignins in hexane-soluble portion obtained at 350 °C/ 5 min (signals of dimers, aprotic solvent and H-donor are not shown).

2.3.2 Effect of temperature on formation behavior

Temperature is the most important variable for thermal degradation of lignin in wood. Primary pyrolysis reactions of lignin occur over a wide temperature range of 200–400°C but become significant around 320–350°C (Asmadi et al., 2011a). Therefore, we studied the formation behavior of lignin-derived products and other fractions first at five different temperatures (270, 300, 320, 350, and 380°C, Fig. 2-6). Because the estimated boiling points of

DPB and the H donor are 374 °C and 354 °C (Scifinder, 2019), respectively, when the reactor temperature was set to 380 °C, the actual treatment temperature for the wood was lower than 380 °C under normal pressure.

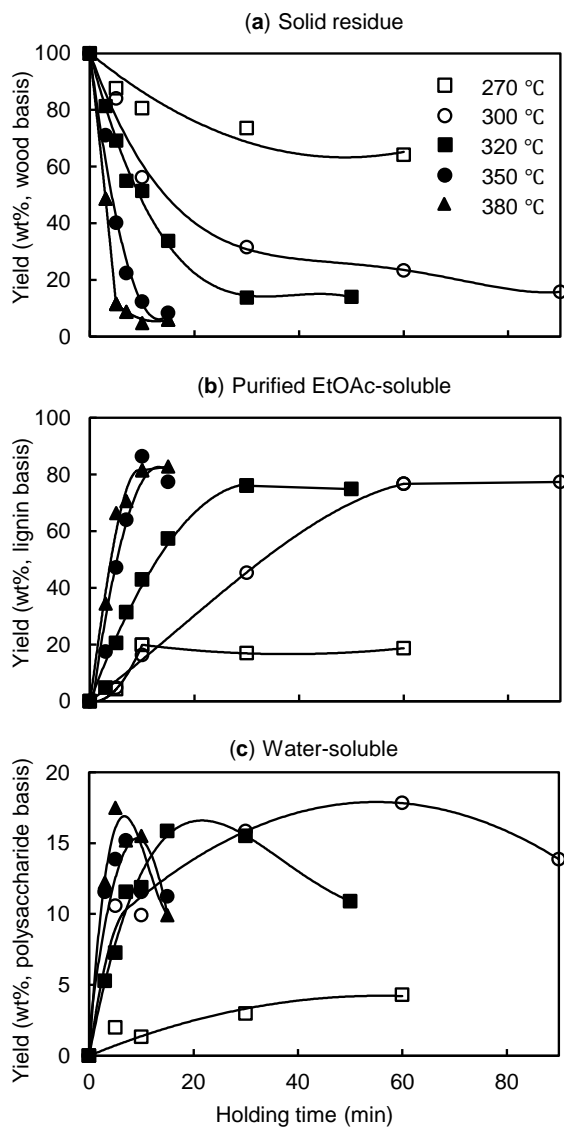


Fig. 2-6 The yield of a) solid residue, and b) purified EtOAc-soluble and c) water-soluble portions from wood pyrolysis in the presence of DPB and H donor at 270–380 °C. Wood (50 mg), DPB (200 mg), H donor (50 mg).

The degradation behavior varied greatly depending on the treatment temperature. At 270 °C, the yield of the purified EtOAc-soluble (lignin) fraction was approximately 20 wt%

(lignin basis) after treatment for 10 min. This yield did not increase even when the treatment time was extended to 60 min. These results indicate that approximately 20% of lignin in softwood is reactive even at a relatively low temperature, whereas the rest of the lignin in wood is not converted into soluble products.

Increasing the temperature to 300 °C increased the yield of oligomers, which reached approximately 80 wt% with heating times of 60 and 90 min. The required heating time decreased to 30 min at 320 °C and 10 min at 350 °C. There was little variation in the heating time at temperatures above 350 °C. These results agree with thermogravimetric analysis of the pyrolysis reactivity of lignin (Asmadi et al., 2011a). Interestingly, the yield of lignin-derived products between 300–380 °C tended to level off at approximately 80 wt%, and increasing the heating time did not decline such yields. These results indicate that most of the lignin in Japanese cedar wood was recovered as a very stable oligomer even at high temperatures.

By contrast, the yield of the water-soluble (polysaccharide) fraction was relatively low (< 20 wt%, polysaccharide basis). Furthermore, the yields tended to decrease as the treatment time increased, especially at temperatures above 300 °C. Therefore, products derived from polysaccharide were unstable under such conditions.

2.3.3 Molecular weight distribution of lignin-derived products

The molecular weight distribution of lignin-derived products (purified EtOAc-soluble fraction) was evaluated by GPC. The chromatogram of the lignin-derived products obtained after treatment at 350 °C for 5 min (Fig. 2-7a) was compared with those of the lignin-derived products obtained in the absence of a H donor (Fig. 2-7b) and in nitrogen (Fig. 2-7c). The broad signal of the lignin-derived products (Fig. 2-7a) showed a peak at approximately 10 min, which corresponded to 1,270 Da for polystyrene (GPC column exclusion limit: 1,500 Da at 9.5 min). Assuming that all monomeric units are coniferyl alcohol (molecular weight 180.2), this is equivalent to a heptamer and indicates that the obtained lignin-derived products are oligomers. This feature was observed for all lignin-derived products (Fig. 2-8) obtained under the pyrolysis conditions shown in Fig. 2-6. Therefore, the molecular weight distribution is fairly similar regardless of the pyrolysis temperature (270–380 °C) and treatment time.

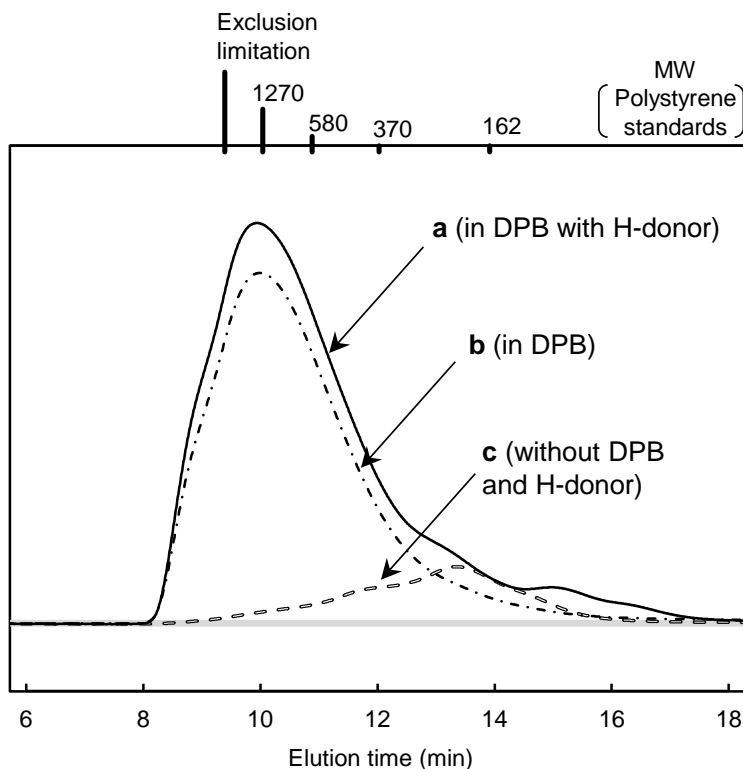


Fig. 2-7 GPC chromatograms of purified EtOAc-soluble fractions obtained from Japanese cedar wood. (a) solid line: neat pyrolysis at 350 °C for 5 min under nitrogen, (b) dotted and dashed line: pyrolysis in an aromatic solvent (diphenoxybenzene, DPB), and (c) dash line: pyrolysis in DPB with a hydrogen donor (1,2,3,10b-tetrahydrofluoranthene).

The GPC profile (Fig. 2-8) tended to shift slightly to the higher molecular weight (MW) region as the yield of lignin-derived products increased. This indicated that the MW range was determined by the yield. These results also indicate that re-condensation of lignin-derived products did not occur actively in DPB and the H donor.

Under nitrogen, the yield of lignin-derived products from Japanese cedar wood was only approximately 10 wt% (lignin basis), and the oligomer signal in the 9–12 min range was relatively very small. Thus, in neat pyrolysis conditions, most of the lignin-derived products re-condense and are converted to char, and only volatile monomers are recovered.

In DPB, the yield of lignin-derived products greatly increased from 10 wt% (under nitrogen) to 40 wt%, and the addition of the H donor further increased the yield to 52 wt%. These results indicate that aprotic solvents are more important than H donors in the production of low MW lignin-derived products from Japanese cedar wood. As discussed below, thermal

degradation of wood polysaccharides may produce H donors that stabilize lignin-derived radicals. Both pyrolysis conditions using DPB show similar oligomer signals in Fig. 2-7. As indicated by Kotake et al., quinone methide formation from lignin pyrolysis products would be effectively inhibited in DPB, an aprotic solvent, by suppressing the proton transfer required for the transformation (Kotake et al., 2014).

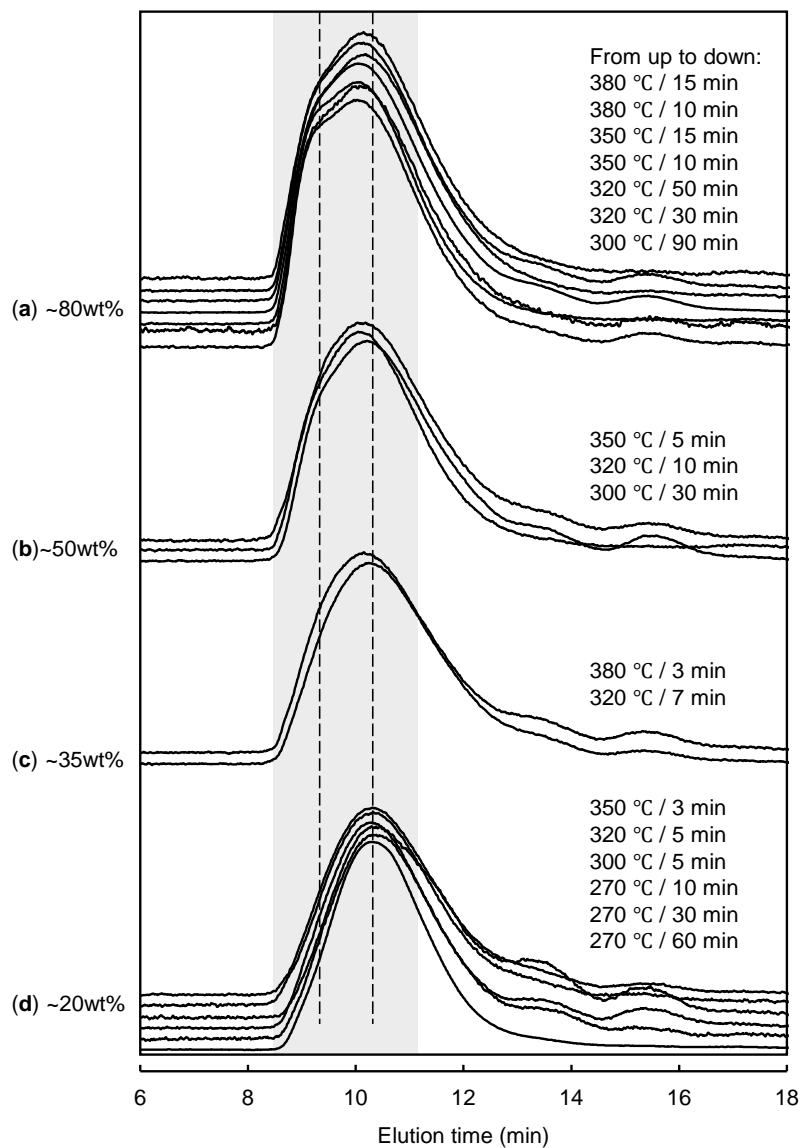


Fig. 2-8 GPC chromatograms of the purified EtOAc-soluble fractions obtained from Japanese cedar wood after treatment at various temperatures and for different times. The results are grouped by the yield of lignin-derived oligomer.

2.3.4 NMR analysis of lignin-derived oligomer

The ^1H -NMR spectra of the lignin-derived products obtained after treatment at 350 °C for 5 min (Fig. 2-4c and d) were compared with that of Japanese cedar MWL (Fig. 2-4e), to evaluate the chemical structure of oligomer derived from lignin. The MWL spectrum (Fig. 2-4e) showed signals for $\underline{\text{H}}\text{-C}_\alpha\text{-OR}$ and $\underline{\text{H}}\text{-C}_\beta\text{-OR}$ at 3.5–6 ppm (Heitner et al., 2016). These signals were much smaller in the spectra of the lignin-derived products (Fig. 2-4c and d), which indicated that these structures containing α - and β -ether linkages almost disappeared. Aldehyde signals (8.5–10 ppm) in the MWL spectrum (Fig. 2-4e) also disappeared in the spectra of the lignin-derived products (Fig. 2-4c and d). By contrast, large signals assigned to saturated alkyl protons were observed between 0.5–3 ppm in the spectrum of lignin-derived products (Fig. 2-4c). These results indicated that the α - and β -ether bonds were cleaved, and the side-chains were converted to saturated alkyls.

The ^1H - ^1H COSY NMR spectra of the lignin-derived products obtained after treatment at 350 °C for 5 min and their acetyl derivatives (Fig. 2-9) were used to evaluate the alkyl side chain structure. Dihydroconiferyl alcohol is reportedly produced by hydrogenation of the C=C double bond of coniferyl alcohol, a primary pyrolysis product, under pyrolysis conditions (Kotake et al., 2014). Signals assigned to the γ -hydroxypropyl side chain were observed in Fig. 2-9a, and the $\text{C}_\gamma\text{-H}$ signal shifted to a lower magnetic field in Fig. 2-9b because of the electron withdrawing effect of the acetyl group. These results confirm that γ -hydroxypropyl is a major alkyl side chain in the lignin-derived oligomer as suggested by the monomer composition (Kotake et al., 2014).

In the ^1H -NMR spectrum (Fig. 2-4d), acetyl methyl protons of aliphatic and phenolic hydroxyl groups were observed at 1.7–2.1 ppm and 2.1–2.3 ppm, respectively, because of the deshielding effect of the aromatic ring. As discussed below, other saturated alkyl signals overlapped with these signals, but the amounts of aliphatic and phenolic OH groups of the lignin-derived products could still be estimated. CDCl_3 was used for NMR of the acetylated derivatives (Fig. 2-4d) to avoid overlap with the solvent signal (acetone: 2.05 ppm, CHCl_3 : 7.26 ppm). The relative peak areas of aromatic, methoxyl, phenolic, and aliphatic acetyl methyl protons were approximately 1:1:0.8:1 (Fig. 2-4d). These values are not accurate because of signal overlap, but the relatively large aromatic proton signal indicates that re-condensation is not important because the guaiacyl unit contains three aromatic protons and three methoxyl protons. Similarly, most repeating units contain a phenolic OH group and one OH group in the side chain (probably C_γ).

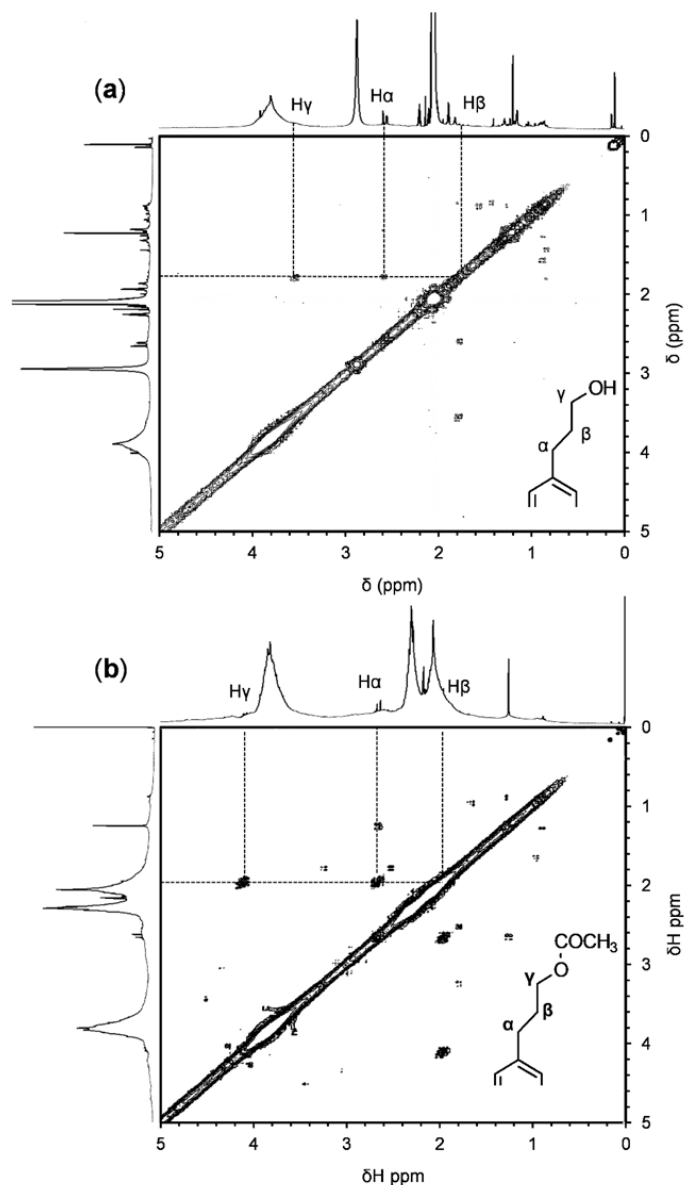


Fig. 2-9 ^1H - ^1H COSY NMR spectra of (a) the purified EtOAc-soluble fraction obtained after treatment at 350 °C for 5 min (NMR solvent: acetone- d_6) and (b) its acetylated derivatives (NMR solvent: CDCl_3).

The signals at 2.5-3 ppm in the NMR spectra of the acetate derivatives of lignin-derived products increased in intensity when the treatment time was increased from 3 min to 10 min, and the yield of lignin-derived products reached 80 wt% (Fig. 2-10). This indicates that large numbers of saturated alkyl side chains form in this period. As explained below, conversion of the vinyl ether structure was considered along with hydrogenation of the coniferyl alcohol type C=C double bond.

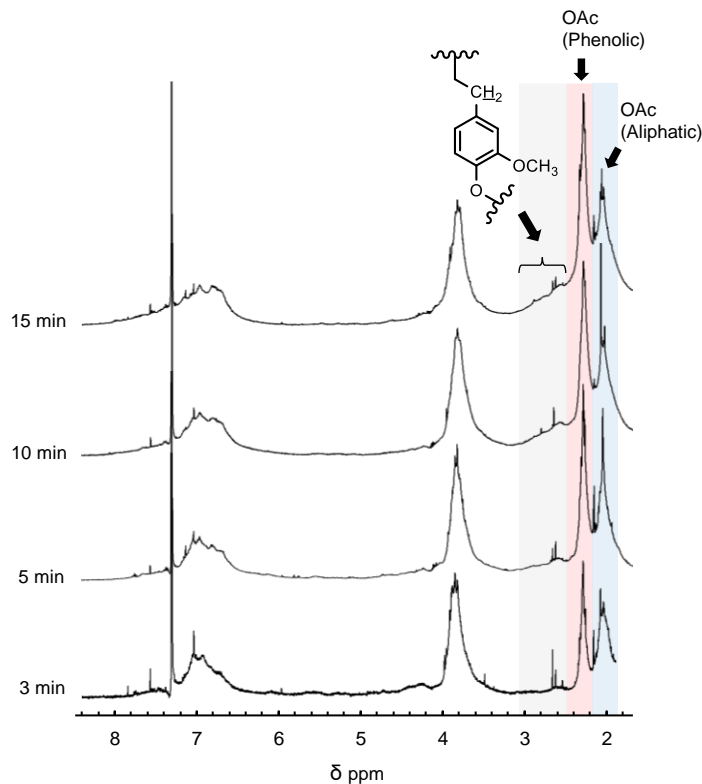


Fig. 2-10 $^1\text{H-NMR}$ spectra of acetylated purified EtOAc-soluble fractions obtained after treatment at $350\text{ }^\circ\text{C}$ for various times.

The relative peak area of the aromatic/aliphatic acetyl methyl protons also slightly increased in this period, which indicated that ether bond cleavage occurred even in the treatment period between 5 and 10 min. When the yield of lignin-derived products reached approximately 80 wt%, the spectra were very similar regardless of the pyrolysis temperature or processing time (Fig. 2-11). The spectrum for the product obtained after treatment at $270\text{ }^\circ\text{C}$ for 60 min (yield 20 wt%) was similar to that for the product obtained after treatment at $350\text{ }^\circ\text{C}$ for 5 min (yield 52 wt%), which indicated that the chemical structure of lignin-derived products was determined by the yield even at a low temperature of $270\text{ }^\circ\text{C}$. These results led to a hypothesis that the chemical structure of lignin-derived products correlated with the pyrolysis reactivity of lignin in wood, because the HSQC NMR spectra of lignin-derived oligomers obtained after treatment at $350\text{ }^\circ\text{C}$ for 5 min (Fig. 2-12b) and $270\text{ }^\circ\text{C}$ for 60 min (Fig. 2-13) were also quite similar.

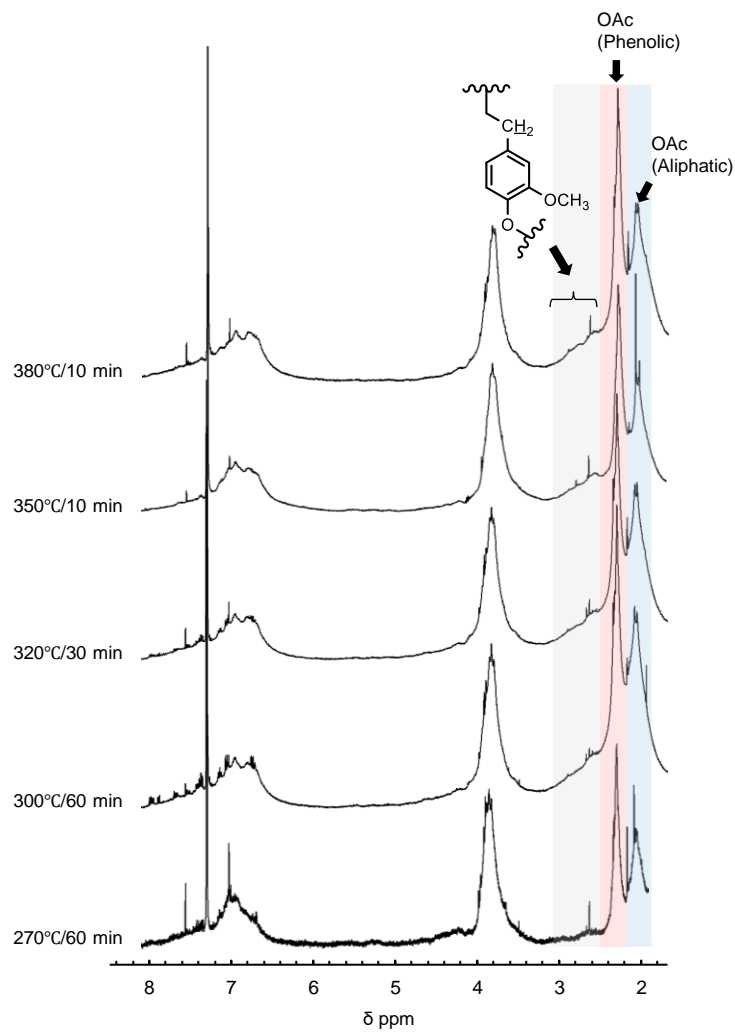
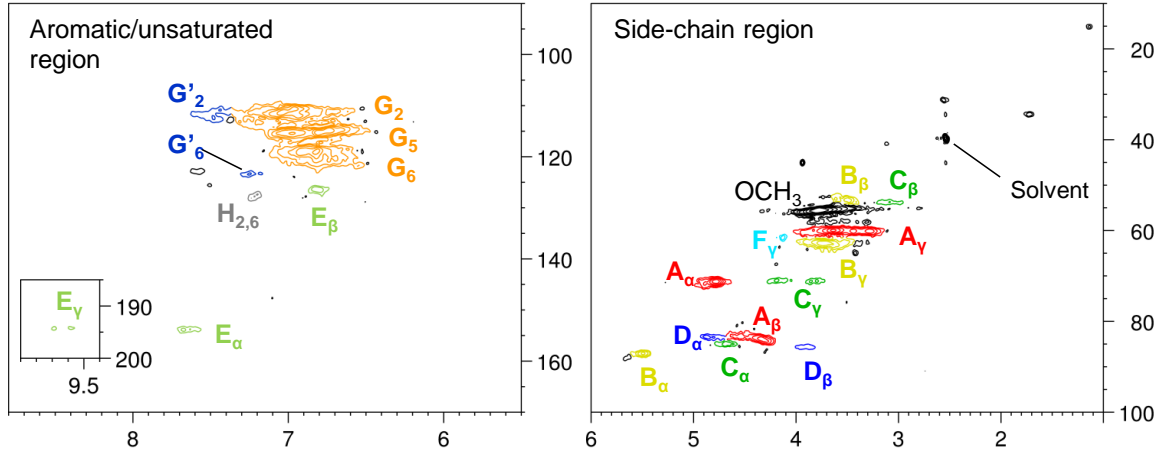
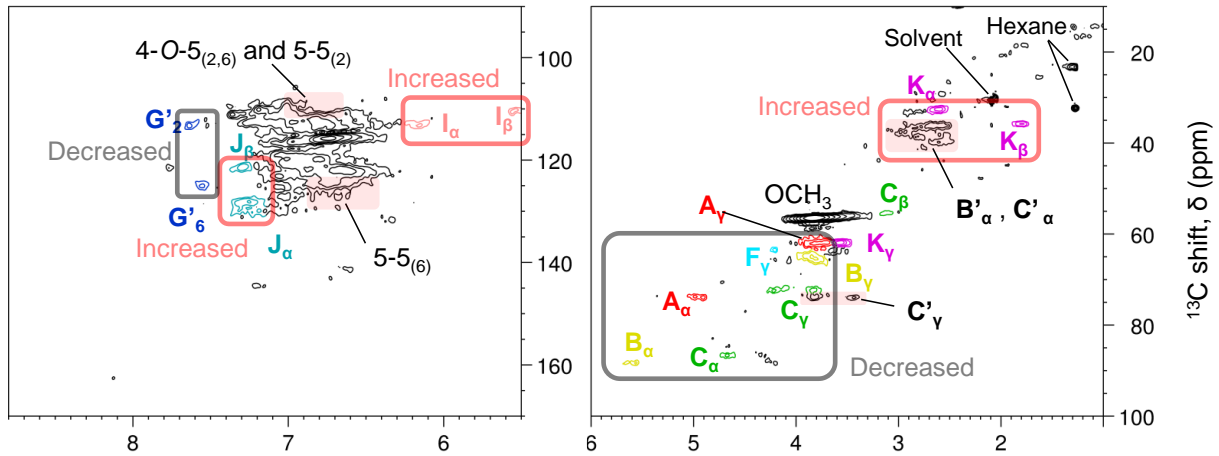


Fig. 2-11 ¹H-NMR spectra of acetylated purified EtOAc-soluble portions obtained under various pyrolysis conditions where the yield of lignin-derived oligomer was maximum at about 80 wt% excluding conditions (270 °C/ 5 min, around 20 wt%).

(a) Cedar MWL (untreated)



(b) 350°C / 5 min



(c) 350°C / 10 min

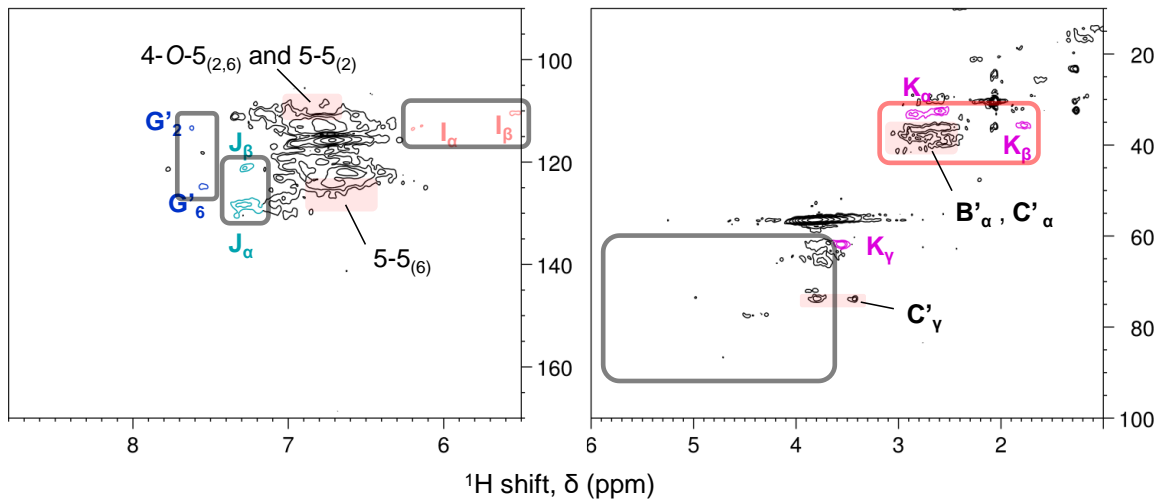


Fig. 2-12 HSQC NMR spectra of (a) Japanese cedar MWL (Solvent: DMSO-*d*₆), and purified EtOAc-soluble portions obtained at 350 °C for (b) 5 min and (c) 10 min.

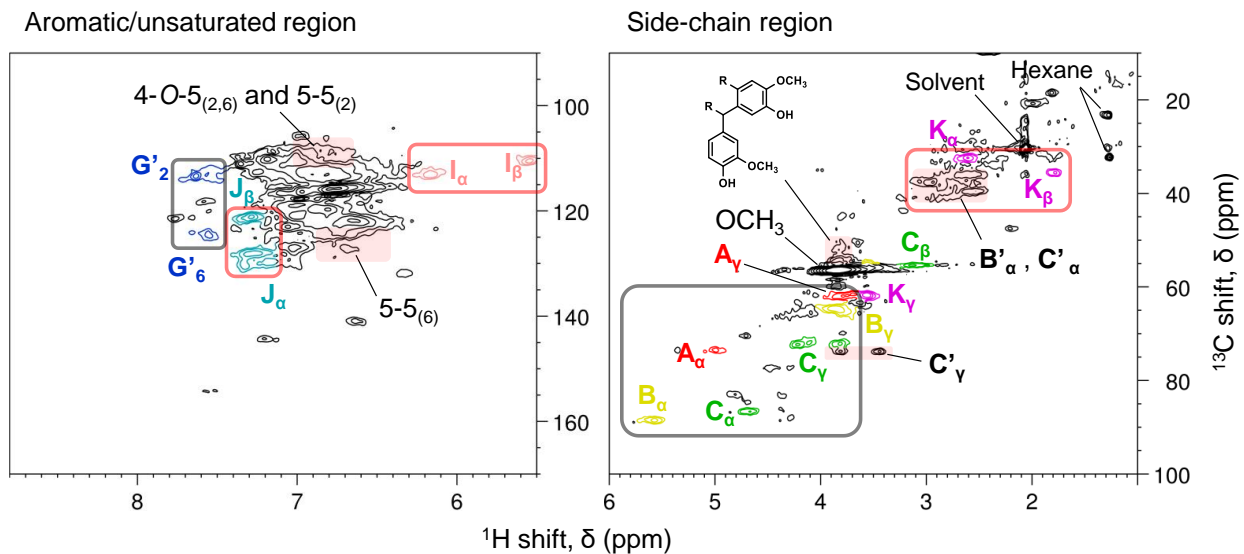


Fig. 2-13 HSQC NMR spectrum of purified EtOAc-soluble portion obtained at 270 °C/ 60 min.

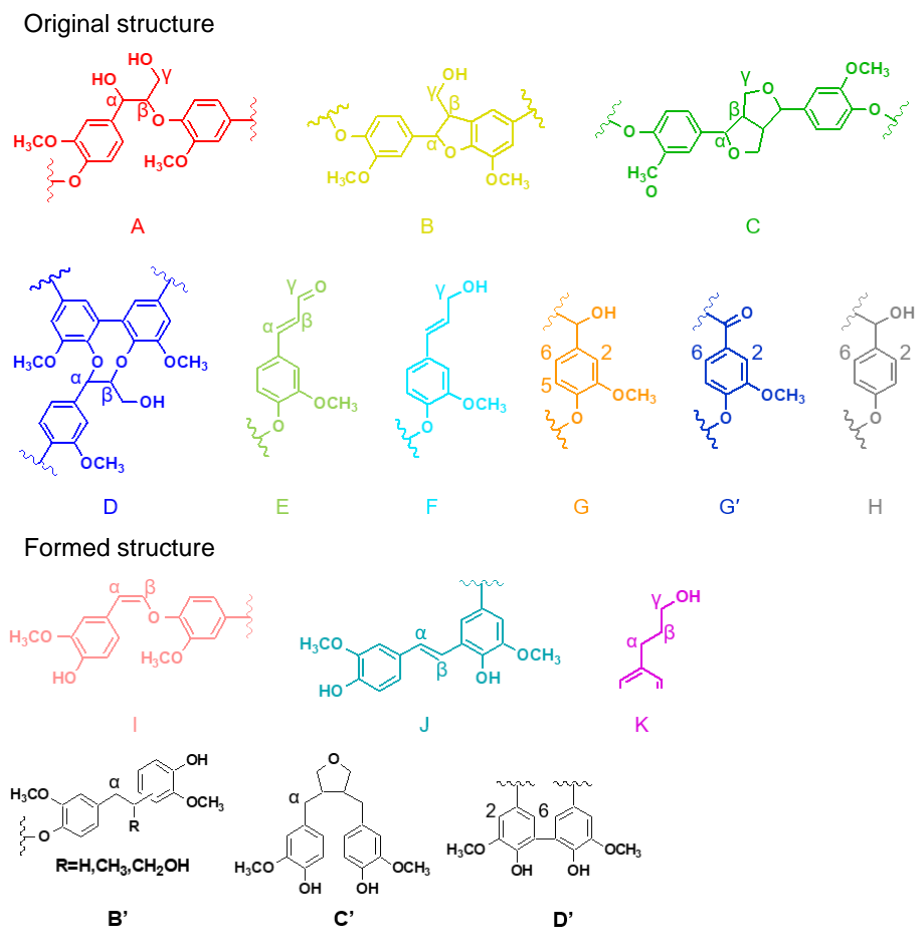


Fig. 2-14 Chemical structures identified by the HSQC NMR spectra.

The HSQC NMR spectra of Japanese cedar MWL and lignin-derived products obtained after treatment at 350 °C for 5 min or 10 min are shown in Fig. 2-12. The chemical structures assigned to the signals are shown in Fig. 2-14. In the δ_C/δ_H 50-90/3-6 ppm region of the MWL spectrum (Fig. 2-12a), signals assigned to the side chains of guaiacylglycerol- β -guaiacyl ether (β -O-4) (A), phenylcoumaran (β -5) (B), pinoresinol (β - β) (C), dibenzodioxocin (D), and coniferyl alcohol (F) type structures were observed (Heitner et al., 2016; Wen et al., 2013). These signals were weak in the spectrum of the lignin-derived products obtained after treatment for 5 min (Fig. 2-12b) and not present in the spectrum of the lignin-derived products obtained after treatment for 10 min (Fig. 2-12c), which supports the above conclusion that α - and β -ether bonds are cleaved within 10 min.

In the alkyl region of the lignin-derived product (δ_C/δ_H 20-50/1.5-3.5 ppm) (Fig. 2-12b and c), several new signals were observed. Signals assigned to the γ -hydroxypropyl side chain (K) (Ralph et al., 2004) formed by hydrogenation of F were observed, and the signal for F disappeared in the spectrum for the product obtained after treatment for 10 min. In addition to these signals, pyrolysis produced large signals at δ_C/δ_H 35-40/2.4-2.7 ppm, labeled as B' $_{\alpha}$ and C' $_{\alpha}$. According to the literature, these signals can be assigned to structures derived from phenylcoumaran (B) and pinoresinol (C) (Sy and Brown, 1998; Van Aelst et al., 2020), with cleavage and rearrangement of the side-chain ring structures (Fig. 2-14). Conversion of B to B' and C to C', would occur during pyrolysis, and this explains the increase in signal strength in the 1.8–3 ppm region with treatment times of up to 10 min (Fig. 2-10). However, these conversions do not contribute to the depolymerization of lignin macromolecules.

The spectra in the aromatic/unsaturated region slightly changed for the lignin-derived products. The signals assigned to the conjugated aldehyde (E) and benzaldehyde (H) disappeared in the spectra for the products obtained after treatment at 350 °C for 5 min or 10 min (Fig. 2-12). Instead, signals appeared for vinyl ether (I) (Zhao et al., 2020), stilbene (J) (Lancefield et al., 2018), and 5-5' (D') (Ralph et al., 2004; Van Aelst et al., 2020). Stilbenes are reportedly formed by pyrolytic degradation of the β -aryl type condensed structure (Kawamoto et al., 2007b; Minami et al., 2003). Large stilbene signals were observed in the spectrum for the product obtained after treatment for 5 min, and the signal strength was not lessened greatly in the spectrum for the product obtained after treatment for 10 min. This indicates that the stilbene C=C

double bonds are stable under the current pyrolysis conditions, even though the coniferyl alcohol type C=C bonds are efficiently hydrogenated as mentioned above.

Vinyl ether is reportedly formed from the β -ether structure (Kawamoto et al., 2007b; Minami et al., 2003). Clear signals were observed for vinyl ether in the spectrum of the product obtained after treatment for 5 min. The signal intensity was much lower in the spectrum of the product obtained after treatment for 10 min. Thus, this structure was degraded during the 5–10 min treatment period. Vinyl ether, particularly in the phenolic terminal unit, is reportedly hydrolyzed during heat treatment in nitrogen to form a β -carbonyl structure (Miyamoto and Kawamoto, 2019). This transformation would occur under the current pyrolysis conditions and increase the content of phenolic OH groups as described above.

The 5-5' signals originated from dibenzodioxocin (D) after cleavage of the α - and β -ether bonds.

On the basis of these results, the side chains of the condensed structures were transformed during the treatment, but these transformations do not contribute to depolymerization of the lignin macromolecules. This is the main reason for production of oligomers rather than monomers.

On the basis of the HSQC NMR analysis results, the changes in the $^1\text{H-NMR}$ spectrum (Fig. 2-7) could be interpreted as follows. The saturated side-chain $\underline{\text{H}}-\text{C}_\alpha-\text{OR}$ and $\underline{\text{H}}-\text{C}_\beta-\text{OR}$ signals (4–5 ppm) almost disappeared even after treatment for only 3 min. Some of the β -ether and β -aryl structures were converted to vinyl ethers and stilbenes, respectively. These double bond signals overlapped with the aromatic proton signals, which resulted in slight overestimation of the peak areas of the aromatic protons. The vinyl ethers were cleaved after treatment for 10 min, which increased the signal intensity for phenolic acetyl methyl protons. The increase in the peak area of the signal at 2.5–3.5 ppm with treatment times of up to 10 min resulted primarily from ring-opening and ring-isomerization of the side chains of phenylcoumaran (B) and pinoresinol (C) structures.

2.3.5 Cell wall effect

Wood is made up of cells with thick cell walls, and each cell is connected by a middle lamella. The cell wall is a nanocomposite of crystalline cellulose microfibrils surrounded by a

matrix of hemicellulose and lignin (Terashima et al., 2009). Such nanostructures are expected to affect the thermal degradation of wood component polymers.

The recoveries of hydrolyzable sugars from solid residues treated at 350 °C for up to 15 min were compared with the yields of lignin-derived oligomers (Fig. 2-15). Japanese cedar contains the hemicelluloses glucomannan and xylan. The percentages of the undecomposed fraction were estimated from the recoveries of mannose and xylose. The yields of hydrolyzable mannose, xylose, and glucose were 10.0, 6.0, and 48.5 wt% (wood basis). Assuming a glucomannan mannose/glucose ratio of 3:1 (Timell and Syracuse, 1967; Tyminski and Timell, 1960), 3.3 wt% glucose comes from glucomannan and the remaining 45.2 wt% comes from cellulose.

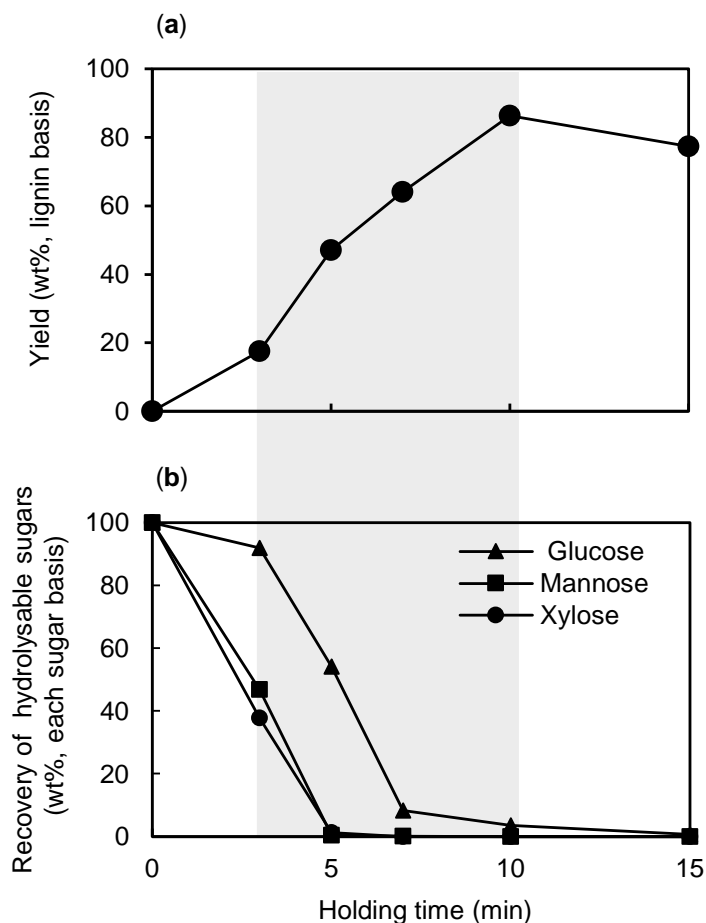


Fig. 2-15 Correlation between (a) yield of lignin-derived oligomer and (b) yields of hydrolysable sugars in solid residues (350 °C at various treatment times).

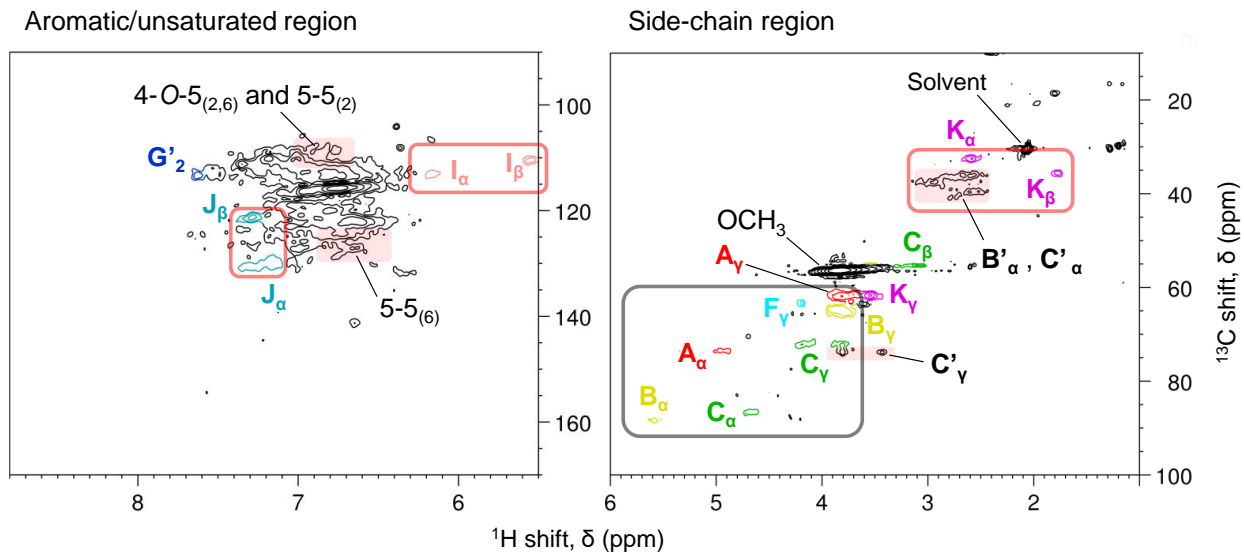


Fig. 2-16 HSQC NMR spectrum of purified EtOAc-soluble portion obtained at 350 °C/ 5 min in the absence of H donor.

After treatment for 3 min, approximately half of the glucomannan and xylan were degraded and/or removed, but most of the cellulose remained in the solid residue. The yield of lignin-derived oligomer was only 20 wt% at this point, and increased as the cellulose decomposed during the 3-10 min treatment period. These results indicate that the formation of lignin-derived oligomers is closely associated with the degradation of cellulose. Similar to the molecular weight distribution described in the GPC results (Fig. 2-7), removal of the H donor did not change the HSQC NMR spectrum of the lignin-derived oligomer obtained after treatment at 350 °C for 5 min (Fig. 2-16). Therefore, wood polysaccharides are expected to function as H donors that stabilize lignin-derived radicals. Conversely, this process may accelerate the thermal degradation of cellulose and hemicellulose.

Cellulose is stable at 270 °C, and the yield of lignin-derived products was limited to approximately 20 wt% even if the treatment time was extended (Fig. 2-6). These results show that approximately 20% of lignin in wood is degraded to oligomers even if cellulose degradation does not proceed. One possible explanation is that the production of these lignin-derived products comes from middle lamella lignin (Fig. 2-17), but further research is needed to confirm this. SEM-EDX has shown that 15–35% of lignin is present in the middle lamella of secondary

walls (Higuchi, 2012). However, cellulose degradation is required for degradation of the remaining bulk lignin and subsequent removal from the cell wall structure (Fig. 2-17).

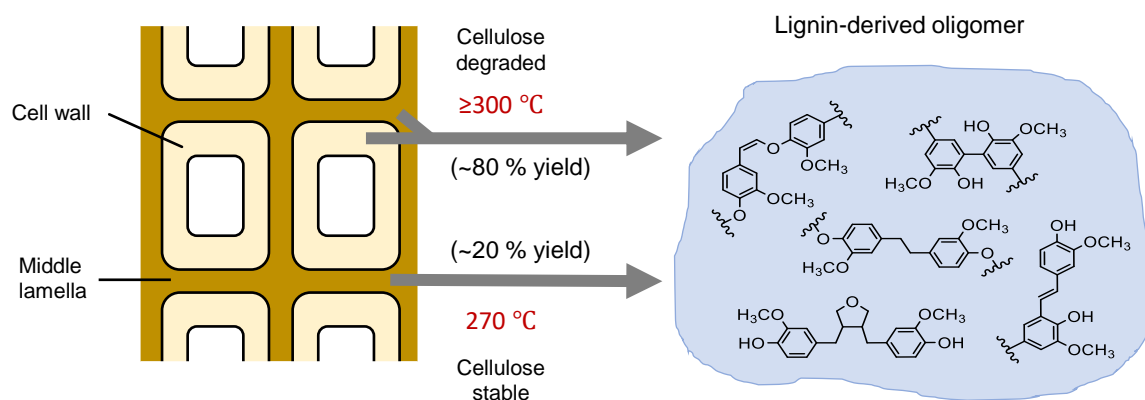


Fig. 2-17 Temperature effect on the production of oligomers from lignin in cell wall during pyrolysis of Japanese cedar wood in aromatic solvent and H donor.

2.4 Conclusions

Pyrolysis of Japanese cedar wood was studied in an aromatic solvent with a H donor at 270–380 °C. Re-condensation was efficiently suppressed to form thermally stable oligomers with yields up to approximately 80 wt% (lignin basis) at temperatures above 300 °C. Extraction with EtOAc/water effectively separated the lignin-derived oligomers from wood polysaccharide-derived products. The yield of lignin-derived oligomer was limited to approximately 20 wt% (lignin basis) at 270 °C, which indicated that approximately 20% of lignin in the Japanese cedar wood was reactive. Decomposition of cellulose was required to obtain lignin-derived oligomers from bulk lignin in wood (cell wall effect). Because wood polysaccharides act as H donors, the use of aromatic solvents is more important than the use of H donors in the production of lignin-derived oligomers. The α - and β -ether bonds were cleaved to form saturated alkyl side chains such as γ -hydroxypropyl, but condensed type β - β , β -aryl and 5-5' bonds remained. The β -aryl type existed as a stilbene in the oligomer. Some β -ether bonds were cleaved via vinyl ether. The obtained lignin-derived oligomer was rich in phenolic and alcohol OH groups. This is advantageous for utilizing lignin-derived oligomers as polyols for biopolymer production.

Chapter 3

Pyrolysis-assisted catalytic hydrogenolysis of softwood lignin at elevated temperatures for the high yield production of monomers

3.1 Introduction

Lignin is the most abundant renewable source of aromatic compounds on the planet and accounts for 20–35 wt% of lignocellulosic biomass materials such as wood and herbaceous plants. Consequently, the conversion of lignin to aromatic monomers could represent a renewable source of commodity chemicals such as phenol and other aromatics and an alternative to the use of petroleum (Wong et al., 2020). The selective depolymerization of lignin is a very important aspect of this strategy and catalytic hydrogenolysis has received a great deal of attention in this regard. It has been reported that catalytic hydrogenolysis conducted under extreme conditions (such as 250–260 °C and 220–240 bar) can convert lignin into saturated cycloalkanes such as cyclohexane that can be used as gasoline substitutes (Cooke et al., 1941; Godard et al., 1941; Harris et al., 1938; Sun et al., 2018). Recently, other work has shown that milder conditions (150–200 °C) can be used during catalytic hydrogenolysis to avoid hydrogenation of the aromatic rings (Sun et al., 2018; Tang et al., 2021) and has demonstrated the selective production of dihydroconiferyl alcohol and dihydrosinapyl alcohol from lignin and wood (Gillet et al., 2017; Schutyser et al., 2018; Sun et al., 2018; Torr et al., 2011). The monomer yields obtainable from hardwood lignins are generally high (on the order of 50 wt%) whereas those from softwood lignins are often less than 30 wt% (Galkin and Samec, 2014; Luo et al., 2022; Van Den Bosch et al., 2015). Accordingly, increasing the monomer yields from softwood lignin remains a challenge.

The varying chemical structures of different types of lignin are one reason for the low monomer yields from softwood lignin. Lignin macromolecules are constructed via the polymerization of cinnamyl alcohols serving as biosynthetic monomers based on one-electron oxidation. The composition of lignin and the types of linkages (that is, ether (C–O–C) or

condensed (C–C) bonds) are determined by the benzene ring substitution pattern of the cinnamyl alcohols, which comprise guaiacyl (4-hydroxy-3-methoxyphenyl, G-type), syringyl (3,5-dimethoxy-4-hydroxyphenyl, S-type) and *p*-hydroxyphenyl (H-type). Softwood lignin contains almost exclusively G-type alcohols while hardwood lignin contains G- and S-types (Obst and Landucci, 1986). The G-type units each contain a site that allows for condensation at the C5 position whereas this position in an S-type unit is occupied by a methoxyl group. Therefore, as summarized in Table 1-2, softwood lignin has a higher proportion of β -5 and 5-5 condensed bonds but a lower proportion of β -O-4-type bonds. As a consequence of the higher dissociation energies of condensed bonds, these linkages are resistant to cleavage (Li et al., 2015; Schutyser et al., 2018; Sun et al., 2018; Zakzeski et al., 2010) during pyrolysis, treatment with acids or bases and exposure to reductive/oxidative environments. This is problematic because the cleavage of these highly stable bonds is required for the efficient conversion of softwood lignin into aromatic monomers.

The present work used a combination of catalytic hydrogenolysis and pyrolysis to induce the conversion of lignin within the temperature range of 250–350 °C, over which range this material is readily degraded even without the use of phenylpropane units in softwood lignin (other than the 4-O-5-type bonds) can be efficiently cleaved to produce coniferyl alcohol (Klein and Virk, 1983; Nakamura et al., 2008). However, the major products from standard pyrolysis are high molar mass compounds rather than coniferyl alcohol owing to the extremely high condensation reactivity of such alcohol (Kotake et al., 2013). During pyrolysis, coniferyl alcohol transitions to a quinone methide serving as a key intermediate for re-condensation. The formation of this intermediate can be inhibited by the hydrogenation of C=C double bond on coniferyl alcohol to produce a saturated alkyl. This effect was thought to be obtainable using catalytic hydrogenolysis conditions. This possibility has been confirmed by observations of lignin pyrolysis in the presence of a hydrogen donor in diphenoxybenzene (an aprotic solvent) to give a thermally stable oligomer with a yield of approximately 80 wt% (Wang et al., 2022) together with various monomers at a yield of 16 wt% (Kotake et al., 2014). The monomer yield remained relatively low because the 4-O-5 and condensed bonds in the lignin were not cleaved. Therefore, if these bonds can be cleaved by high temperature catalytic hydrogenolysis, the monomer yield should be significantly improved.

It is known that substituents on aromatic rings in lignin can be removed by replacement with hydrogen radicals during pyrolysis (Kawamoto, 2017). Although these substitution reactions do not proceed rapidly, catalytic conditions could potentially improve the reactivity. There are several approaches to promoting cleavage of the condensed bonds in lignin, including the use of C α -aryl-type dimers with CoS $_2$ at 250 °C (Shuai et al., 2018), β -1-type dimers in supercritical water at 400 °C (Yamaguchi et al., 2017) and 5-5 type-dimers with a catalyst at 600 °C in conjunction with microwave irradiation (Wang et al., 2020). However, trials using real lignin specimens have continued to provide low yields of aromatic monomers even using these optimized conditions.

The work reported herein examined the catalytic hydrogenolysis of milled wood lignin (MWL) and organosolv lignin, both of which were isolated from Japanese cedar (*Cryptomeria japonica*, a softwood), using Pd/C in anisole (an aprotic solvent) over the temperature range of 200–350 °C. Various model dimers, including those containing 4-*O*-5, C α -aryl and 5-5 bonds, were also used to elucidate the conversion mechanisms.

3.2 Experimental

3.2.1 Materials

The sapwood of Japanese cedar (*Cryptomeria japonica*) was ground into a fine flour and sieved to obtain particles less than 150 μ m in size, after which the material underwent Soxhlet extraction with acetone. The MWL was subsequently prepared from the extracted wood flour according to a procedure previously reported by Björkman (Björkman A, 1956). The MWL was determined to contain the hydrolysable sugars glucose (at 0.6 wt%), xylose (0.7 wt%), mannose (0.3 wt%) and arabinose (0.2 wt%). Organosolv lignin was prepared using an acid-assisted ethanol organosolv process (Pan et al., 2006). Briefly, a 500 mg quantity of the extracted wood flour was dispersed in 5 mL of an aqueous ethanol solution (65%, v/v) containing H $_2$ SO $_4$ (1%, w/w) and then heated at 195 °C for 40 min. Only 0.07 wt% carbohydrates and 1.14 wt% acid-soluble lignin remained in the resulting organosolv lignin. The compounds 4-phenoxyphenol (**1**), 2,2'-methylenediphenol (**2**) and 2,2'-dihydroxy-3,3'-dimethoxy-5,5'-dimethylbiphenyl (**3**) were selected as model dimers having 4-*O*-5, α -aryl and 5-5 linkages, respectively. Compounds **1**

(>99%, Tokyo Chemical Industry Co., Ltd., Tokyo, Japan) and **2** (98%, Sigma-Aldrich Co. LLC, St. Louis, MO, USA) were purchased while **3** was synthesized from methyl guaiacol (guaranteed reagent grade, Nacalai Tesque, Inc., Kyoto, Japan) according to a literature procedure (Kratzl and Vierhapper, 1971). The purity of this compound was confirmed by $^1\text{H-NMR}$ to be 99%.

3.2.2 Pyrolysis-assisted catalytic hydrogenolysis

Samples of the model dimers, Japanese cedar MWL and organosolv lignin were subjected to pyrolysis-assisted catalytic reactions in a batch reactor (Fig. 3-1) (Ehara and Saka, 2002). In each case, a sample mass of approximately 10 mg was placed in a sealed 5 mL reaction vessel together with a specific amount of 5% Pd/C (extra pure reagent, Nacalai Tesque, Inc.) and 2 mL of anisole (>99%, guaranteed reagent, Nacalai Tesque, Inc.). The free space in the vessel (approximately 3 mL) was filled with H_2 at 0.1 or 1.0 MPa using a compressor. After being filled, the reactor was immersed in a salt bath preheated to a temperature in the range of 200–350 °C and agitated by imparting a swinging motion. After a set time, the reactor was transferred to a water bath to quench the reaction. The time spans required to heat the reactor to the target temperature and to cool it to the quenching temperature were approximately 30 sec each and so were negligibly short compared with the reaction time. It should be noted that the 3 mL of H_2 at 0.1 and 1.0 MPa added to the reactor equated to approximately 0.13 and 1.3 mmol and so was equivalent to 2.4 and 24 times the number of guaiacyl propanoid (C9) units in 10 mg of the lignin sample (approximately 0.056 mmol), respectively. During the reaction, the pressure in the reactor would have increased to the vapor pressure of anisole. Calculations based on the Soave-Redlich-Kwong model using the Pro/II simulator 2021 software package (AVEVA Group plc, London, UK) indicated that the pressure was between 0.3 and 3.3 MPa when the reaction temperature was between 200 and 350 °C, such that the majority of the 2 mL of anisole was in the liquid phase.

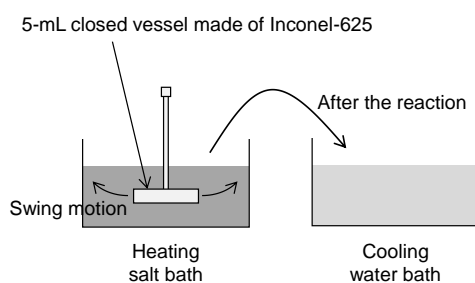


Fig. 3-1 A diagram of the closed batch-type reaction system.

After the reaction, the reactor was washed several times using a total of 18 mL of methanol to recover the reaction mixture, giving a turbid dispersion with a volume of approximately 20 mL containing a solid residue, the Pd/C and anisole. A portion of this suspension was centrifuged to remove solids after which the reaction products were analyzed.

3.2.3 Product analysis

GPC was used to analyze the methanol-soluble portion of the product mixture as a means of determining the MW distribution of the products. This analysis was performed using an LC-10A system (Shimadzu Corporation, Kyoto, Japan) with a Shodex KF-801 column (exclusion limit 1500 Da as the polystyrene equivalent; Showa Denko K.K., Tokyo, Japan), tetrahydrofuran as the eluent at 0.6 mL/min, a column oven temperature of 40 °C and an ultraviolet detector operating at 280 nm.

GC/MS was also used to assess the methanol-soluble portion of the reaction mixture following trimethylsilyl derivatization. This analysis employed a GCMS-QP2010 Ultra instrument (Shimadzu Corporation) with a CPSil 8CB column (length: 30 m, inner diameter: 0.25 mm, film thickness: 0.25 µm; Agilent Technologies, Inc., Santa Clara, CA, USA), He as the carrier gas at 2.09 mL/min, an injector temperature of 250 °C and a split ratio of 1/10. The column oven temperature was initially 70 °C (2 min hold) then ramped at 4 °C/min to 150 °C (1 min hold) and subsequently ramped at 10 °C/min to 300 °C (1 min hold). Prior to each analysis, the methanol was removed from the methanol-soluble portion by heating at 30 °C under vacuum. This relatively low temperature was used because some products, such as guaiacol, were partly lost by heating at 40 °C or above. An aliquot of 1,3,5-triphenylbenzene was added to the resulting specimen as an internal standard, followed by the addition of pyridine (100 µL), hexamethyldisilazane (150 µL) and trimethylchlorosilane (80 µL) with subsequent heating at 60 °C for 30 min for trimethylsilylation. The products were quantified using calibration curves prepared from the analysis of standards. The molar yield, M_i , of each monomeric product, i , was calculated as

$$M_i \text{ (mol\%)} = \frac{\text{Mass of } i}{\text{MW of } i \times n_{C9}} \times 100$$

where n_{C9} is the moles of phenylpropanoid (C9) units in the lignin sample, calculated as

$$n_{C9} \text{ (mol)} = \frac{\text{Sample mass (approximately 0.01 g)}}{\text{Average MW of phenylpropanoid units}}$$

The average MW values of the phenylpropanoid units in the MWL and in the ethanol organosolv lignin obtained from softwood have been reported to be 182 and 168 Da (Lange and Schweers, 1980; Lin and Dence, 1992), respectively, and these values were used in the present study.

NMR analyses were conducted using an AC-400 spectrometer (400 MHz, Varian Medical Systems, Palo Alto, CA, USA). The chemical shifts and coupling constants (J) are presented herein as δ (ppm) and in units of Hz, respectively. Prior to each analysis, the methanol was removed from the methanol-soluble portion by heating under vacuum at 30 °C and the resulting dry oil was dissolved in dimethyl sulfoxide- d_6 for the analysis of MWL or in acetone- d_6 for the analysis of organosolv lignin.

3.2.4 Gas phase catalytic reaction of guaiacol

Approximately 1 μ L of guaiacol (>99%, Wako Pure Chemical Industries, Ltd., Osaka, Japan) was injected into a tandem micro-reactor system (Rx-3050TR, Frontier Laboratories Ltd., Fukushima, Japan) as shown in Fig. 3-2. This aliquot was volatilized in the first reactor after which the resulting vapor was transferred to the second reactor via a flow of H₂ carrier gas. A column packed with Pd/C (inner diameter: 3 mm, height of Pd/C layer: 20 mm) was situated in this second reactor to promote the catalytic conversion of the guaiacol. The first and second reactors were both held at the same temperature of between 260 and 360 °C. The resulting products were introduced into a GC/MS system (GCMS-QP2010 SE, Shimadzu Corporation) and analyzed in real-time. This system included an Ultra ALLOY⁺-1 column (length: 30 m, inner diameter: 0.25 mm, film thickness: 2 μ m; Frontier Laboratories Ltd.) connected to a vent-free adaptor N-50 (length: 50 cm, inner diameter: 0.15 mm), H₂ as the carrier gas at 1.20 mL/min, an injector temperature of 250 °C and a split ratio of 1/24.9. The column oven temperature was initially 50 °C (5 min hold) followed by a ramp at 10 °C/min to 270 °C (3 min hold).

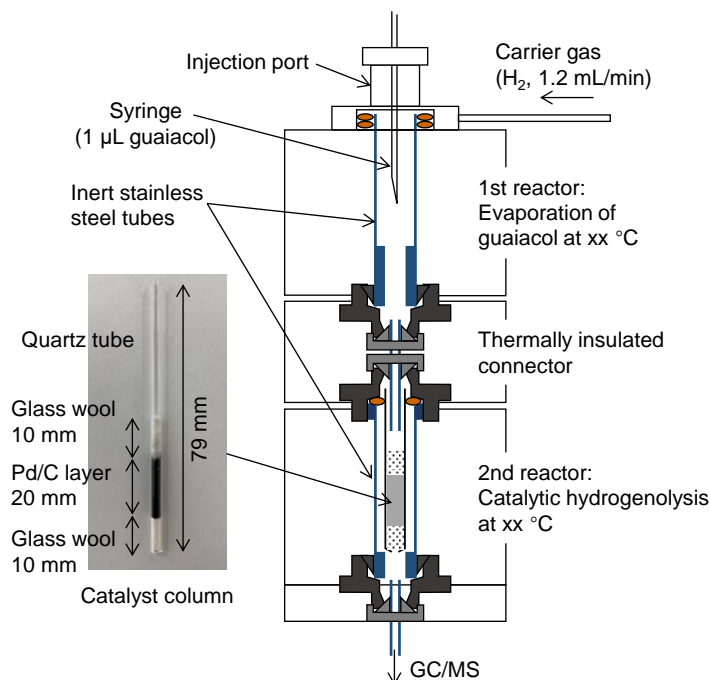


Fig. 3-2 A photograph and diagram of the tandem micro-reactor GC/MS system.

3.3 Results and discussion

3.3.1 Monomer formation from Japanese cedar MWL

Fig. 3-3 presents the gel permeation chromatography (GPC) data acquired from the analysis of Japanese cedar MWL treated with Pd/C and H₂ in anisole at various temperatures and for different durations. During these trials, relatively low amounts of H₂ (3 mL at 0.1 MPa, corresponding to 2.4 equivalents relative to the moles of aromatic rings in each specimen) were used to avoid saturation of the aromatic moieties. These chromatograms indicate the retention times of the monomer and dimer/trimer fractions based on prior analyses of model compounds. Note that, during the trial performed at 350 °C, a small amount of the anisole was converted to phenol.

In the case of the sample reacted at 200 °C, a peak assigned to dihydroconiferyl alcohol (DHCA) can be observed together with various high molecular weight (MW) products that eluted over the time span of 9–12 min. Increasing the processing temperature evidently reduced the product MWs, with this effect especially apparent at 300 and 350 °C, indicating that

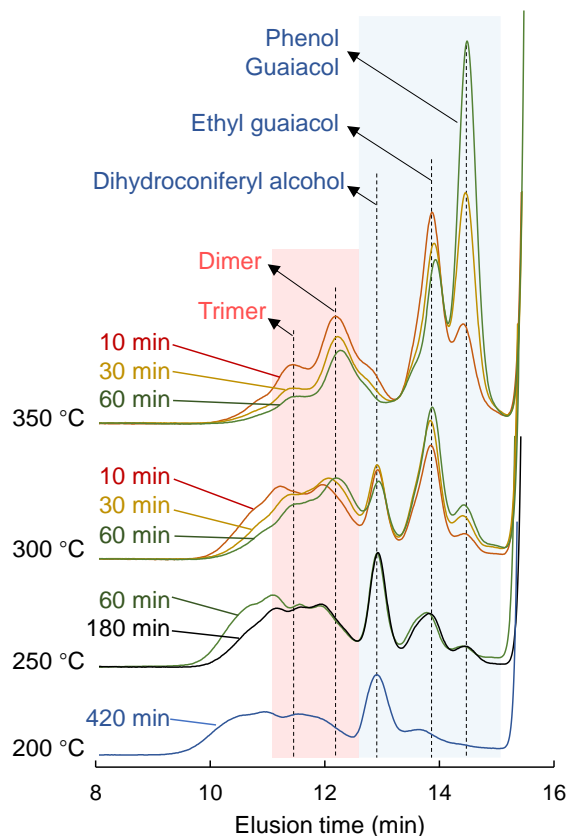


Fig. 3-3 Gel permeation chromatograms of the reaction mixtures obtained from the pyrolysis-assisted catalytic hydrogenolysis of Japanese cedar MWL in anisole at 200–350 °C (MWL: 10 mg, Pd/C: 10 mg, anisole: 2 mL, H₂: 3 mL at 0.1 MPa). GPC column exclusion limit: 1500 Da at 9.5 min.

depolymerization proceeded in this temperature range. The intensity of the various peaks in the monomer region of each chromatogram also changed at these higher temperatures, confirming variations in the types or proportions of monomers.

Table 3-1 presents the molecular structures of the monomers discussed herein while the yields of the products (in mol%, based on the quantity of aromatic rings in the lignin) obtained from these conversions are summarized in Fig. 3-4. At 200 °C, the monomer yield increased by extending the duration from 180 min (18.0 mol%) to 360 min (26.0 mol%) and tended to plateau at 420 min (27.4 mol%), where DHCA was obtained in a yield of 18.4 mol% and accounted for 67% of all monomers. The monomer yield increased to 53 mol% upon increasing the temperature to 250 °C, indicating that temperature had a very important effect on monomer production. It should also be noted that the monomer yield and composition did not change with

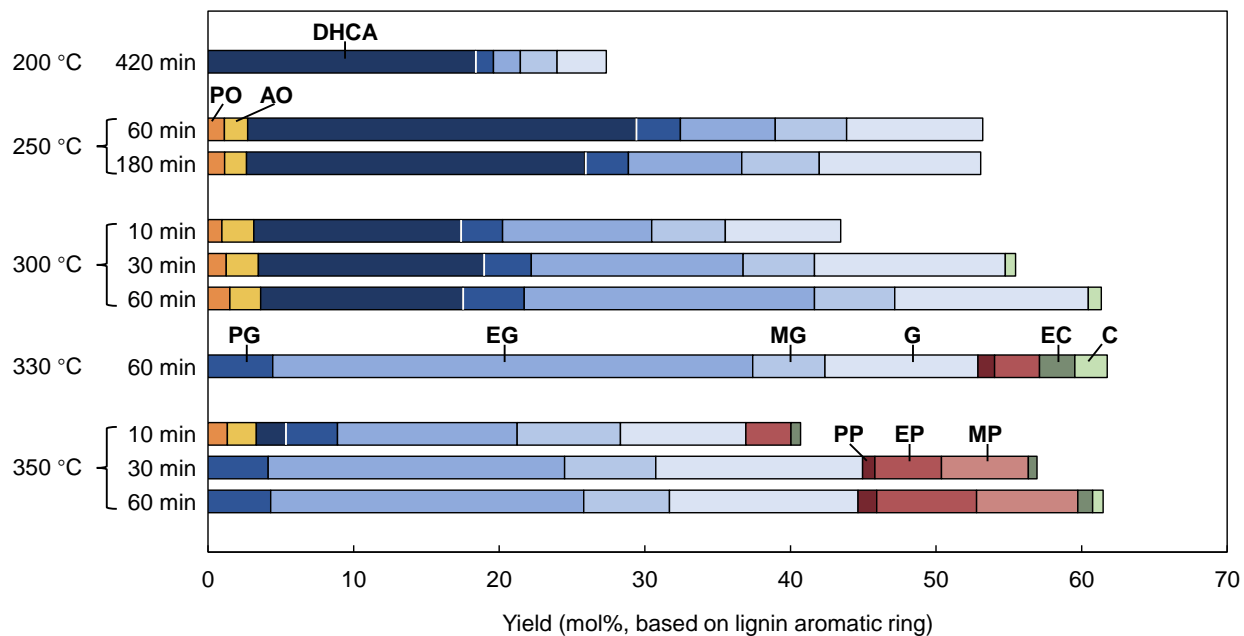
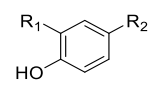


Fig. 3-4 The yields of monomers obtained from the pyrolysis-assisted catalytic hydrogenolysis of Japanese cedar MWL at varying temperatures and for different durations (MWL: 10 mg, Pd/C: 10 mg, anisole: 2 mL, H₂: 3 mL at 0.1 MPa). PO: propiovanillone, AO: acetovanillone, DHCA: dihydroconiferyl alcohol, PG: propyl guaiacol, EG: ethyl guaiacol, MG: methyl guaiacol, G: guaiacol, PP: propyl phenol, EP: ethyl phenol, MP: methyl phenol, EC: ethyl catechol, C: catechol.

variations in the treatment duration at 250 °C (based on trials running for 60 and 180 min), suggesting that these monomers were stable and did not decompose on prolonged heating. The proportions of guaiacol and alkyl guaiacols (methyl, ethyl and propyl) in the monomers were also found to increase at 250 °C. These results also indicate that 60 min is sufficient to generate monomers from MWL at temperatures above 250 °C.

The overall monomer yield was further increased at 300 °C, reaching 61 mol% after 60 min. Ethyl guaiacol and guaiacol were the primary monomeric products from this trial while the DHCA yield was slightly decreased. At 330 °C, no DHCA was obtained but a significant amount (33 mol%) of ethyl guaiacol was produced. From these data, it is evident that the DHCA was converted to ethyl guaiacol. The maximum monomer yield was on the order of 60 mol% over the temperature range of 300–350 °C. Lignin itself is known to rapidly degrade via pyrolysis within 10 min at 350 °C and 60 min at 300 °C in aromatic solvents without the addition of catalysts (Wang et al., 2022). Therefore, pyrolysis would have played a role in the decomposition of lignin in the present work at these high temperatures.

Table 3-1 Molecular structures and abbreviations for the various monomeric products.

	Legends		
		R ₁	R ₂
Vanillic acid	VA	OCH ₃	COOH
Isoeugenol (<i>cis</i>)	IE (<i>cis</i>)	OCH ₃	CHCHCH ₃
Isoeugenol (<i>trans</i>)	IE (<i>trans</i>)	OCH ₃	CHCHCH ₃
Eugenol	E	OCH ₃	CH ₂ CHCH ₂
Vinyl guaiacol	VG	OCH ₃	CHCH ₂
Coniferyl aldehyde	CALD	OCH ₃	CHCHCHO
Vanillin	VO	OCH ₃	CHO
Propiovanillone	PO	OCH ₃	COCH ₂ CH ₃
Acetovanillone	AO	OCH ₃	COCH ₃
Dihydroconiferyl alcohol	DHCA	OCH ₃	CH ₂ CH ₂ CH ₂ OH
Propyl guaiacol	PG	OCH ₃	CH ₂ CH ₂ CH ₃
Ethyl guaiacol	EG	OCH ₃	CH ₂ CH ₃
Methyl guaiacol	MG	OCH ₃	CH ₃
Guaiacol	G	OCH ₃	H
Propyl phenol	PP	H	CH ₂ CH ₂ CH ₃
Ethyl phenol	EP	H	CH ₂ CH ₃
Methyl phenol	MP	H	CH ₃
Ethyl catechol	EC	OH	CH ₂ CH ₃
Catechol	C	OH	H

At 350 °C, alkylphenols (representing the demethoxylation products) were generated at a proportion of approximately 15 mol%. Phenol may also have been produced but the yield could not be determined because the anisole used as a solvent also generated a small amount of phenol throughout the reaction. The demethylation products catechol and ethyl catechol were also detected, although the yields of both were minimal. The demethylation and demethoxylation of the guaiacol moiety evidently began to occur over the temperature range of 300–330 °C.

To better understand the effects of pyrolysis, the catalyst (Pd/C) and the H₂, Japanese cedar MWL specimens were heated at 350 °C for 10 min in anisole under either N₂ or H₂ and with or without the Pd/C catalyst. The resulting monomer yields and GPC profiles are presented in Fig. 3-5 and Fig. 3-6, respectively. The trial with N₂ but without Pd/C in anisole produced coniferyl aldehyde, DHCA, isoeugenol (both *cis* and *trans*), eugenol, vinyl guaiacol, acetovanillone,

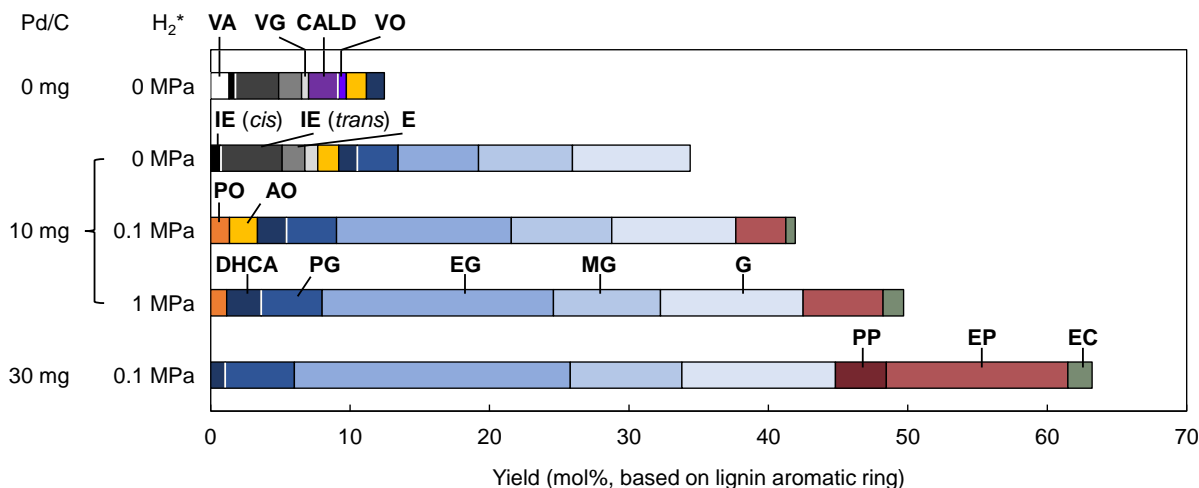


Fig. 3-5 The yields of monomers obtained from the pyrolysis-assisted catalytic hydrogenolysis of Japanese cedar MWL at 350 °C for 10 min with varying amounts of Pd/C and H₂ (MWL: 10 mg, anisole: 2 mL, H₂: 3 mL at 0.1 or 1.0 MPa). VA: vanillic acid, IE (*cis*): isoeugenol (*cis*), IE (*trans*): isoeugenol (*trans*), E: eugenol, VG: vinyl guaiacol, CALD: coniferyl aldehyde, VO: vanillin, PO: propiovanillone, AO: acetovanillone, DHCA: dihydroconiferyl alcohol, PG: propyl guaiacol, EG: ethyl guaiacol, MG: methyl guaiacol, G: guaiacol, PP: propyl phenol, EP: ethyl phenol, EC: ethyl catechol. *H₂ pressure at room temperature prior to the reaction. A value of 0 MPa indicates that N₂ was used instead of H₂.

vanillin and vanillic acid as typical pyrolysis monomers at a total yield of 12.5 mol%. Coniferyl alcohol, which was predicted to form in significant amounts based on cleavage of the β -ether bonds in the lignin, was not detected, likely as a result of secondary degradation (Fig. 3-7). In prior work, coniferyl aldehyde, DHCA, isoeugenol and vinyl guaiacol were obtained from the pyrolysis of coniferyl alcohol (Kotake et al., 2013). The acetovanillone, vanillin and vanillic acid may have been formed via different pyrolysis pathways. As noted, coniferyl alcohol also tends to re-condense via a quinone methide intermediate to form thermally stable condensed products containing C _{α} - and C _{γ} -aryl bonds (Nakamura et al., 2007), although this condensation is suppressed in aromatic solvents such as anisole. The low monomer yield from this trial is attributed to the 4-*O*-5 and condensed bonds in the sample, which resisted cleavage (Wang et al., 2022).

The addition of Pd/C significantly increased the monomer yield (from 12.5 to 34.4 mol%) even under N₂, with the appearance of guaiacol and alkyl guaiacols (methyl, ethyl, and propyl) among the products. The GPC data also show that the peaks related to a high MW fraction in the

products (Fig. 3-6) appearing over the range of 9–12 min were shifted to a lower MW region. This result demonstrates that some bonds in the oligomers produced by pyrolysis were cleaved by the incorporation of the Pd/C, resulting in an improved monomer yield.

Although the monomer yield was increased further upon using H₂ instead of N₂ (from 34.4 to 41.9 mol% at 0.1 MPa and to 49.8 mol% at 1.0 MPa), these relative improvements were much less than those obtained by adding Pd/C. This finding was supported by the GPC data, which exhibited minimal change on going between H₂ and N₂ in the presence of Pd/C. Consequently, the incorporation of Pd/C was more important than the addition of H₂ with regard to promoting

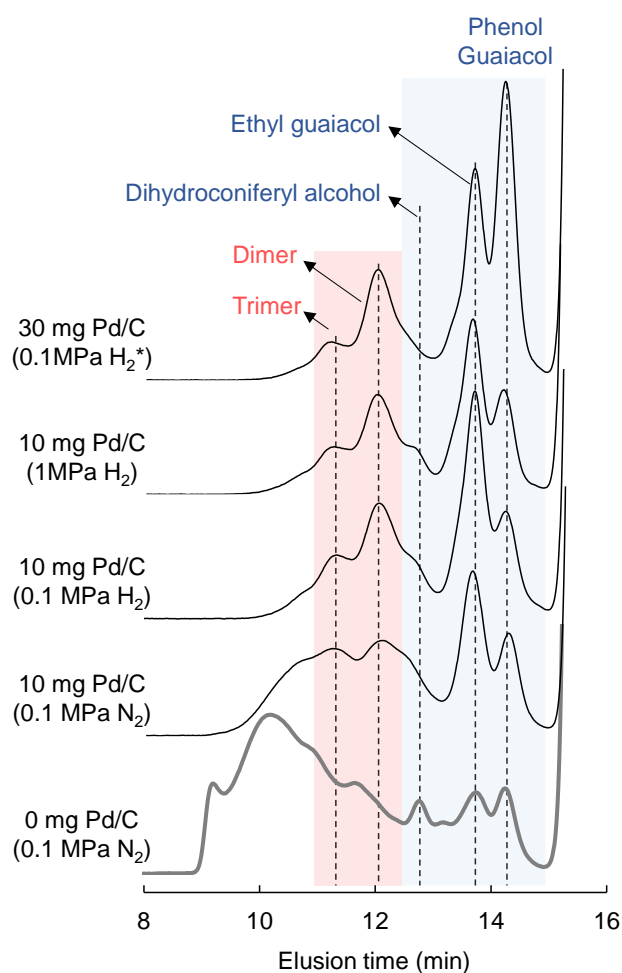


Fig. 3-6 Gel permeation chromatograms of the reaction mixtures obtained from the pyrolysis-assisted catalytic hydrogenolysis of Japanese cedar MWL in anisole at 350 °C for 10 min with varying amounts of Pd/C and H₂ (MWL: 10 mg, anisole: 2 mL, H₂: 3 mL at 0.1 or 1.0 MPa). GPC column exclusion limit: 1500 Da at 9.5 min.*H₂ pressure at room temperature prior to the reaction.

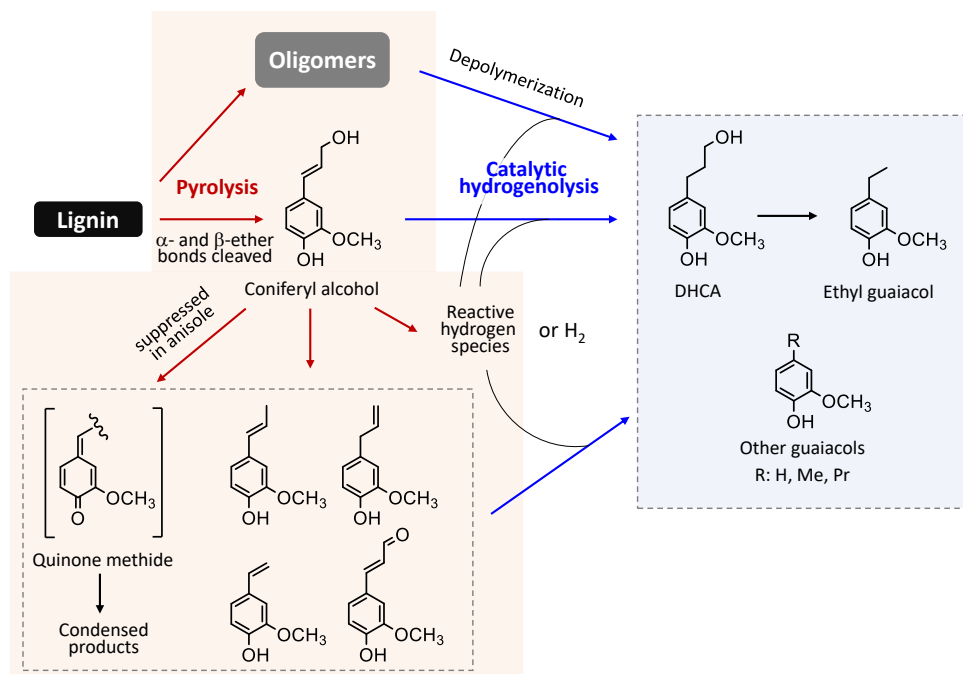


Fig. 3-7 Proposed reaction pathways for monomer production via the catalytic hydrogenolysis of lignin with pyrolysis, Pd/C and H_2 at 250–350 °C.

the depolymerization of lignin-derived oligomers, although using H_2 did slightly increase the degree of conversion. Reactive hydrogen species may have been present in the reaction mixtures but further studies will be required to identify these species. The monomers obtained with N_2 but without Pd/C (as described above) were not produced under H_2 with Pd/C, presumably as a result of the hydrogenation of side-chain double bonds.

Increasing the amounts of H_2 and Pd/C improved the extent of lignin conversion but did not significantly change the composition of the monomeric product mixture. It should also be noted that extensive saturation of the aromatic rings in the lignin did not occur even with the use of H_2 at 1.0 MPa, corresponding to 24 equivalents relative to the moles of aromatic rings in the MWL. As discussed below, efficient ring saturation did not proceed at such high temperatures. Ethyl phenol and ethyl catechol were detected only after reactions under H_2 and in the presence of Pd/C, suggesting that both H_2 and Pd/C were required for demethoxylation and demethylation.

Fig. 3-7 summarizes the proposed roles of pyrolysis, Pd/C and H_2 during high-temperature catalytic hydrogenolysis at 250–350 °C. Although the MWL was not soluble in anisole, this material underwent thermal depolymerization to generate soluble oligomers along with monomers via the cleavage of α - and β -ether bonds as a consequence of the pyrolysis. As a result,

the subsequent conversion of oligomers to monomers proceeded more efficiently on the surface of the solid Pd/C catalyst. Reactive hydrogen species formed during the pyrolysis were also important and the addition of very small amounts of H₂ ensured a sufficient supply of these species. The monomers generated in this system had alkyl side chains (methyl, ethyl and propyl). In particular, ethyl groups were formed via the pathway γ -hydroxypropenyl (representing a coniferyl alcohol) \rightarrow γ -hydroxypropyl (a DHCA) \rightarrow ethyl. A large amount of unsubstituted guaiacol was also produced. One possible pathway for guaiacol formation proceeded via vanillin and related intermediates, and this will be discussed in the chapter 5.

3.3.2 Dimer production from Japanese cedar MWL

The data discussed above suggest that bonds in the lignin-derived oligomers that are normally difficult to cleave were broken after adding Pd/C. An analysis of the chemical structures of the dimers was therefore performed to better understand the associated reactions. Fig. 3-8 shows the dimer regions of the gas chromatography-mass spectrometry (GC/MS) total ion chromatograms of the mixtures obtained from Japanese cedar MWL after reactions using 0.1 MPa H₂ and Pd/C in anisole at 300 and 350 °C, following trimethylsilylation.

Biphenyl (5-5, a-d) and β -aryl (β -1 and β -5, e-i)-type dimers were detected within the retention time ranges of 30–32 and 33–37 min, respectively, indicating that these bonds were relatively stable even under the pyrolysis-assisted catalytic hydrogenolysis conditions. It should also be noted that the chromatograms were quite complex as a consequence of the conversion reactions of side chains on the products. As was observed when assessing the monomers, γ -hydroxypropyl, methyl, ethyl and propyl side chains were attached to the various products, although unsubstituted compounds were also generated. Accordingly, similar side chain transformations evidently occurred in the case of the dimers and possibly the oligomers.

Stilbene, which is a typical pyrolysis product of β -aryl-type structures, can be hydrogenated to produce the diarylethane-type dimers labeled e-i in Fig. 3-8. Dimers g, h, and i tended to be converted to dimers e and f, as can be clearly seen in the chromatogram of the sample processed at 300 °C. Dimers h and i, each of which contained two alkyl side chains, were derived from the β -5 bonds in lignin and converted to dimer f, whereas dimer g (with only one alkyl side chain) was obtained from a β -1 bond and converted to dimer e. For these reasons, the

peaks related to dimers e and f were more intense in the chromatogram of the sample heated at 350 °C for 10 min. However, these signals were decreased in intensity after the treatment time was extended to 30 or 60 min, suggesting that even stable β -aryl bonds could be cleaved at such high temperatures. Similar trends were observed for the 5-5-type dimers.

The heteronuclear single quantum coherence (HSQC) nuclear magnetic resonance (NMR) spectrum obtained from the Japanese cedar MWL indicated the presence of 5-5, β -aryl and β - β -type condensed bonds along with α - and β -ether bonds (Fig. 2-12a). The α - and β -ether bonds (structures A, B, C and D in Fig. 2-14) could be pyrolytically cleaved within the temperature range of 250–350 °C (Wang et al., 2022). However, dimers containing β - β bonds (structure C) and 4-*O*-5 bonds (undetectable in the HSQC spectra) were not present in the dimer regions of the various chromatograms (Fig. 3-8). These bonds might therefore have been cleaved following the addition of Pd/C and H₂.

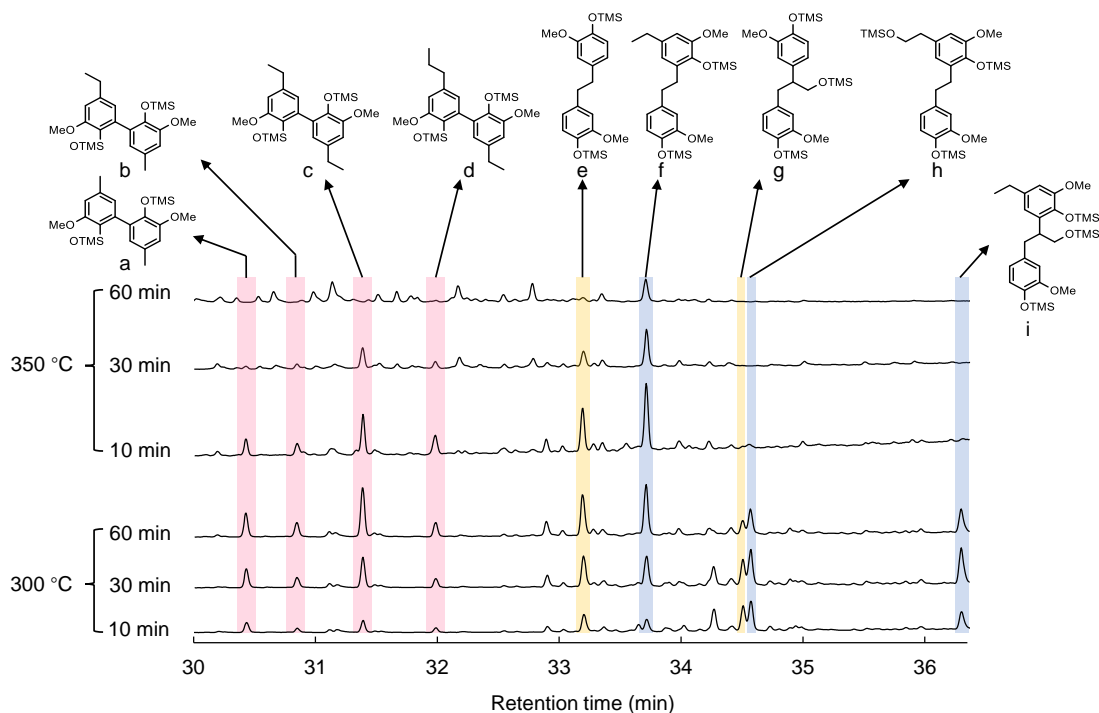


Fig. 3-8 The dimer regions of GC/MS total ion chromatograms acquired from the trimethylsilyl (TMS) derivatives of products obtained from the pyrolysis-assisted catalytic hydrogenolysis of Japanese cedar MWL in anisole at 300 or 350 °C (MWL: 10 mg, Pd/C: 10 mg, anisole: 2 mL, H₂: 3 mL at 0.1 MPa).

3.3.3 Model compound study

Three model dimers having 4-*O*-5 (**1**, 4-phenoxyphenol), α -aryl (**2**, 2,2'-methylenediphenol) and 5-5 (**3**, 2,2'-dihydroxy-3,3'-dimethoxy-5,5'-dimethyl biphenyl)-type bonds were treated at 200, 250, 300 or 350 °C for 60 min in anisole with Pd/C and H₂. The GPC data obtained from the reaction mixtures are shown in Fig. 3-9. Here, the number attached to each peak represents either the dimer recovery or the product yield (in mol%) as determined by GC/MS (Fig. 3-10, Fig. 3-11 and Fig. 3-12). Phenol yields at temperatures above 300 °C were not determined because the anisole used as a solvent produced some phenol under these conditions, as noted earlier.

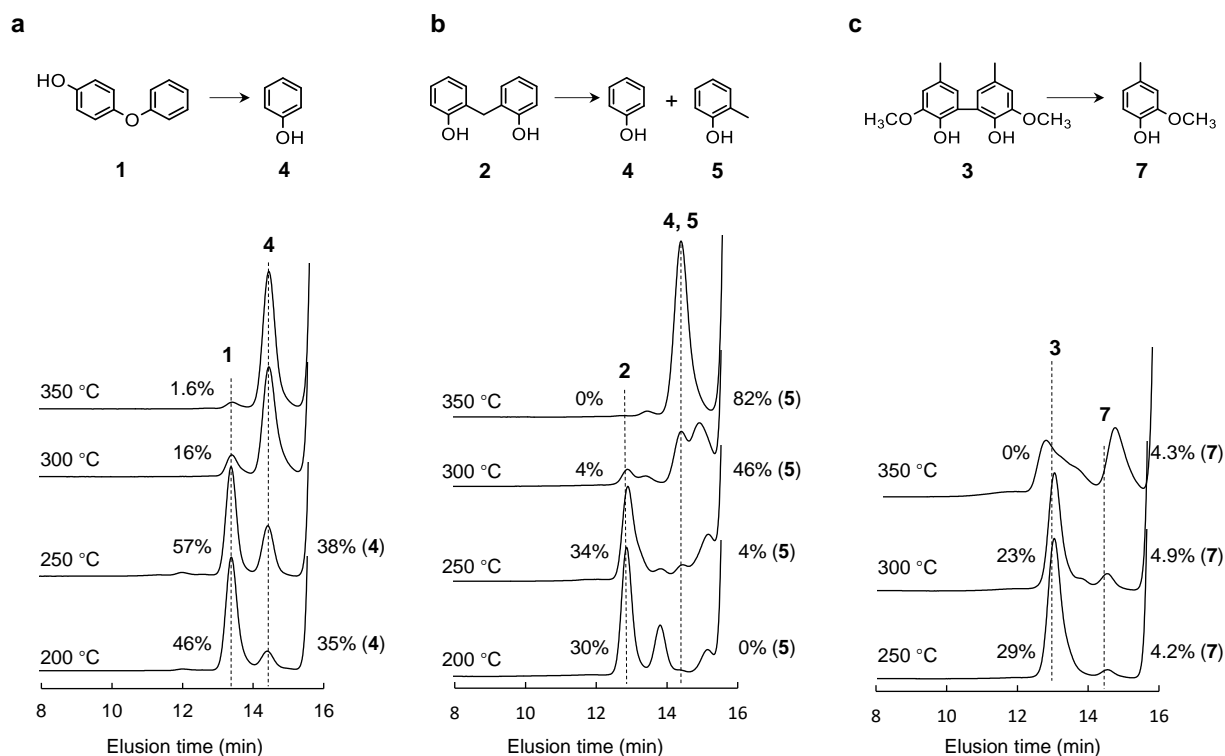


Fig. 3-9 Gel permeation chromatograms of the reaction mixtures obtained from the pyrolysis-assisted catalytic hydrogenolysis of the model dimers **a** (having 4-*O*-5 bonds; **1**), **b** (having α -aryl bonds; **2**) and **c** (having 5-5 bonds; **3**) at 200–350 °C for 60 min in anisole (Model: 10 mg, Pd/C: 10 mg, anisole: 2 mL, H₂: 3 mL at 0.1 MPa). The numerical value attached to each signal indicates the recovery or yield (mol%, based on aromatic rings). GPC column exclusion limit: 1500 Da at 9.5 min.

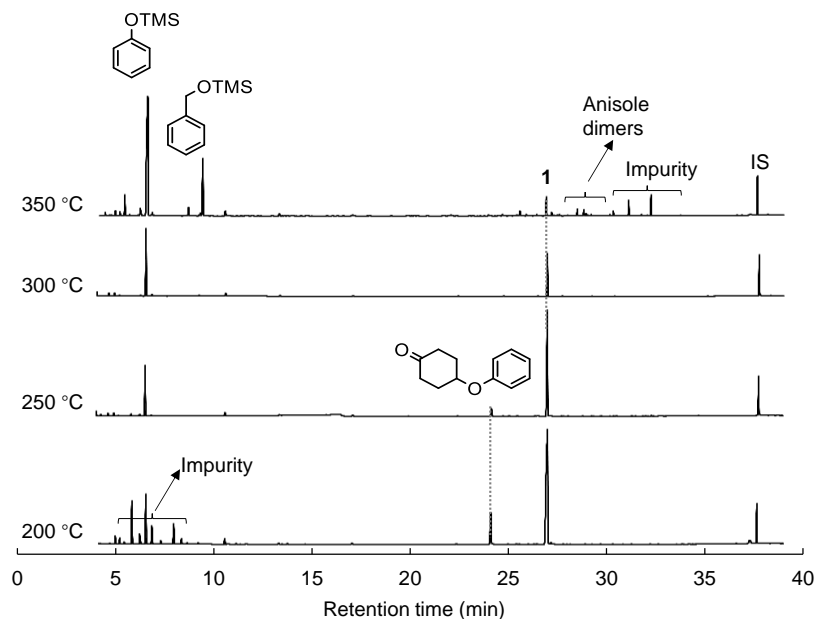


Fig. 3-10 The GC/MS total ion chromatograms of the TMS-derivatives of reaction mixtures obtained from the pyrolysis-assisted catalytic hydrogenolysis of the 4-*O*-5 model compound (**1**) in anisole at 200–350 °C for 60 min.

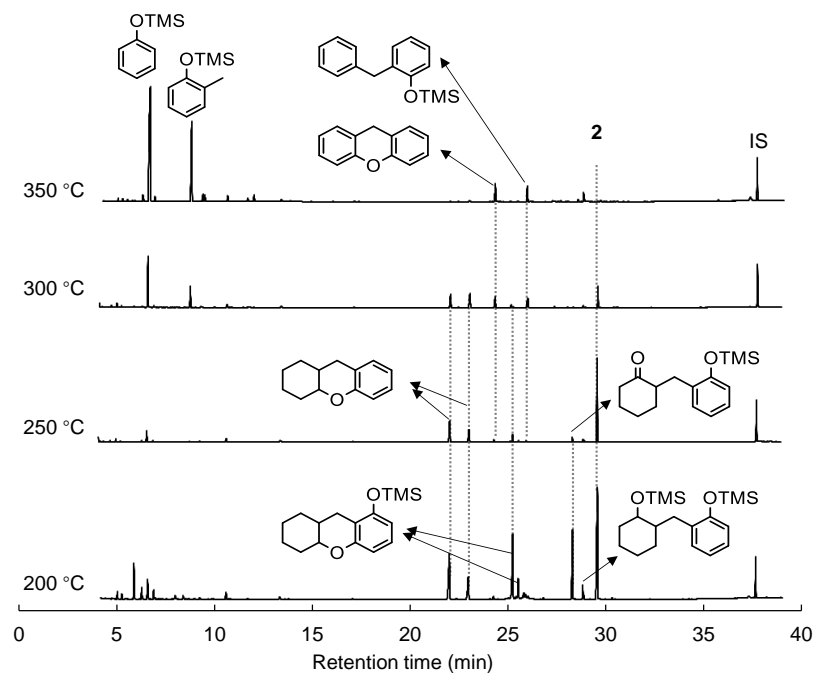


Fig. 3-11 The GC/MS total ion chromatograms of the TMS-derivatives of reaction mixtures obtained from the pyrolysis-assisted catalytic hydrogenolysis of the α -aryl model compound (**2**) in anisole at 200–350 °C for 60 min (Compound **2**: 10 mg, Pd/C: 10 mg, anisole: 2 mL, H₂: 3 mL at 0.1 MPa).

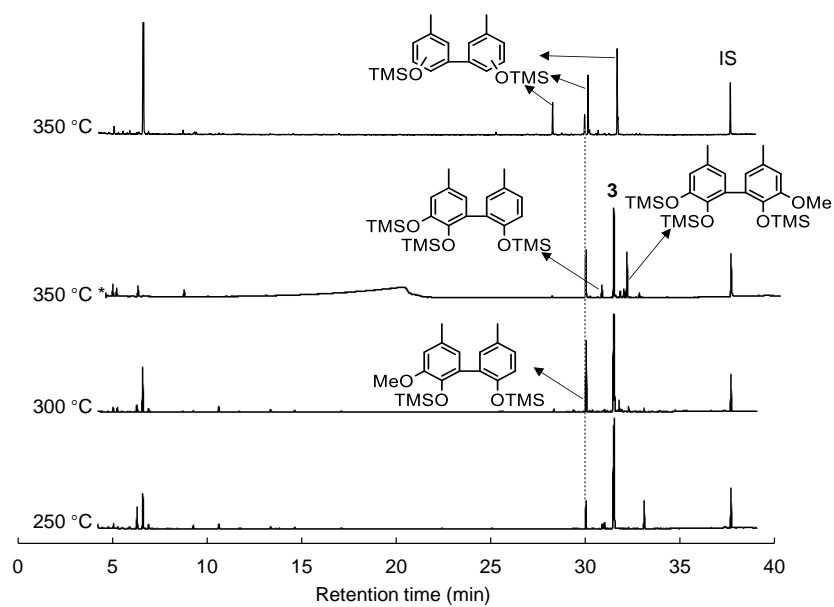


Fig. 3-12 The GC/MS total ion chromatograms of the TMS-derivatives of reaction mixtures obtained from the pyrolysis-assisted catalytic hydrogenolysis of the 5-5 model compound (**3**) in anisole at 250–350 °C for 60 min (Compound **3**: 10 mg, Pd/C: 10 mg, anisole: 2 mL, H₂: 3 mL at 0.1 MPa). *Treatment time: 10 min.

In all experiments, no GPC peaks appeared at retention times shorter than those of the model dimers, suggesting that these dimers did not condense under these conditions. However, the reactivity of each dimer was dependent on its structure. Specifically, the 4-*O*-5 bond of dimer **1** was broken at the lowest temperature of 200 °C and increasing reactivity was observed with increases in temperature. In contrast, the α -aryl bond of dimer **2** was cleaved at 300 and 350 °C to form 2-methylphenol. These data suggest that these two types of bonds were cleaved during pyrolysis-assisted catalytic hydrogenolysis at high temperatures.

Although α -aryl bonds are not present in natural lignins, these bonds can be formed by the re-condensation of quinone methide intermediates during pyrolysis, pulping and other conversion processes. Therefore, the efficient cleavage of α -aryl bonds under the current reaction conditions promoted the production of monomers from the lignin. In particular, this effect could be demonstrated using organosolv lignin, as discussed below. Thus, even if these bonds were formed, they could be cleaved under the current pyrolysis-assisted catalytic hydrogenolysis conditions.

On the contrary, the 5-5 bond in dimer **3** was much less reactive with regard to monomer less than 5% (compared with a theoretical yield of 200%, based on the quantity of aromatic rings in the model) in the temperature range of 250–350 °C. These results are consistent with the composition of the dimer fraction obtained from the MWL (products labeled a-d, Fig. 3-8). As discussed below, demethylation and demethoxylation occurred selectively in the case of the 5-5-type dimer.

Fig. 3-12 provides the GC/MS total ion chromatograms of the reaction mixtures generated in trials using the 5-5 dimer model **3**. Although the bond attaching the methyl substituent of this compound was not cleaved, demethoxylation and demethylation occurred efficiently to form dimers having catechol and phenol moieties, in contrast to the results obtained with dimers **1** and **2**. This specificity is attributed to the unique conformation of the 5-5 dimer, in which two aromatic rings are arranged perpendicular to one another as a consequence of the steric repulsion between the hydrogens and hydroxyl groups at ortho positions (Grein, 2002), as depicted in Fig. 3-13. In this conformation, the parallel association of the two benzene rings of the 5-5 dimer with Pd is difficult, such that one ring must be positioned vertically with respect to the Pd. This scenario could lead to increases in demethoxylation and demethylation reactivity. The association of the benzene ring with the catalyst in a perpendicular configuration during catalytic hydrogenation is known to result in deoxygenation whereas a planer configuration favors hydrogenation of the ring (Zhang et al., 2020). However, both rings of the 4-*O*-5 (He et al., 2014) and α -aryl dimers can be associated in parallel with the Pd atom.

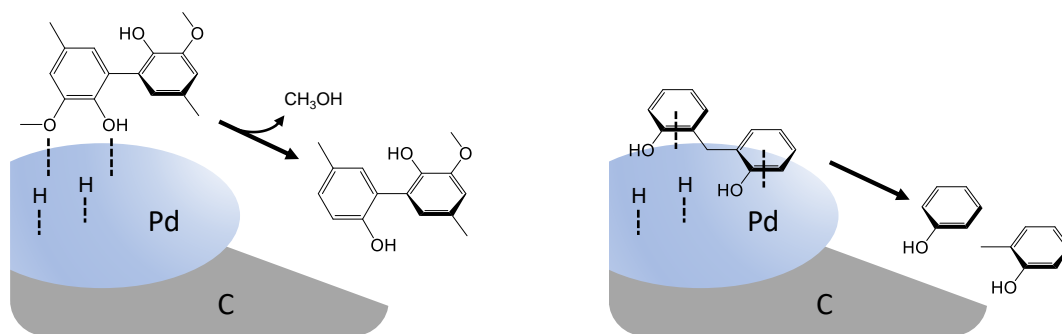


Fig. 3-13 Diagrams showing the proposed interactions of biphenyl (**3**)- and diarylmethane (**1**)-type dimers on a Pd surface determining reaction selectivity.

Saturated ring products were also formed from the 4-*O*-5 and α -aryl dimers while no such products were detected in trials using the 5-5 dimer, most likely because of the unique conformation discussed above. The GC/MS total ion chromatograms obtained from the 4-*O*-5 and α -aryl dimers are shown in Fig. 3-10 and Fig. 3-11, respectively. Interestingly, the signals assigned to the saturated ring products decreased with increases in the reaction temperature and almost disappeared at 300 and 350 °C. The signal observed as a large peak around 14 min only at 200 °C in Fig. 3-9b would originate from the ring-saturation products identified in Fig. 3-11. Ring saturation therefore occurred at a relatively low temperature of 200 °C but was not significant at higher temperatures. This effect illustrates the advantage of high-temperature catalytic hydrogenolysis for the production of aromatic monomers.

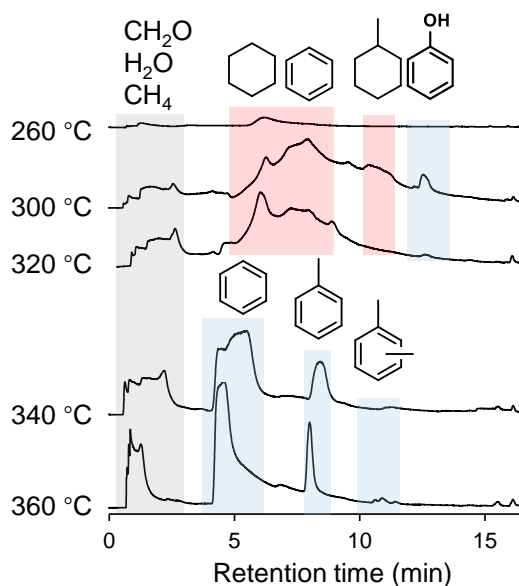


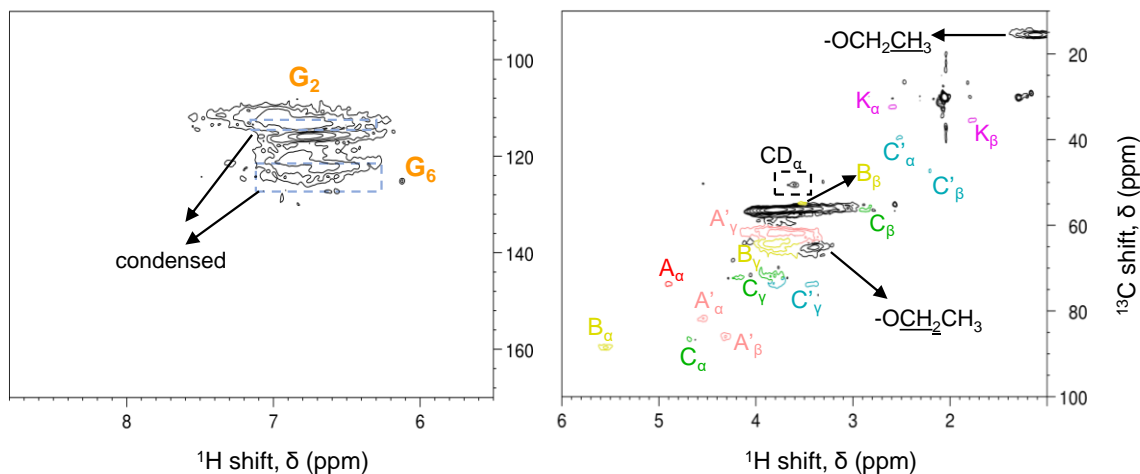
Fig. 3-14 The GC/MS total ion chromatograms obtained from reactions mixtures following the catalytic hydrogenolysis of gas phase guaiacol over Pd/C at different temperatures in a micro-reactor with H₂ as the carrier gas.

The same results were obtained from the gas phase catalytic conversion of guaiacol using Pd/C with a tandem micro-reactor GC/MS system under a H₂ flow at different temperatures. The results are shown in Fig. 3-14. Here, the peaks obtained sooner than 3 min are attributed to formaldehyde, methane and water. At 260 °C, only trace amounts of cyclohexane were detected and most of the guaiacol was adsorbed on the Pd/C. A mixture of cyclohexane and benzene was obtained upon raising the temperature to 300 or 320 °C along with small amounts of

methylcyclohexane and phenol. The product composition changed to benzene, toluene and xylenes at 340 and 360 °C. These results indicate that the extent of ring saturation decreased with increasing temperature. The less efficient adsorption of H₂ at such high temperatures (Carlos A. Leon y Leon and Vannice, 1991) evidently reduced the degree to which ring saturation occurred.

3.3.4 Japanese cedar organosolv lignin

The present pyrolysis-assisted catalytic hydrogenolysis conditions were also applied to organosolv lignin isolated from Japanese cedar wood using 65% ethanol with 1% H₂SO₄ in conjunction with heating at 195 °C for 40 min. Organosolv lignin is an emerging resource in the biorefinery industry. As indicated by the HSQC NMR spectrum of this material (Fig. 3-15), the bond types were very different from those in the MWL (see Fig. 2-12a). Specifically, the majority of α - and β -ether bonds were cleaved during the extraction process and a large number



Unique structures in ethanol organosolv lignin

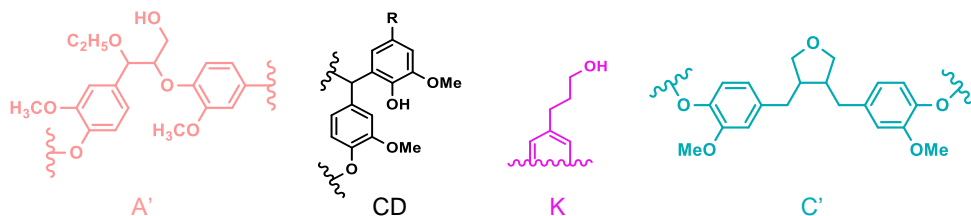


Fig. 3-15 The HSQC NMR spectrum of Japanese cedar organosolv lignin, acquired in acetone-*d*₆ (Structure A, B, C refer to Fig. 2-14).

of α -aryl bonds were formed by re-condensation, in agreement with literature reports (Bouxin et al., 2015; Guo et al., 2015).

The GPC data and monomer yields obtained from processing organosolv lignin are summarized in Fig. 3-16 and Fig. 3-17, respectively. Unlike the results obtained from the MWL trials, the MW distribution of the products was not significantly different from that of the

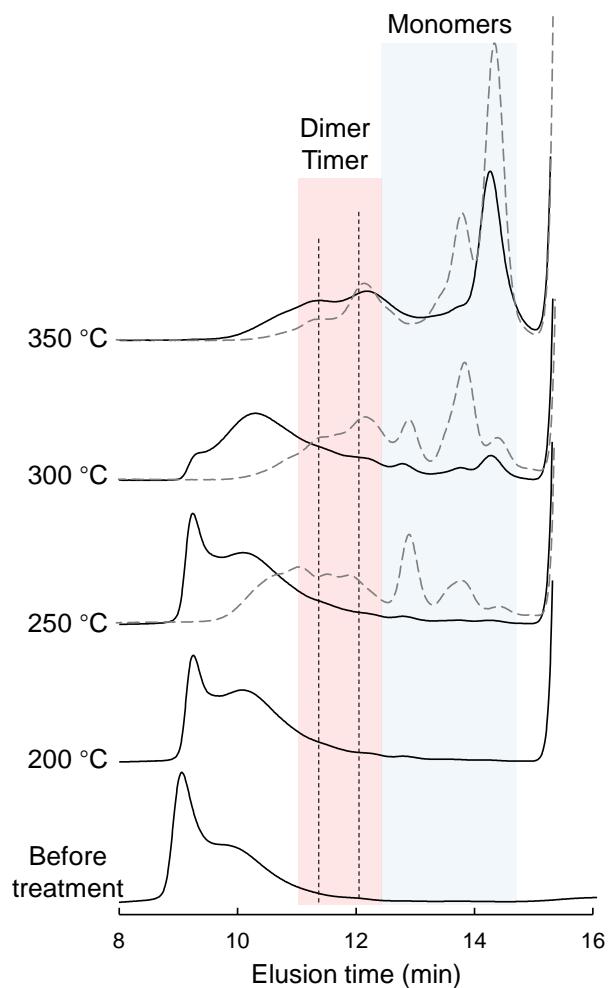


Fig. 3-16 Gel permeation chromatograms of the reaction mixtures obtained from the pyrolysis-assisted catalytic hydrogenolysis of Japanese cedar organosolv lignin in anisole at 200–350 °C for 60 min. Chromatograms obtained from MWL are also included as dashed gray curves for comparison (Organosolv lignin: 10 mg, Pd/C: 10 mg, anisole: 2 mL, H₂: 3 mL at 0.1 MPa). GPC column exclusion limit: 1500 Da at 9.5 min.

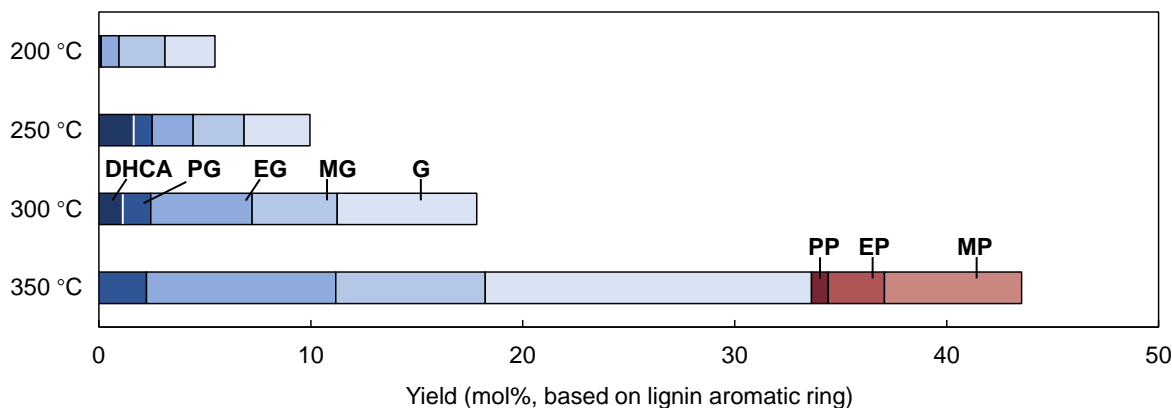


Fig. 3-17 The yields of monomers obtained from the pyrolysis-assisted catalytic hydrogenolysis of Japanese cedar organosolv lignin in anisole at 200–350 °C for 60 min (Organosolv lignin: 10 mg, Pd/C: 10 mg, anisole: 2 mL, H₂: 3 mL at 0.1 MPa). DHCA: dihydroconiferyl alcohol, PG: propyl guaiacol, EG: ethyl guaiacol, MG: methyl guaiacol, G: guaiacol, PP: propyl phenol, EP: ethyl phenol, MP: methyl phenol.

original organosolv lignin even after processing at 250 °C. This stability can be explained by the type of linkages in this material, which primarily comprised condensed bonds. As a result, the monomer yields were limited to 5.5 mol% (at 200 °C) and 9.9 mol% (at 250 °C).

Depolymerization was greatly enhanced above 300 °C and the monomer yields showed corresponding increases to 17.8 mol% (at 300 °C) and 43.5 mol% (at 350 °C). Based on the reactivity of the α -aryl type dimer **2** (Fig. 2-9b), the α -aryl bonds that are abundant in organosolv lignin are likely to be cleaved in this temperature range. High-temperature catalytic hydrogenolysis can therefore efficiently convert highly condensed lignin-derived products to monomers.

The compositions of the monomer mixtures generated by the organosolv lignin and MWL were also slightly different. Specifically, the proportions of guaiacol and methyl guaiacol were greater in the case of the former material. This result can possibly be ascribed to differences in the side-chain reactions involved in the organosolv pulping and pyrolysis processes. Organosolv lignins tended to preferentially form unsubstituted guaiacol, likely due to their high content of α -aryl linkages, as discussed in Fig. 3-15. This bond is cleaved at 350 °C to produce guaiacol.

3.4 Conclusions

This work examined the catalytic hydrogenolysis of MWL isolated from Japanese cedar wood (a softwood) in anisole using Pd/C over the temperature range of 250–350 °C, within which lignin is pyrolyzed. A high yield of monomers (over 60 mol%, based on the lignin aromatic rings) could be achieved when the catalytic process was carried out at temperatures above 250 °C. The insoluble MWL was first thermally converted to soluble oligomers and monomers by pyrolysis, after which depolymerization of the oligomers and monomer conversion occurred under catalytic conditions. Based on the dimer composition and the reactivity of 4-*O*-5-, α -aryl- and 5-5-type model dimers, the high monomer yield is attributed to the cleavage of these normally stable bonds in the oligomers. Ring saturation was also found to be significantly suppressed at these high temperatures. DHCA was the predominant monomer below 200 °C whereas guaiacol and alkyl guaiacols (methyl, ethyl and propyl, especially ethyl guaiacol) were formed above 300 °C. Demethylation and demethoxylation were initiated above 330 °C, particularly in the case of the 5-5 dimer, which had a unique conformation in which the two aromatic rings were arranged perpendicular to one another. The presence of the Pd/C catalyst was determined to be more important than the addition of H₂ with regard to catalytic depolymerization. The data from this work allowed the roles of pyrolysis, the catalyst and hydrogen in monomer production to be evaluated. This high temperature process, termed pyrolysis-assisted catalytic hydrogenolysis, was also effectively applied to organosolv lignin isolated from Japanese cedar, giving monomers in 43.5 mol% yield at 350 °C based on the cleavage of α -aryl bonds formed by re-condensation during organosolv pulping.

Chapter 4

Pyrolysis-assisted catalytic hydrogenolysis of pinoresinol

4.1 Introduction

Lignin is an aromatic polymer and one of the three main components of woody plants. In recent years, lignin has gained great interest due to its potential as a renewable resource for the production of chemicals and fuels. The production of industrial lignins, as a byproduct of pulping industries, has been increasing annually, with Kraft lignin expected to be the largest contributor in the near future. The conversion of technical lignin into high-value chemicals and fuels offers an opportunity to enhance the profitability of the pulping industry and meet the growing demand for sustainable resources.

Pyrolysis is a thermal conversion process conducted in the absence of oxygen at elevated temperature. Subjecting lignin to pyrolysis results in the breakdown of the polymer into smaller organic molecules, including phenolic compounds and polycyclic aromatic hydrocarbons (PAHs). The presence of PAHs in lignin pyrolysis products is of concern due to their toxicity and potential adverse effects on human health and the environment.

Naphthalenes are typical PAHs, and their formation is widely believed to arise from phenolic compounds generated from thermal degradation of lignin. This formation pathway is supported by model pyrolysis experiments conducted with phenols,(Buryan, 1991; Kim et al., 2020) and dimer.(Wang et al., 2017) Phenol undergoes decarbonylation to generate cyclopentadiene, which then undergoes Diels–Alder reaction and aromatization to produce naphthalene at temperature higher than 600 °C.(Egsgaard et al., 2014; Sharma and Hajaligol, 2003) However, the limited naphthalene yields (< 10%) observed in model pyrolysis experiments performed at 600-800 °C (Buryan, 1991; Kim et al., 2020) do not align with the notable presence of naphthalene in lignin pyrolysis(Kim et al., 2018; Shen et al., 2016) Furthermore, studies have shown that naphthalene can also be formed from lignin at temperature lower than 600 °C.(Jiang et al., 2014; Oasmaa and Johansson, 1993; Setter et al., 2020; Zhou et al., 2016) This suggests that there may be an additional pathway for the naphthalene formation

during lignin pyrolysis, for example, the transformation of linkages between aromatic units in lignin.

Common linkages found between phenylpropane units in kraft lignin are β -O-4, β - β , β -5, and α -5. The resinol structure is significantly important for hardwood kraft lignin, as it presents at up to 12.9%. (Zhao et al., 2019) It was found that β - β structure is transformed into naphthalene structure under acid-catalyzed phenolation condition at 120 °C. (Li et al., 2020) The analysis of dimer products obtained from milled wood lignin pyrolysis with the existence of Pd/C in anisole reveals that 5-5 and β -aryl type linkages are unlikely to be responsible for the naphthalene formation. Therefore, we believe that the β - β structure can generate the naphthalene structure during pyrolysis. However, there is currently no evidence to support such a proposal.

In this study, the catalytic hydrogenolysis of pinoresinol was performed using Pd/C and hydrogen at 250-350 °C to investigate whether the naphthalene structure was formed from the resinol structure during pyrolysis. Anisole is an aprotic solvent used to suppress condensation of the model. (Kotake et al., 2014) Pd/C helps to reduce side chains, thereby further inhibiting condensation. Pinoresinol was chosen as a model because its product can be simpler than that of syringyl-type resinol.

4.2 Experimental

4.2.1 Materials

The pinoresinol was prepared by the treatment of coniferyl alcohol with FeCl₃ in acetone/water (Lancefield and Westwood, 2015). And kraft lignin was purchased from Nacalai Tesque. Coniferyl alcohol was obtained from coniferyl aldehyde by aldehyde reduction with Sodium borohydride (NaBH₄). The purities of synthesized chemicals were confirmed by NMR.

4.2.2 Catalytic reaction

Pinoresinol (10 mg) or kraft lignin (10 mg), was mixed with 5% Pd/C (10 mg) and anisole (2 mL) in a closed reactor (5 mL volume) with the agitation system. The air inside the reactor was replaced by H₂ to 1 atm. The reactor was heated at 250, 300, and 350 °C and the mixture was agitated for 1 h in a preheated salt bath, before cooled in water. According to the

temperature profile of agitation heating equipment, it took only about 40 s for the reactor to reach the salt temperature.

The thermalcatalytic products (including solid Pd/C) in solvent (2 mL) were extracted with MeOH (6x3 mL). The organic extracts were combined to give a 20 mL turbid solution. A certain portion of suspension was centrifuged to remove Pd/C before products analysis.

4.2.3 Product analysis

Gel-permeation chromatography (GPC) was conducted to show the molecular weight distribution of MeOH-soluble portion by using a Shimadzu LC-10A system with a Shodex KF-801 column (exclusion limit molecular weight: 1,500 Da, polystyrene standard) at a flow rate of 0.6 mL/min and a temperature of 40 °C. THF was used as the eluent with a UV detector at 280 nm.

A portion of the MeOH-solubles was added with 1,3,5-triphenylbenzene (Internal standard) and then silylated by adding pyridine (100 μ L), hexamethyldisilazane (HMDS, 150 μ L), and trimethylchlorosilane (TMCS, 80 μ L) in conjunction with stirring and heating at 60 °C for 30 min. These trimethylsilyl derivatives were analyzed and quantified by GC-MS using a Shimadzu-2010 Plus gas chromatograph (Shimadzu Corporation, Kyoto, Japan) coupled with a Shimadzu QP 2010 Ultra mass spectrometer (Shimadzu Corporation, Kyoto, Japan). Agilent CPSil 8CB (length: 30 m, diameter: 0.25 mm) was used as the column. Helium was used as carrier gas at a flow rate of 2.09 mL/min. The injector temperature was 250 °C, and the split ratio is of 10. The temperature program was set as following: 70 °C (2 min), 4 °C/min to 150 °C, 150 °C (1 min), 10 °C/min to 300 °C, 300 °C (1 min). The MS scan parameters included a scan range of 35–600 m/z and a scan interval of 0.3 s.

The NMR spectra were measured by a Varian AC-400 (400 MHz) spectrometer (Varian, CA, USA). The chemical shifts and coupling constants (J) were shown as δ (ppm) and Hz, respectively.

4.3 Results and discussion

Pinoresinol (compound **10**) was treated at 250, 300 or 350 °C for 60 min in anisole with Pd/C and H₂. The Gel-permeation chromatography of products obtained from the reaction

mixtures are shown in Fig. 4-1. Here, the number attached to each peak represents either the dimer recovery or the product yield (in mol%) as determined by GC/MS (Fig. 4-2).

In all temperatures, no peaks appeared at retention times shorter than 11.8 min, suggesting that pinoresinol did not condense under these conditions. The yield of monomer increased from 5 to 16.8 mol% (compared with a theoretical yield of 200%, based on the quantity of aromatic rings in the model) when temperature increased from 250 to 350 °C. This indicates that the C-C bond of the pinoresinol structure was not easily broken under pyrolysis-assisted catalytic hydrogenolysis conditions. Although there were large peaks at around 12 min, the recovery of pinoresinol was always 0. Therefore, the two aromatic rings in pinoresinol were still connected, and the dimers were the main product.

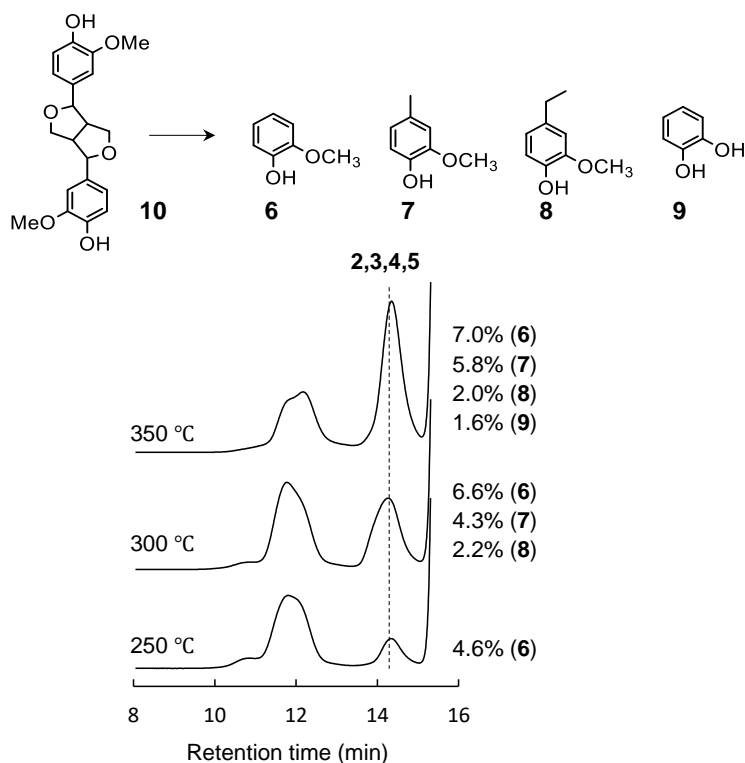


Fig. 4-1 Gel-permeation chromatography of products recoveries from β - β model. (Holding times are 1 h).

Fig. 4-2 and Fig. 4-3 provides the GC/MS total ion chromatograms of monomer region and dimer region. The peaks of the monomeric products were pretty small compared to the peaks of the dimers (as shown in Fig. 4-4), so the signal intensities in Fig. 4-2 were amplified by 20 times.

The dimeric products of pinoresinol still owned aromatic ring, unlike the products obtained from compound **1** and compound **2** especially at 250 °C. The low monomer yield and non-ring-saturated products suggest that resinol structure is unlikely undergoing catalytic C-C cleavage and ring-saturation. Fig. 4-5 shows the 3D structure of pinoresinol. The plane of the guaiacyl nuclei is not in the same plane of five-membered ring of the side chain. This steric hindrance would thwart aromatic ring being adsorbed.

Treated at 250 °C for 1 h, the predominant dimer products obtained were compound **u**, which has the tetrahydrofuran (THF) type side chain, compound **o**, and **q**, which have the tetralin type side chain, and also traces of compound **t** and **v**, which have both tetralin and THF structures in side chain. With the temperature rose to 350 °C, the peak area of compound **u** was noticeably declined, while those of compound **n**, which has the alkyl side chain, and compound **p**, **r**, and **s**, which has the naphthalene structure, were increased. In the meantime, the productions of guaiacyl monomers and some naphthalene products (compound **j**, **k**, **l**, and **m**) were increased. The identification of these compounds was deduced from the MS spectrum shown in Fig. 4-6.

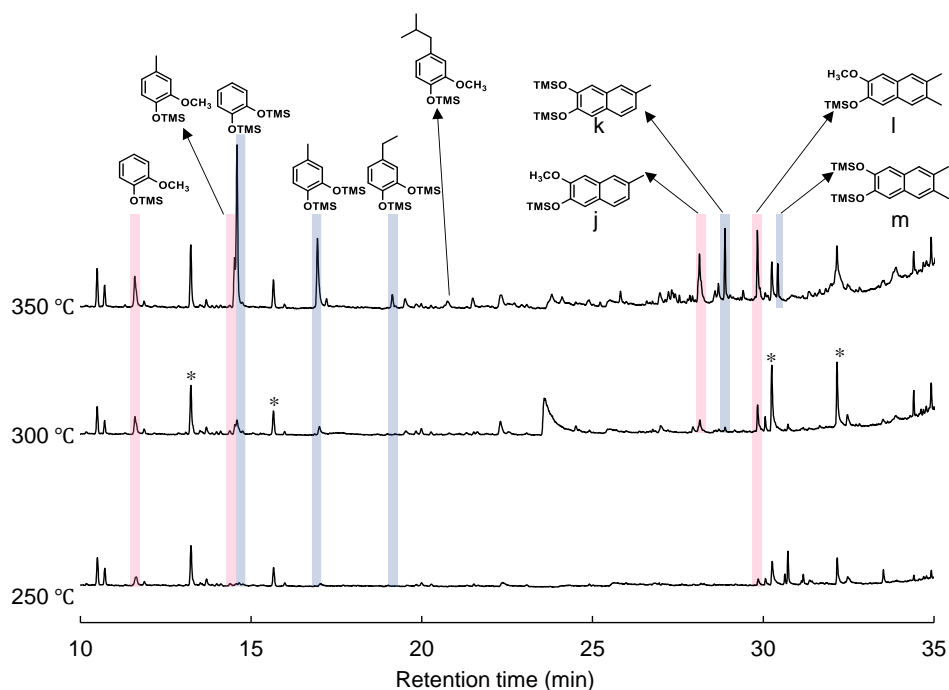


Fig. 4-2 The GC/MS total ion chromatograms (monomer region) of the TMS-derivatives of reaction mixtures obtained from the thermocatalytic hydrogenolysis of the pinoresinol model compound (10) in anisole at 200–350 °C for 60 min. (Enlarged by 20 times) Asterisk mark is from impurities.

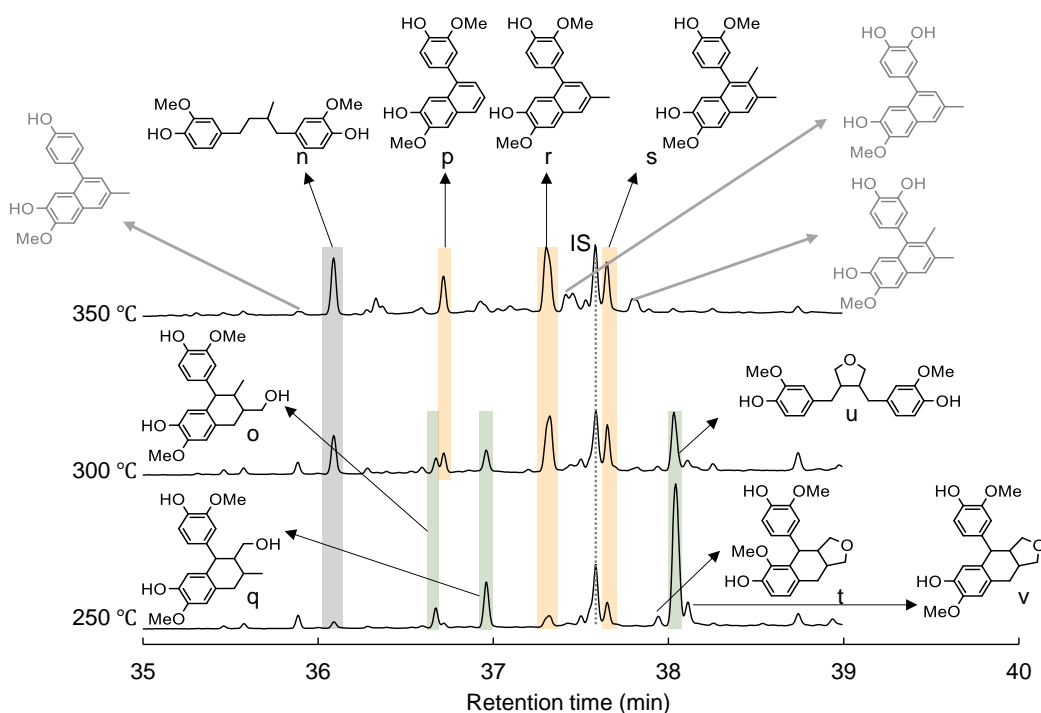


Fig. 4-3 The GC/MS total ion chromatograms (dimer region) of the TMS-derivatives of reaction mixtures obtained from the thermocatalytic hydrogenolysis of the pinoresienol model compound (10) in anisole at 250–350 °C for 60 min.

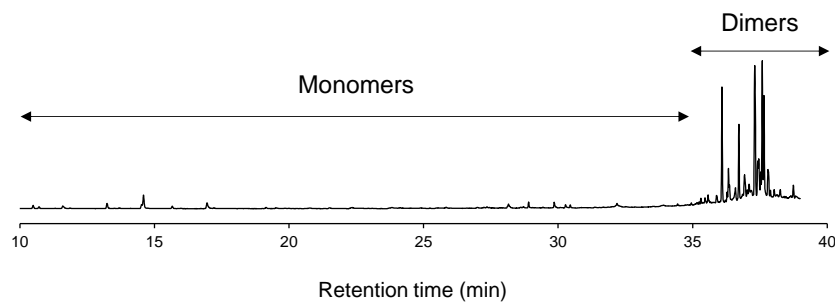


Fig. 4-4 The GC/MS total ion chromatograms of the TMS-derivatives of reaction mixtures obtained from the thermocatalytic hydrogenolysis of the pinoresienol model compound (10) in anisole at 350 °C for 60 min.

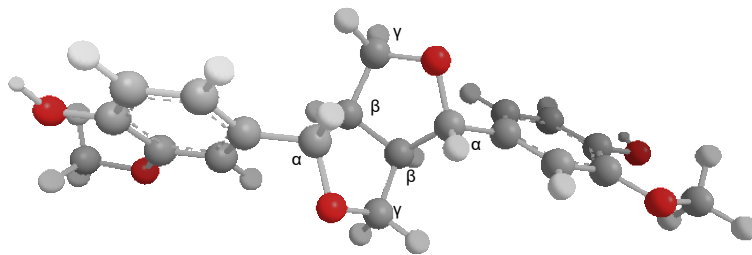


Fig. 4-5 3D configuration of β - β model.

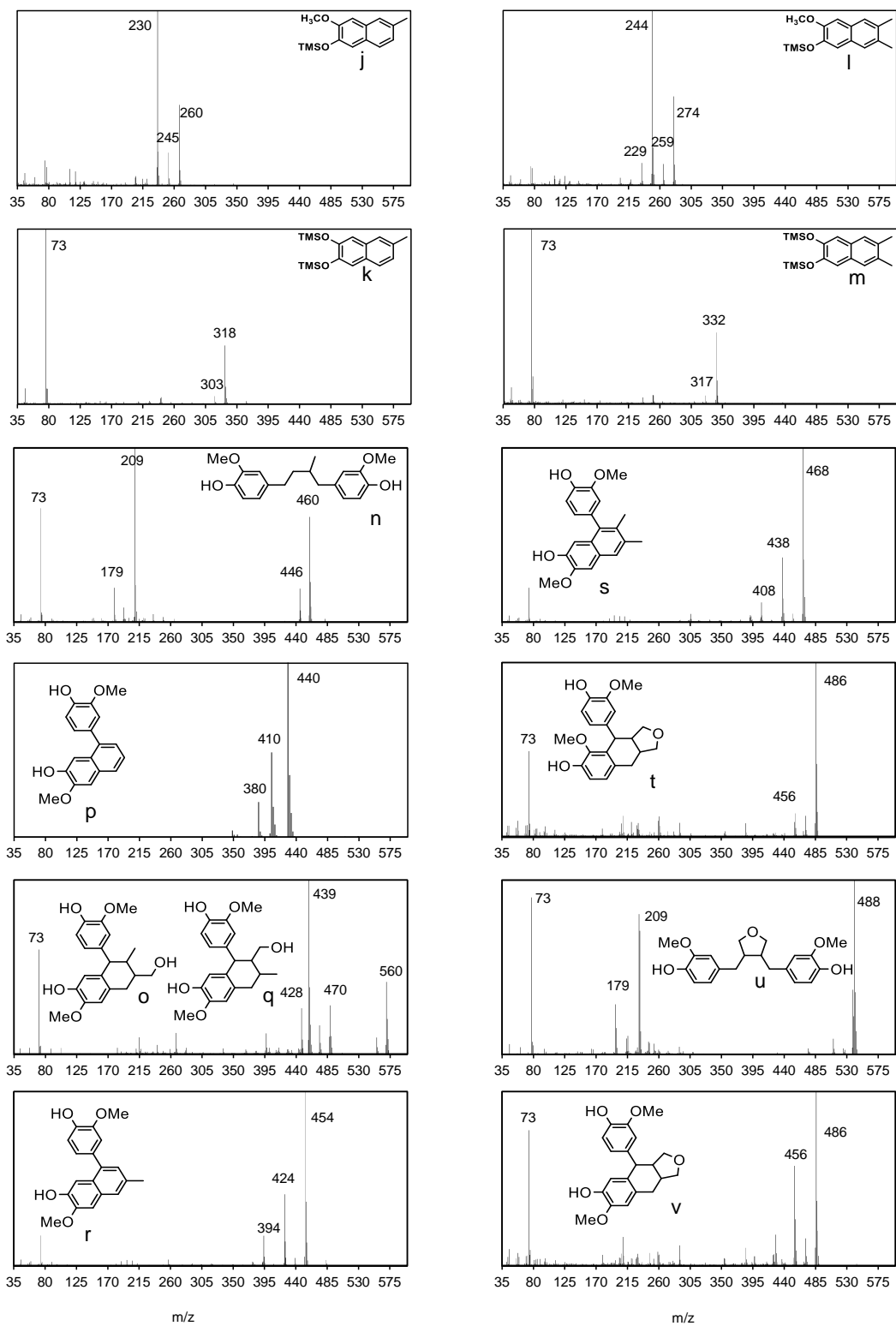


Fig. 4-6 The mass spectra of various dimers corresponding to the compounds shown in Fig. 4-2, Fig. 4-3.

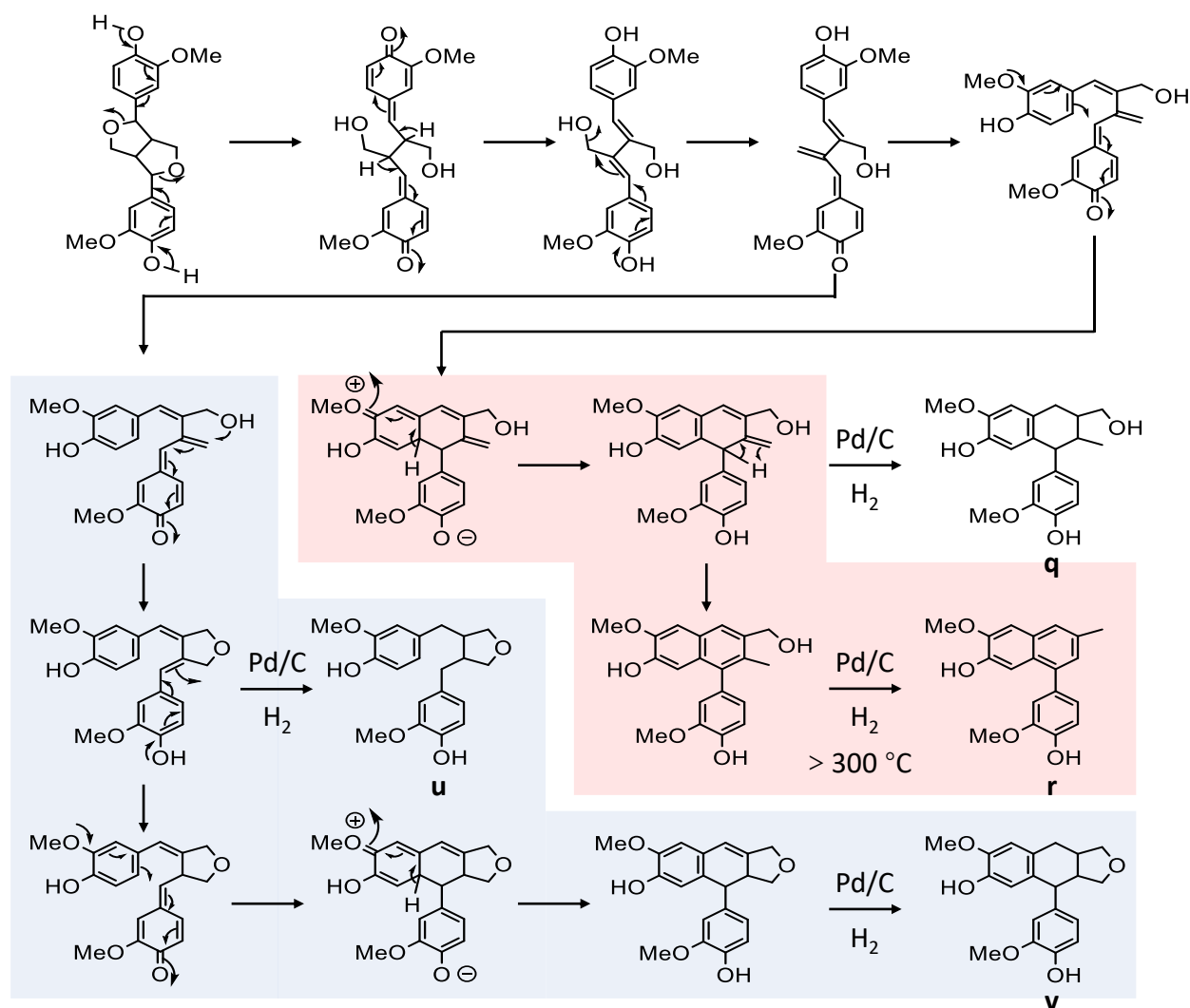


Fig. 4-7 Proposed pathways for the products from pinoresinol.

The proposed pathways for compound **o** to **v** were shown in Fig. 4-7. Recovery of compound **u**, the tetrahydrofuran (THF) type product, has been reported from the hydrogenolysis products from resinol structure (Van Aelst et al., 2020). Compounds **q** and **o** are tetralin type products, and their yields ranked the second at 250 °C. Also, traces of compounds **t** and **v** were identified. The difference in the yields of these products might be related to the number of intermediate products. It takes only 5 steps to convert pinoresinol to compound **u**, 6 steps to compound **q**, and 8 steps to compound **v**. The keto-enol tautomerism of pinoresinol could produce some intermediates with conjugated C_α and C_β. Such high conjugation would favor the

formation of six-member ring six-member ring structure, which facilitate the contact of C_{α} with aromatic nuclei. As the consequence of α -2 or α -6 condensation, THF type compound **t** and **v**, and phenyl-naphthalene type compounds **r** and **s** could be generated.

At higher than 300 °C, hydrogenolysis of compound **u** would convert the ether on side chain to alcohol, which would like to undergo deformylation to give compound **n**. Such deformylation reaction will be discussed in the **chapter 5**. Also, catalytic deformylation of compound **q** followed by H-donation might generate Phenyl-naphthalene type compounds **p**, **r**, **s**. Guaiacol was the major monomer product, which were likely to be derived from the hydrogenolysis of phenyl-naphthalene in a way discussed in **section 3.3.3**.

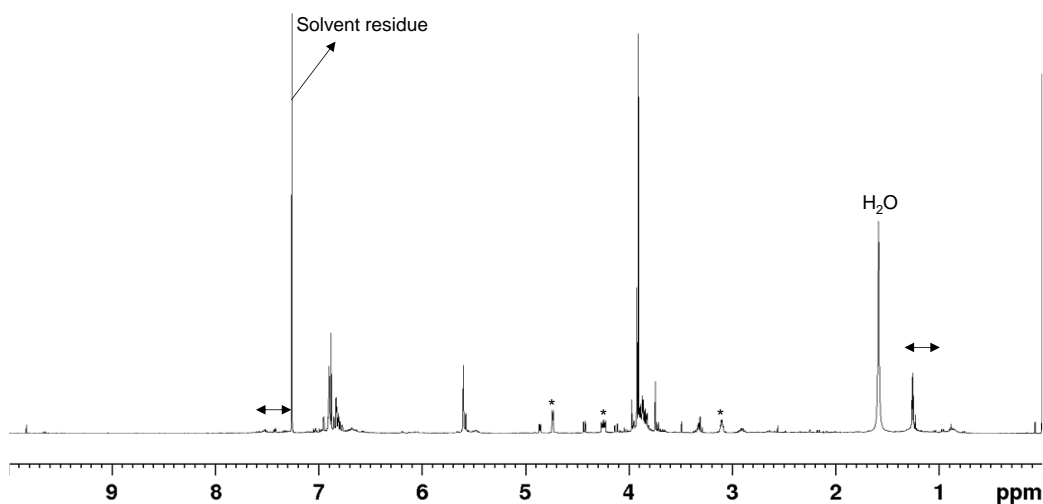


Fig. 4-8 ^1H NMR spectra of TLC-purified products obtained from pinoresinol pyrolysis in the presence of an aromatic solvent and a hydrogen donor at 350°C for 10 min. Asterisk mark is from pinoresinol.

Fig. 4-8 shows the NMR spectrum of main products separated from the pinoresinol products after pyrolysis in DPB and H-donor at 350 °C for 10 min as described in **chapter 2**. This spectrum supports the proposed structures deduced in Fig. 4-6. Compared to the protons on guaiacyl nuclei that have chemical shift in 6.5-7.5 ppm, the peaks of aromatic-H located at 7.5-8.0 ppm should be more deshielded. These peaks might from the proton of middle benzene in phenyl-naphthalene, which was deshield by the three ring currents. The peaks at 1.25 ppm could come from the alkyl-Hs that are not linked with oxygen or aromatic ring, which might

from the methyl group in compound **o** and **q**. However, these structures should be further confirmed by TLC separation.

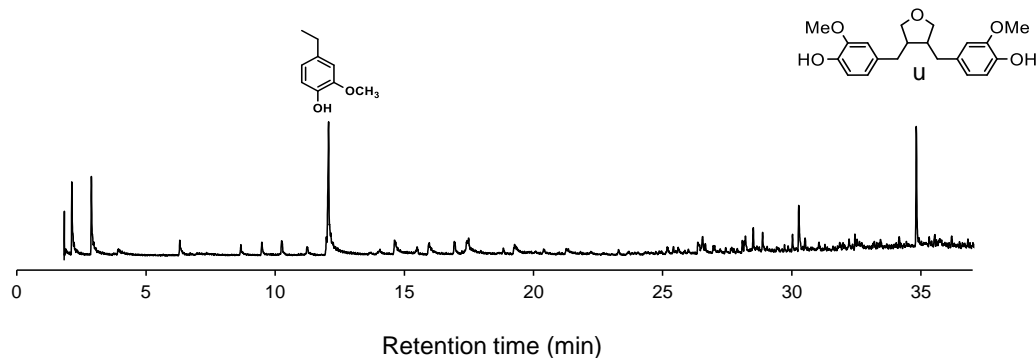


Fig. 4-9 The GC/MS total ion chromatograms of the reaction mixtures obtained from the pyrolysis-assisted catalytic hydrogenolysis of kraft lignin in anisole at 350 °C for 10 min.

Fig. 4-9 shows the GC/MS total ion chromatograms acquired from products obtained from the pyrolysis-assisted catalytic hydrogenolysis of kraft lignin in anisole at 350 °C for 10 min. The monomer yield is around 15%, and the main product is the ethyl guaiacol and compound **u**. The low monomer yield could be due to the poisoning of sulfur to Pd. This demonstrated that kraft lignin is a possible source for the production of anhydrosecoisolariciresinol (compound **u**).

4.4 Conclusions

Pyrolysis-assisted catalytic hydrogenolysis of pinosresinol gave phenylanthracene structure, especially at 350 °C. C-C bonds in β - β were hard to cleave. These results suggest that naphthalene structure can also be derived from β - β , and this could be the reason for the formation of polycyclic aromatic hydrocarbons during lignin pyrolysis.

Chapter 5

Role of pyrolysis in pyrolysis-assisted catalytic hydrogenolysis of lignin and mechanistic insights into catalytic conversion

5.1 Introduction

Lignin is an aromatic polymer that constitutes 20%–30% of lignocellulosic biomass and is attracting attention as a renewable resource that can replace petroleum-derived aromatic chemicals. For this purpose, it is important to selectively depolymerize lignin to aromatic monomers.

Catalytic hydrogenolysis has been actively investigated in recent years as a method for producing aromatic monomers from lignin. Generally, this process is conducted at a relatively low temperature range around 200 °C or lower. Aromatic monomers can be obtained in relatively high yields from hardwood lignins, whereas yields from softwood lignins are limited because of the higher contents of condensed linkages (β -1, β -5, β - β , and 5-5) that resist cleavage (Van Den Bosch et al., 2015). Another concern is the inability of lignin polymers to efficiently access solid catalysts, even if catalytic hydrogenolysis of monomers and dimers is successful.

Even without the assistance of a catalyst, the α - and β -ether bonds of lignin will cleave spontaneously at high temperatures above 250 °C (especially above 300 °C), causing depolymerization of lignin macromolecules (Nakamura et al., 2008; Wang et al., 2022). However, repolymerization occurs rapidly via a quinone methide intermediate formed from a conjugated C=C structure of the product, yielding higher molecular weight (MW) products that are ultimately converted to char (Kotake et al., 2013). This repolymerization process has been found to be effectively inhibited in aprotic solvents (Kotake et al., 2014), such as aromatic solvents, to selectively give thermally stable oligomers (Wang et al., 2022). By adding Pd/C and a small amount of hydrogen to this system (Wang et al., 2023), the side chain C=C structure is hydrogenated and the product is stabilized against repolymerization. In addition, by cleaving diphenyl ether and condensed structures, which are difficult to cleave by pyrolysis, aromatic

monomers can be produced in 60 mol% yield or higher (based on lignin aromatic rings) even from softwood lignin, which was previously difficult. This technique is called pyrolysis-assisted catalytic hydrogenolysis because it utilizes the assistance of lignin pyrolysis. Conventional catalytic hydrogenolysis of softwood lignin at temperatures below 200 °C gives dihydroconiferyl alcohol (DHCA) with good selectivity (Song et al., 2013; Torr et al., 2011), whereas guaiacols and alkyl guaiacols (methyl, ethyl, and propyl; particularly ethyl) are produced by pyrolysis-assisted catalytic hydrogenolysis at temperatures above 300 °C.

In pyrolysis-assisted catalytic hydrogenolysis, the composition of the pyrolysis products of lignin is expected to determine the composition of the final aromatic monomers. However, at present, the factors at play in this process are not well understood. Therefore, in this study, we focused on the side-chain structure of monomers obtained by pyrolysis of softwood lignin. Guaiacols with various side-chain structures (alkyl guaiacols, dihydroconiferyl alcohol, coniferyl alcohol, coniferyl aldehyde, eugenol, isoeugenol, acetovanillone, and vanillin) are typical monomeric products of pyrolysis (Asmadi et al., 2011a; Saiz-Jimenez and De Leeuw, 1986). They were subjected to catalytic hydrogenolysis in anisole containing Pd/C and hydrogen at 300 and 350 °C to determine how the side-chain structure was transformed. Coniferyl alcohol produced by the cleavage of β -ether was investigated in detail because it is the most important pyrolysis product from softwood lignins (Nakamura et al., 2008). We also examined the role of side-chain functional groups in transformations by their interactions with the Pd/C surface.

5.2 Experimental

5.2.1 Materials

Guaiacyl acetone (98%) was purchased from Alfa Aesar (Ward Hill, MA, USA). 1-Guaiacyl ethanol (97%), coniferyl aldehyde (98%), propyl guaiacol (99%), and homovanillyl alcohol (99%) were purchased from Sigma-Aldrich (St. Louis, MO, USA). Isoeugenol (*trans/cis* mixture, extra pure reagent [EP]), eugenol (EP), acetovanillone (EP), vanillin (guaranteed reagent [GR]), and methyl guaiacol (GR) were purchased from Nacalai Tesque (Kyoto, Japan). Vanillyl alcohol (98%), ethyl guaiacol (98%), and guaiacol (98%) was purchased from Tokyo Chemical Industry (Tokyo, Japan). Coniferyl alcohol was synthesized by the reduction of coniferyl aldehyde with NaBH₄ and dihydroconiferyl alcohol was obtained by the hydrogenation

of coniferyl alcohol on Pd/C under H₂ at room temperature. Analysis of these synthesized compounds by nuclear magnetic resonance spectroscopy confirmed the purities to be approximately 99%.

5.2.2 Catalytic reaction

The catalytic reaction of the monomeric model compounds were conducted in a sealed 5-mL batch reaction vessel, as described in section 3.2.2. In each trial, 10 mg of a compound and 10 mg of 5% Pd/C (EP, Nacalai Tesque) were placed in the vessel with 2 mL of anisole (GR, Nacalai Tesque) as solvent. The space left in the vessel (approximately 3 mL) was filled with H₂ or N₂ at 1 atm; the added H₂ was equivalent to a molar excess of 2.4–3.5 times relative to the 10-mg sample. The vessel was then immersed in a salt bath preheated to a temperature in the range of 200–350 °C for the catalytic reaction with agitation. After a set time, the reaction was quenched by transferring the vessel to a water bath.

After the reaction, the contents of the vessel were washed several times with methanol (18 mL in total) to recover the turbid reaction mixture, which contained the derived products, Pd/C, and anisole. A portion of the suspension was centrifuged to remove Pd/C before analysis.

5.2.3 Product analysis

Molecular weight distribution of the methanol-soluble products was determined by GPC. Analysis by GC–MS was performed to quantify the products in the reaction mixture after trimethylsilyl derivatization. The methods for products analysis were same with the description in section 3.2.3.

The molar yield, M_i , of each monomeric product, i , was calculated as:

$$M_i \text{ (mol\%)} = \frac{\text{Mass of } i}{\text{MW of } i \times n} \times 100,$$

Herein, n is the number of moles of the model compound treated, calculated as:

$$n \text{ (mol)} = \frac{\text{Sample mass (approximately 0.01 g)}}{\text{Average MW of model sample}}.$$

5.3 Results and discussion

5.3.1 Coniferyl alcohol and dihydroconiferyl alcohol

CA is expected to form in significant yields from softwood lignin, but the yields of CA in typical pyrolysis are quite low because of the condensation of CA into higher MW products upon formation (Kotake et al., 2013). The hydrogenation product, DHCA, is produced with a good selectivity by catalytic hydrogenolysis of softwood lignin at relatively low temperatures below 200 °C, indicating that the lignin → CA → DHCA pathway is included in these transformations. Therefore, the reactivity of CA and DHCA with Pd/C and H₂ in anisole was investigated in detail in the temperature range of 200–350 °C (duration time: 60 min). A relatively small amount of H₂ was used, corresponding to 2.4 times the number of moles of aromatic rings. Two additional conditions (with Pd/C in N₂ and N₂ without Pd/C) at 350 °C were also used to understand the roles of catalyst and hydrogen.

Fig. 5-1 shows the GPC profiles of the reaction mixtures obtained by catalytic

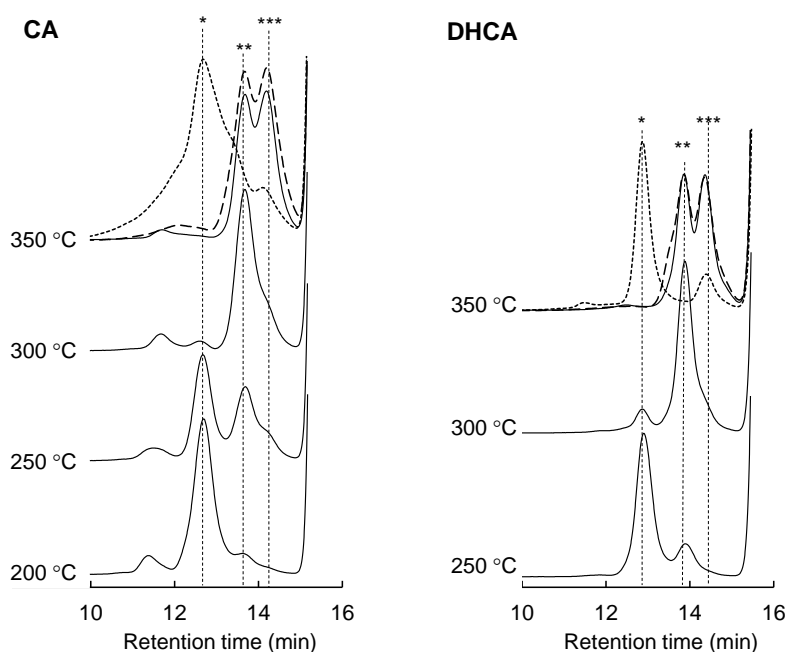


Fig. 5-1 Gel-permeation chromatograms of the reaction mixtures obtained from the catalytic hydrogenolysis of coniferyl alcohol (CA, left) and dihydroconiferyl alcohol (DHCA, right) in anisole at 200–350 °C for 60 min. Solid line: Pd/C, H₂; dashed line: Pd/C, N₂; dotted line: no catalyst, N₂; asterisk: retention time of CA, DHCA, coniferyl aldehyde, isoeugenol (*cis/trans*), eugenol; double asterisk: retention time of ethyl guaiacol; triple asterisk: retention time of guaiacol, methyl guaiacol.

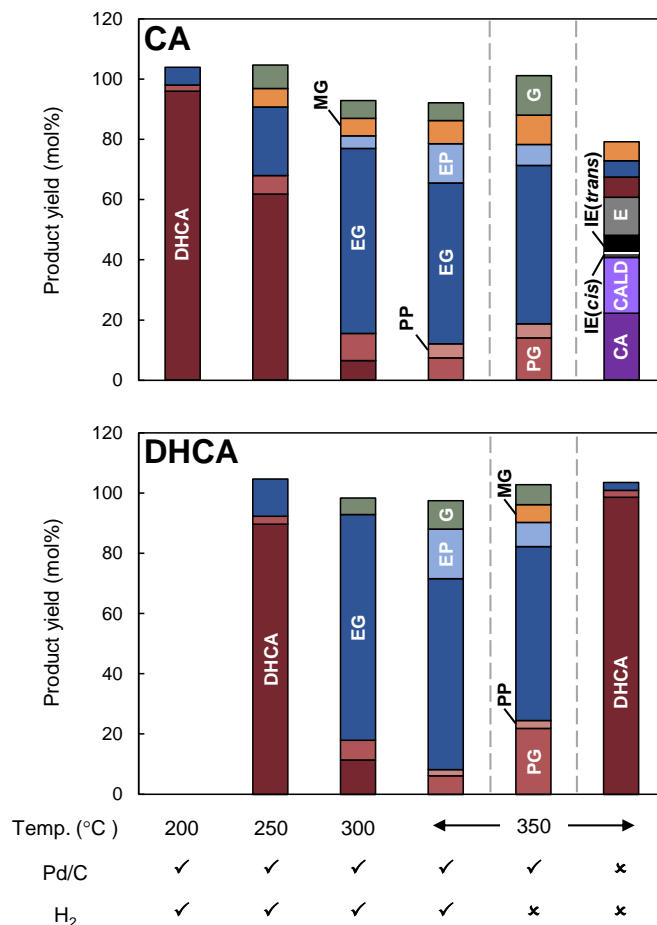
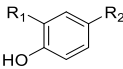


Fig. 5-2 Recovery and yield of monomers obtained by catalytic hydrogenolysis of coniferyl alcohol (top) and dihydroconiferyl alcohol (bottom) in anisole at 200–350 °C for 60 min.

hydrogenolysis of CA and DHCA at 200–350 °C for 60 min (solid black lines). The chromatograms of the products obtained using Pd/C in N₂ and N₂ without Pd/C are shown by dashed lines and dotted lines, respectively. Monomer yields are summarized in Fig. 5-2 and abbreviations and chemical structures of monomers are shown in Table 5-1.

Even in the absence of Pd/C in N₂, limited GPC signals were observed at retention times shorter than that for CA. Thus, CA was effectively stabilized against condensation in anisole even at 350 °C and was recovered as monomer as part of a 79 mol% yield: 22 mol% of CA and 57 mol% of other monomers (DHCA, coniferyl aldehyde, *cis/trans*-isoeugenol, eugenol, ethyl guaiacol, and methyl guaiacol) (Fig. 5-2, top right: in N₂ without Pd/C). Formation of these monomers from CA was also reported by Kotake et al (Kotake et al., 2013). These pyrolytic transformations may compete with catalytic processes for CA when CA is formed by the

Table 5-1 Chemical structures of monomeric products and their abbreviations.

	Legends		
		R ₁	R ₂
Guaiacylacetone	GAC	OCH ₃	CH ₂ COCH ₃
Coniferyl alcohol	CA	OCH ₃	CHCHCH ₂ OH
Coniferyl aldehyde	CALD	OCH ₃	CHCHCHO
Isoeugenol (<i>trans</i>)	IE (<i>trans</i>)	OCH ₃	CHCHCH ₃
Isoeugenol (<i>cis</i>)	IE (<i>cis</i>)	OCH ₃	CHCHCH ₃
Eugenol	E	OCH ₃	CH ₂ CHCH ₂
Dihydroconiferyl alcohol	DHCA	OCH ₃	CH ₂ CH ₂ CH ₂ OH
Propyl guaiacol	PG	OCH ₃	CH ₂ CH ₂ CH ₃
Propyl phenol	PP	H	CH ₂ CH ₂ CH ₃
Propyl catechol	PC	OH	CH ₂ CH ₂ CH ₃
Acetophenol	AP	H	COCH ₂ CH ₃
Acetovanillone	AO	OCH ₃	COCH ₂ CH ₃
Ethyl guaiacol	EG	OCH ₃	CH ₂ CH ₃
Ethyl phenol	EP	H	CH ₂ CH ₃
Ethyl catechol	EC	OH	CH ₂ CH ₃
Methyl guaiacol	MG	OCH ₃	CH ₃
Methyl phenol	MP	H	CH ₃
Methyl catechol	MC	OH	CH ₃
Guaiacol	G	OCH ₃	H
Phenol	P	H	H

pyrolysis of lignin.

Catalytic hydrogenation of CA to DHCA was near complete even at temperatures as low as 200 °C. This indicates that this catalytic conversion occurred much faster than the pyrolytic conversions described above. Further conversion of DHCA to ethyl guaiacol became significant in treatments performed at 250–350 °C, and small amounts of guaiacol, methyl guaiacol, and propyl guaiacol were also produced. Given that DHCA was stable at 350 °C in the absence of Pd/C in N₂ but then became reactive by the addition of Pd/C, these conversions are catalytic processes that do not require the addition of H₂. Similar results were obtained in a previous study using milled wood lignin (MWL) (Wang et al., 2023). These results are explained by the generation of reactive hydrogen species during the conversion, which is discussed below.

It is noted that the composition of the products depended on the reaction temperature (Fig. 5-2) but was very similar between the treatments of CA and DHCA. This can be explained by the

very high reactivity in conversion of CA to DHCA observed at 200 °C. Only small differences were observed. The conversion rate of DHCA → ethyl guaiacol was greater for CA (discussed below), and methyl guaiacol was produced from CA but not from DHCA. Methyl guaiacol may be formed via the pyrolysis pathway. In the GPC profile (Fig. 5-1), a small signal is observed in the higher MW region (shorter retention time than CA) only in the case of CA conversion. These differences are likely to arise from competing pyrolysis pathways, although the effects are only small.

5.3.2 Other pyrolysis intermediates and conversion pathway from lignin

The final composition of the monomers is alkyl guaiacols and guaiacol, as reported for pyrolysis-assisted catalytic hydrogenolysis of MWL and organosolv lignin (Wang et al., 2023). This indicates that alkyl side chains are stable during the transformation. The yields of monomers obtained by catalytic hydrogenolysis of guaiacol and methyl-, ethyl-, and propyl-guaiacol using Pd/C and H₂ in anisole at 300 and 350 °C are summarized in Fig. 5-3 (duration

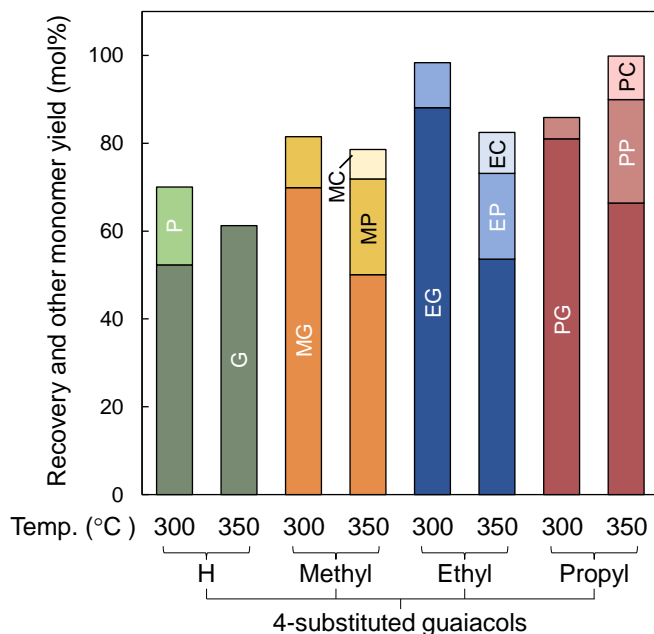


Fig. 5-3 Recovery and yields of monomers obtained by catalytic hydrogenolysis of 4-substituted guaiacols (H-, methyl-, ethyl-, and propyl-) in anisole at 300 and 350 °C for 60 min. Asterisk: percentage recovery of original side-chain structure in identified monomers.

time: 60 min). Values attached to the graph indicate the percent recovery of the original side-chain structure. Demethoxylation took place for all guaiacols at 300 and 350 °C, although the phenol yield from guaiacol (350 °C) is not shown because a small amount of phenol was formed from anisole (solvent) at this temperature. Demethylation to give catechols also occurred to a lesser extent, except for guaiacol, which has no alkyl group. Saturated alkyl groups may accelerate the demethylation. However, no modification of the alkyl groups occurred during the transformation. Therefore, the resulting lignin-derived monomers tended to have saturated alkyl (methyl, ethyl, or propyl) side chains along with unsubstituted ones.

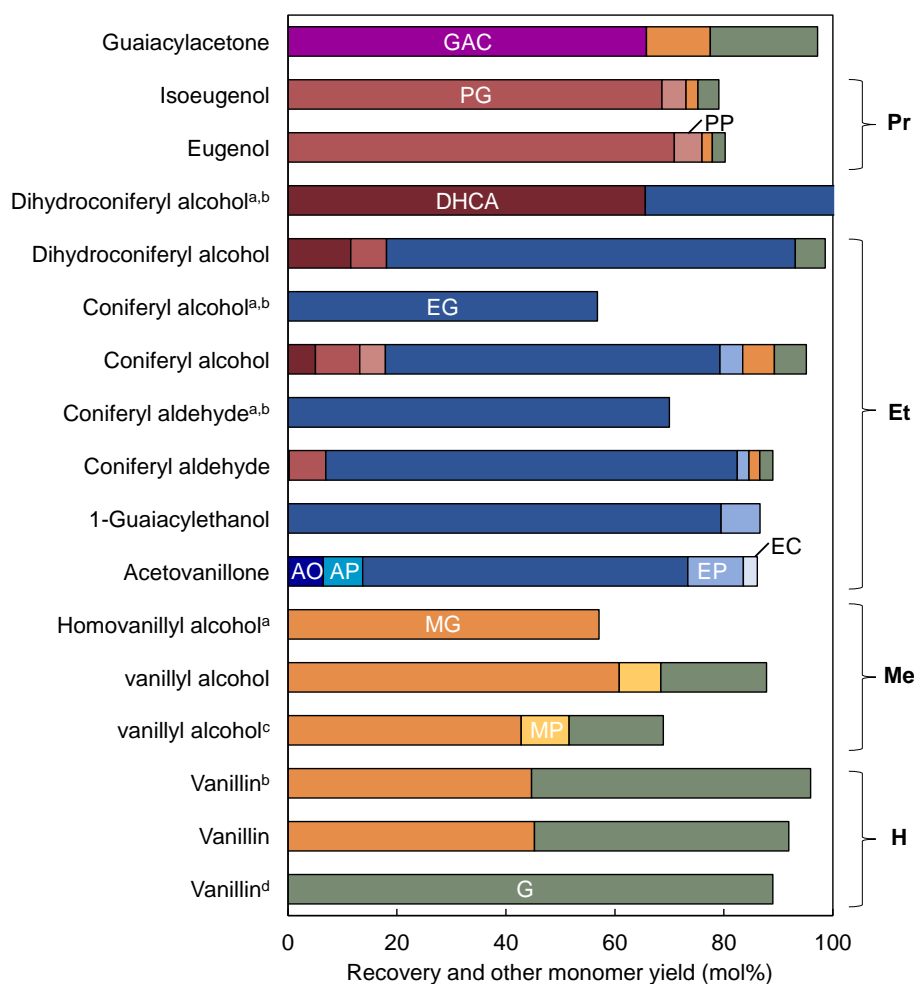


Fig. 5-4 Yields of monomers obtained by catalytic hydrogenolysis of various monomers produced during lignin pyrolysis in anisole at 300 °C for 60 min. a: H₂ used as carrier gas in GC-MS analysis (others used He); b: reaction time 2 min; c: conducted at 350 °C; d: conducted in N₂.

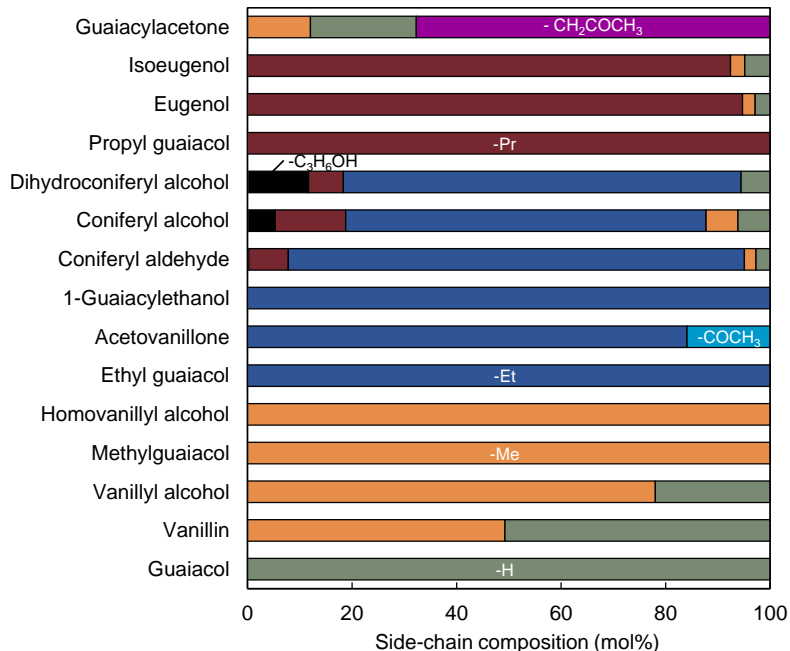


Fig. 5-5 Side-chain composition of monomers obtained by catalytic hydrogenolysis of various monomers produced during lignin pyrolysis in anisole at 300 °C for 60 min.

As illustrated in Fig. 5-2, coniferyl aldehyde, eugenol, isoeugenol, DHCA, ethyl guaiacol, and methyl guaiacol are typically produced via CA during the pyrolysis of lignin. Other monomers such as vanillin and acetovanillone are also produced from lignin via alternative pathways. To understand the roles of these intermediates on the final monomer composition, the reactivities of these compounds were investigated using Pd/C and H₂ at 300 °C in anisole (duration time: 60 min). The monomer yields, side-chain compositions, and conversion pathways obtained are summarized in Fig. 5-4 to Fig. 5-6, respectively.

Unlike saturated alkyl groups, the functional groups on the side chains of these compounds were reactive, yielding propyl, ethyl, methyl, and unsubstituted H groups. Isoeugenol and eugenol mainly yielded propyl guaiacol by hydrogenation of alkenyl C=C bonds, with minor amounts (~ 5 mol%) of methyl guaiacol and guaiacol. In addition to CA and DHCA, coniferyl aldehyde, acetovanillone, and 1-guaiacyl ethanol selectively gave ethyl guaiacol. Methyl guaiacol was produced in high yield from homovanillyl alcohol, vanillyl alcohol, and vanillin. Guaiacol was mainly produced from vanillin and vanillyl alcohol. Therefore, these results suggest that the composition of the side chains of the final products depends on the composition

of the functional groups in the side chains of intermediates formed by the pyrolysis of lignin and varies with the chemical structure of the original lignin.

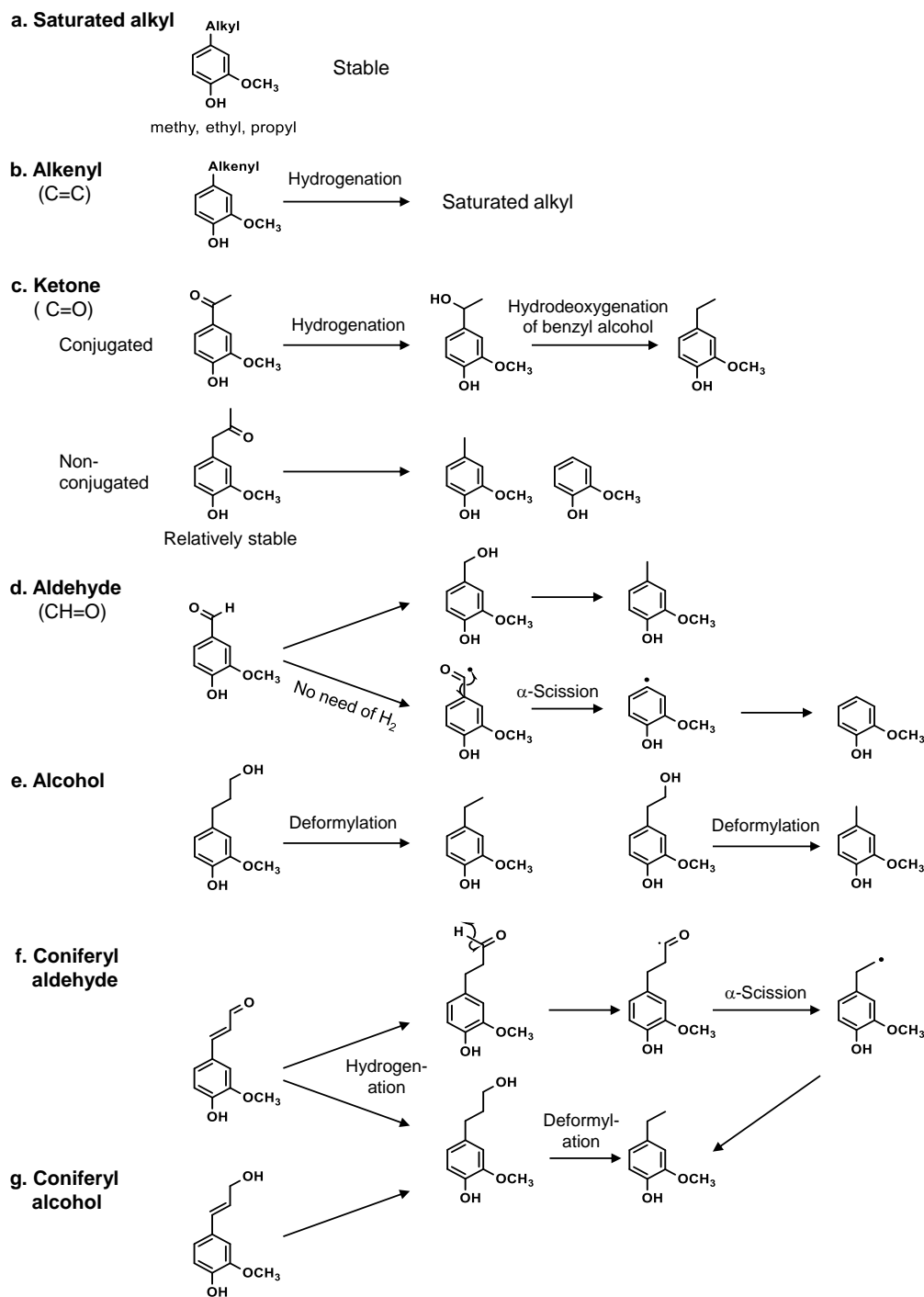


Fig. 5-6 Proposed pathways for various types of monomers produced by pyrolysis of lignin during pyrolysis-assisted catalytic hydrogenolysis using Pd/C and H₂ in anisole at 300 and 350 °C.

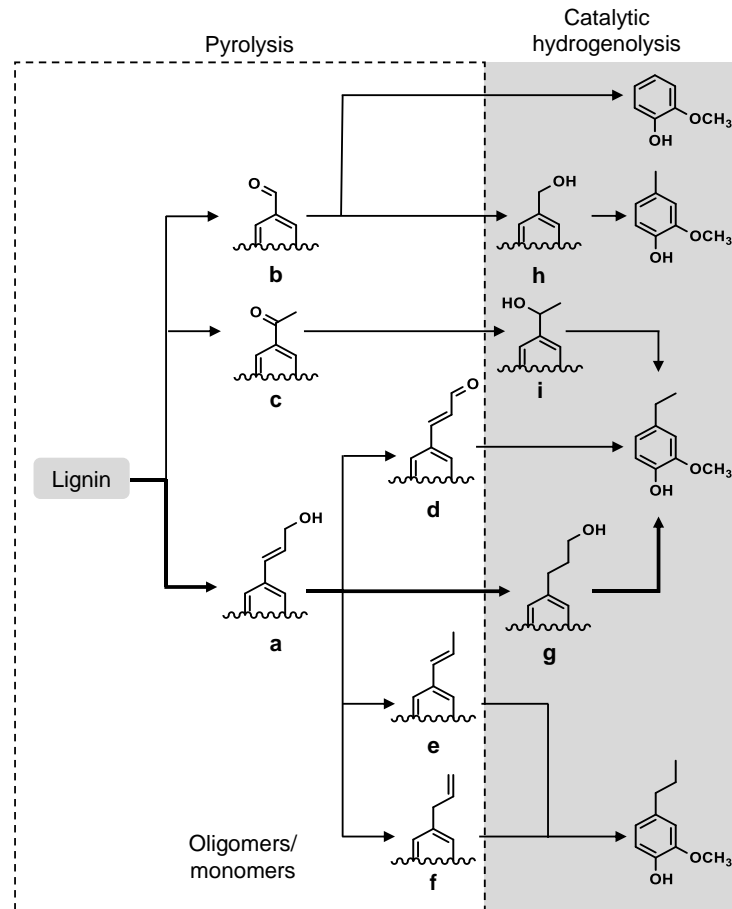


Fig. 5-7 Proposed roles of lignin pyrolysis in pyrolysis-assisted catalytic hydrogenation of lignin.

Based on these results, a pathway of pyrolysis-assisted catalytic hydrogenolysis of lignin at 300 °C was proposed as shown in Fig. 5-7. Given that lignin is a high MW polymer, it could not interact effectively with solid catalysts. This is noticeable when lignin is suspended in a solvent. In this situation, lignin is pyrolyzed to form oligomers and smaller amounts of monomers. Because the condensed-type C–C bonds are not pyrolytically cleaved, oligomers are the major products, especially for softwood lignins.³ As primary pyrolysis products, CA-type (a) and carbonyl-type (b and c) side chains are formed on oligomers and monomers (Fig. 5-7). The CA-type (a) side chains are further converted to coniferyl aldehyde- (d), isoeugenol- (e), eugenol- (f), and DHCA-type (g) side chains by pyrolysis. These pyrolysis reactions compete with catalytic hydrogenolysis: cleavage of 4-*O*-5 and condensed bonds, and side-chain transformations as discussed above.

5.3.3 Role of side-chain functional group in catalytic conversion

The reactivity of the catalytic conversion of guaiacol derivatives greatly depended on the side-chain structure. This is probably because the adsorption of guaiacol derivatives to the catalyst surface differs depending on the side-chain structure as discussed below, although further systematic studies are necessary to conclude the proposed association mechanisms.

Conjugated C=C and C=O side chains were especially reactive compared with other types of side chains. Conversions of CA, coniferyl aldehyde, and vanillin were completed even for a short duration time of 2 min (Fig. 5-4). Because the typical pyrolysis products of lignin contain these conjugated double bonds in their side chains, these side chains would be rapidly transformed. Such high reactivity is reasonably explained by efficient adsorption on the Pd/C surface, considering that the benzene ring and the C=C and C=O structures are coplanar as illustrated in Fig. 5-8a–c. The special stability of alkyl side chains can be explained by less effective association with the catalyst because of the repulsive forces between the hydrophobic alkyl group and polar Pd (Fig. 5-8d).

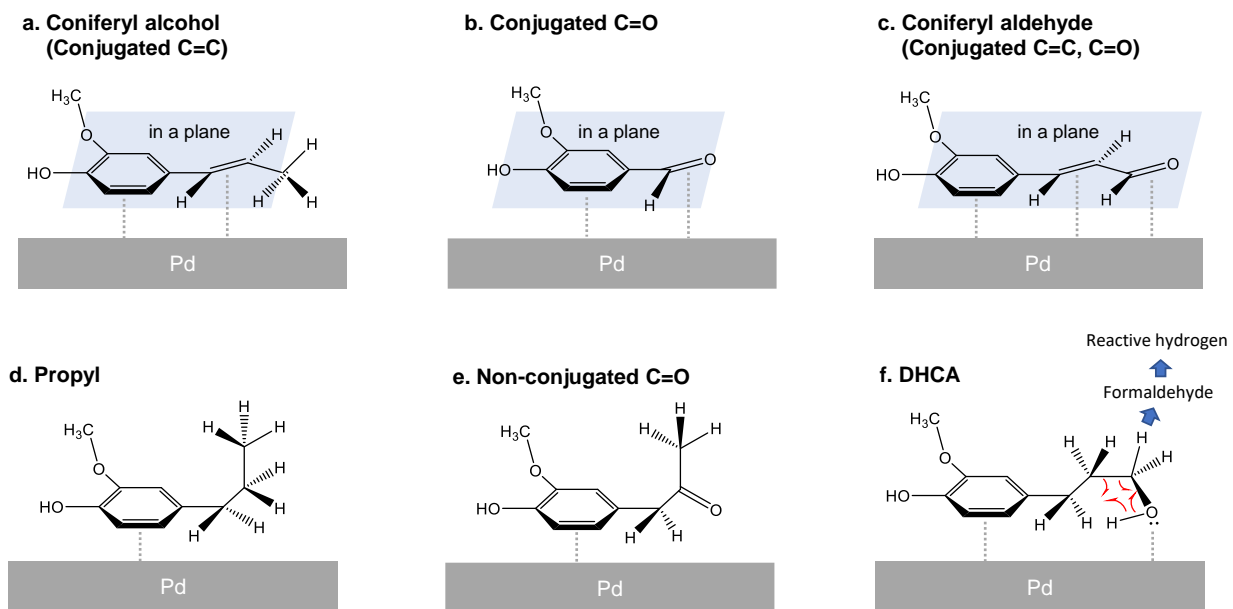


Fig. 5-8 Proposed effects of side-chain functional groups of 4-substituted guaiacols on their ability to adsorb onto the Pd surface, governing reactivity and reaction pathways.

Interestingly, even after 60 min of treatment, guaiacyl acetone with unconjugated C=O side chain was recovered in 65.8% yield (Fig. 5-4). Such a low reactivity was observed because the methylene group of C_α sterically inhibits the parallel association of C=O with the Pd/C surface so that the π electrons of C=O cannot associate effectively with Pd/C (Fig. 5-8e). The conjugated ketone of acetovanillone was efficiently converted to ethyl guaiacol through hydrogenation of C=O, followed by hydrodeoxygenation of benzyl alcohol (Fig. 5-6). These reactions did not proceed at the unconjugated C=O of guaiacyl acetone; instead, the aromatic C–C_α and C_α–C_β bonds were cleaved to yield guaiacol and methyl guaiacol, respectively (Fig. 5-4 and Fig. 5-6c). This result also supports the association described in Fig. 5-8e.

The alcohol-type side chains of DHCA and homovanillyl alcohol had intermediate reactivity and were selectively deformylated (Fig. 5-6e). In addition, the conversion of DHCA to ethyl guaiacol did not require the addition of H₂ as discussed before. Conformational analysis revealed that a lone pair of OH oxygen electrons can be associated with the Pd/C surface, as illustrated in Fig. 5-8f. Ethyl guaiacol and formaldehyde can be generated directly from DHCA by intramolecular hydrogen transfer from OH to C_β at the four-center transition state. Furthermore, the generated formaldehyde may serve as a source of reactive hydrogen through the catalytic decomposition pathway of formaldehyde → H• + •CH=O and •CH=O → H• + CO.

Product selectivity was affected by the environment (H₂ or N₂) in the CA and DHCA treatments in Fig. 5-2 (350 °C for 60 min). Side-chain compositions (in mol%) are compared in Table 5-2. By changing from N₂ to H₂, the percentage of ethyl side chain increased from 59.6 to 70.1 mol% (CA) and from 65.9 to 80.0 mol% (DHCA). The selectivity increase can be explained with reference to Fig. 5-8f as follows. Deformylation in N₂ requires the adoption of the four-centered transition state, whereas in H₂, Pd/C-activated hydrogens are available, increasing the conformational flexibility of the OH group.

The role of hydroxymethyl groups as sources of reactive hydrogen is supported by the reactivity of DHCA and isoeugenol. Without the addition of H₂, DHCA was readily converted to ethyl guaiacol, whereas isoeugenol was very stable. Unreacted isoeugenol was recovered in 79.5% yield even after 60 min at 300 °C (Pd/C in N₂). Therefore, the in-situ production of reactive hydrogen species did not occur in the treatment of isoeugenol. In contrast, when a mixture of DHCA (10 mg) and isoeugenol (10 mg) was treated, 4.7 mg of propyl guaiacol was produced.

Table 5-2 Influences of environment (N₂ or H₂) on the side-chain composition of the guaiacols produced by catalytic hydrogenolysis of coniferyl alcohol and dihydroconiferyl alcohol at 350 °C for 60 min.

		Side chain composition (mol%)			
		Pr	Et	Me	H
Coniferyl alcohol	N ₂	18.6	59.6	9.7	13.1
	H ₂	12.0	70.1	7.7	5.9

Dihydroconiferyl alcohol	N ₂	24.6	65.9	5.9	6.7
	H ₂	8.3	80.0	0.0	9.4

Assuming that propyl guaiacol is produced from DHCA alone (24.6 mol% in Table 5-2), the yield of propyl guaiacol would be expected to be 2.3 mg. This discrepancy indicates that the hydrogenation of isoeugenol to propyl guaiacol must occur in the presence of DHCA. Reactive hydrogen species produced by the conversion of DHCA would be utilized for the hydrogenation of isoeugenol. These lines of evidence support the proposal of in-situ formation of reactive species from the catalytic conversion of hydroxypropyl group, probably via formaldehyde (Fig. 5-8f).

The reaction pathway of vanillin depended on the environment (H₂ or N₂). In the presence of Pd/C and H₂, methyl guaiacol (45 mol%) and guaiacol (47 mol%) were produced from vanillin through hydrogenation of C=O, followed by hydrodeoxygenation of benzyl alcohol and α -scission of the formyl radical intermediate, respectively (Fig. 5-6d). However, by changing the environment from H₂ to N₂, methyl guaiacol was not produced because of the limited amount of reactive hydrogen. Guaiacol was formed in N₂ because the α -scission pathway does not require H₂.

Two possible routes are considered for the conversion of coniferyl aldehyde to ethyl guaiacol (Fig. 5-6f), but it is currently unclear which one is suitable. Hydrogenation of conjugated C=C can occur as for CA, and when the aldehyde is reduced to an alcohol, ethyl guaiacol is produced via DHCA. However, the α -scission pathway via the formyl radical intermediate could also generate ethyl guaiacol.

At 250 °C, the conversion of DHCA to ethyl guaiacol proceeded to a greater extent with the treatment of CA than with DHCA (Fig. 5-2). This effect may be related to the high adsorption of CA on the Pd/C surface, as mentioned above. To confirm this hypothesis, the reactivities of CA and DHCA were compared using Pd/C and H₂ at 300 °C for a short duration (2 min). Coniferyl aldehyde and CA decomposed completely to give ethyl guaiacol selectively, but unreacted DHCA was recovered in 65.6% yield by treatment of DHCA. These results suggest that once CA and coniferyl aldehyde adsorbed on the Pd/C surface, successive transformations to the final products, mainly ethyl guaiacol, occur before desorption (Fig. 5-9).

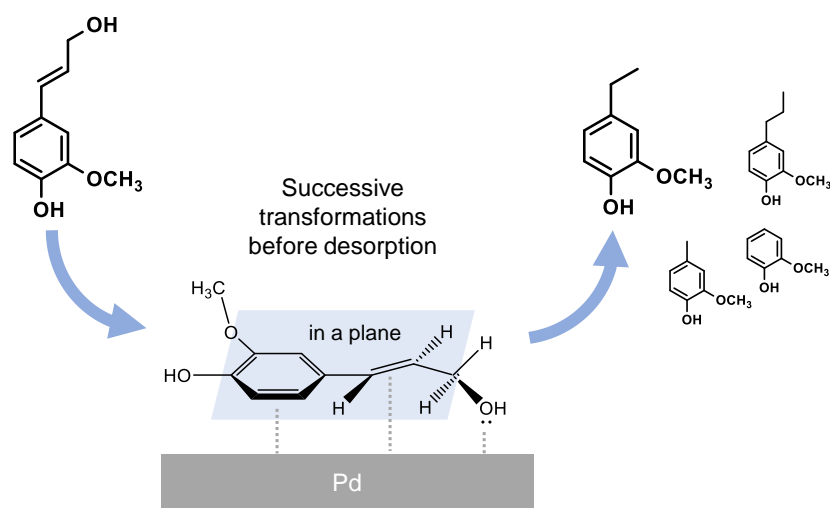


Fig. 5-9 Successive transformations proposed for catalytic hydrogenolysis of coniferyl alcohol with strong adsorption on the Pd surface.

5.4 Conclusions

Intermediate compounds formed by the pyrolysis of lignin were used to investigate the role of pyrolysis in the pyrolysis-assisted catalytic hydrogenolysis of lignin using Pd/C and H₂ in anisole at 300 and 350 °C. The following conclusions were drawn. The side-chain transformation of CA occurred instead of condensation during the pyrolysis of CA in anisole. By adding Pd/C in this system, the hydrogenation to DHCA, followed by deformylation to ethyl guaiacol, occurred much more efficiently than the pyrolytic conversion. No addition of H₂ was required because of the in-situ supply of reactive hydrogens by the decomposition of the product formaldehyde. Saturated alkyl (methyl, ethyl, and propyl) guaiacols were quite stable, so they are end products

along with non-substituted guaiacol. Side-chain functional groups formed by pyrolysis of lignin, particularly those with conjugated C=C and C=O bonds that can be coplanar with the aromatic ring, were highly reactive because of efficient adsorption onto the Pd/C surface. Successive transformations occurred before desorption. Intramolecular hydrogen transfer via a four-centered transition state was proposed to explain the deformylation of the alcohol-type side chains under N₂. Conjugated aldehydes and ketones were hydrogenated and subsequently hydrodeoxygenated to produce alkyl groups, whereas non-conjugated ketones adsorbed less effectively onto the catalyst for steric reasons and were thereby stable. Finally, routes from lignin to final products are proposed, including pyrolysis followed by catalytic conversion. These lines of information provide insights into lignin valorization by pyrolysis-assisted catalytic conversion.

Chapter 6

Solvent effect on monomer formation in pyrolysis-assisted catalytic hydrogenolysis of softwood lignin

6.1 Introduction

Our previous study has shown that the yield of monomers from softwood lignin can be increased to over 60% by catalytic hydrogenolysis conducted at higher temperatures, preferably $>300\text{ }^{\circ}\text{C}$, in anisole (phenyl methyl ether), an aprotic solvent. In this process, pyrolytic degradation of insoluble lignin into soluble intermediates occurs first, making subsequent catalytic reactions efficient (Fig. 6-1). In addition, thermally stable 4-*O*-5 and condensed C–C linkages are catalytically cleaved at such high temperatures. Formation of α -aryl bonds by condensation via a quinone methide (QM) intermediate occurs during pyrolysis and pulping processes and suppresses the monomer production. Since the α -aryl bonds efficiently cleave by pyrolysis-assisted catalytic hydrogenolysis, this method was also demonstrated to be effective for organosolv lignin, a technical lignin. Undesired aromatic-ring saturation was also effectively suppressed at such high temperatures.

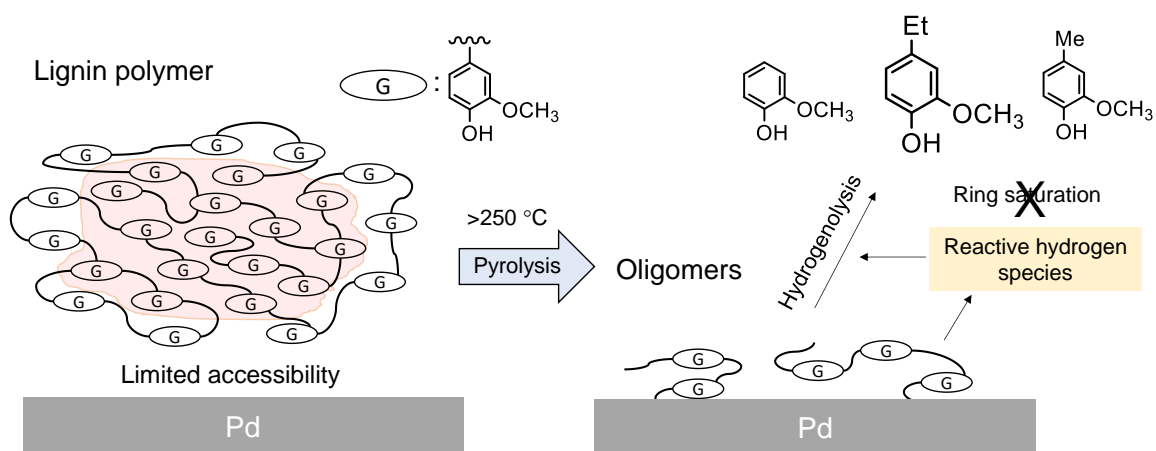


Fig. 6-1 A proposed scheme for the production of monomers from lignin polymers under pyrolysis-assisted catalytic hydrogenolysis conditions

We already reported that the composition of lignin-derived monomers depended on the chemical structure of the intermediates formed by pyrolysis. Solvent type may affect the pyrolysis and subsequent catalytic hydrogenolysis processes of lignin. Various studies reported the yield and composition of monomers in high temperature treatment of softwood lignins in water,(Phaiboonsilpa et al., 2010) methanol,(Minami and Saka, 2003) dioxane,(Dorrestijn et al., 1999) and 1,3-diphenoxybenzene(Kotake et al., 2014) under pyrolysis (no catalyst) conditions. To our best knowledge, there are no systematic works on the solvent effects in the pyrolytic conversion of lignin to monomers, dimers and oligomers, which subsequently undergo catalytic conversions.

For conventional catalytic hydrogenolysis approaches, various solvents including methanol, ethanol, dioxane, water, and their binary mixtures have been utilized, but there are only few studies discussing solvent effects. Schutyser et al.(Schutyser et al., 2015) compared the monomer yields by conducting catalytic hydrogenolysis of birch wood lignin in hexane, dioxane, tetrahydrofuran, alcohols, or water at 200 °C and reported that the monomer yield varied from 1.8 % (in hexane) to 43.8 % (in water) depending on the solvent. However, the temperature 200 °C is too low for lignin pyrolysis to occur effectively. Héroguel et al. (Héroguel et al., 2019) conducted the hydrogenolysis of aldehyde-stabilized beech wood lignin in isooctane at 250 °C, but their major products were cyclohexanes and cyclohexanones with the total yield only 13%.

In this study, solvent effects on pyrolysis-assisted catalytic hydrogenolysis of milled wood lignin (MWL) isolated from Japanese cedar (*Cryptomeria japonica*) wood were studied by using Pd/C in various solvents. Since lignin is rapidly degraded at 350 °C,(Asmadi et al., 2011a; Nakamura et al., 2008) this temperature was chosen throughout the experiments. Model compound studies using coniferyl alcohol (CA) were conducted first under both pyrolysis (no Pd/C in N₂) and catalytic (Pd/C in N₂ or H₂) conditions, since CA is the important primary pyrolysis product formed by the cleavage of β -ether bond that is the most abundant linkage type in lignin.(Kawamoto and Saka, 2007) Then, the results of MWL are discussed with the CA data. The solvents used are categorized to protic (water and methanol), aprotic (anisole, toluene, and 1,4-dioxane) and hydrophobic (hexane) types.

6.2 Experimental

6.2.1 Materials

Coniferyl alcohol, and milled wood lignin (MWL) were prepared with the same methods as described in section 5.2.1, and section 3.2.1.

6.2.2 Thermal reaction

The thermal reaction of the monomeric model compounds was conducted in a sealed 5-mL batch reaction vessel, as described in section 3.2.2. In each trial, 10 mg of solid reaction compound were placed in the vessel with optional addition of 10 mg of 5% Pd/C (EP, Nacalai Tesque). After the loading of 2 mL of solvent (water, methanol, acetone, dioxane, anisole, toluene, benzene, hexane), the space left in the vessel (approximately 3 mL) was filled with H₂ or N₂ at 1 atm. The added H₂ was equivalent to a molar about 2.4 times relative to the mole number of phenylpropane units in 10 mg sample. The vessel was then immersed in a salt bath preheated to a temperature in the range of 350 °C for the thermal reaction with agitation. After a set time, the reaction was quenched by transferring the vessel to a water bath.

After the reaction, the contents of the vessel were washed several times with methanol (18 mL in total) to recover the turbid reaction mixture, which contained the derived products, Pd/C, and anisole. In the case of water as the solvent, EtOAc was used to extract the reaction products in water, and to wash the reaction vessel. A portion of the suspension was centrifuged to remove Pd/C before analysis.

6.2.3 Product analysis

Molecular weight distribution of the methanol-soluble products was determined by GPC. Analysis by GC-MS was performed to quantify the products in the reaction mixture after trimethylsilyl derivatization. The methods for products analysis were same with the description in section 3.2.3.

The molar yield, M_i , of each monomeric product, i , was calculated as:

$$M_i \text{ (mol\%)} = \frac{\text{Mass of } i}{\text{MW of } i \times n} \times 100,$$

Herein, n is the number of moles of the model compound treated, calculated as:

$$n(\text{mol}) = \frac{\text{Sample mass (approximately 0.01 g)}}{\text{Average MW of model sample}}.$$

The average MW values of the phenylpropanoid units in the MWL from softwood was be 182 Da as described in section 3.2.3

6.3 Results and discussion

6.3.1 Pyrolysis of coniferyl alcohol (CA)

Coniferyl alcohol (CA), a major primary pyrolysis product from softwood lignin, was heated with solvent at 350 °C for 60 min in a closed batch reaction vessel under pyrolytic (no Pd/C in N₂) and catalytic (Pd/C in N₂ or H₂) conditions. The amount of H₂ (3 mL) introduced into the vessel at 0.1 MPa corresponds to 2.4 times moles of CA under the catalytic hydrogenolysis conditions. Gel permeation chromatographic (GPC) profiles of the reaction mixtures are shown in Fig. 6-2. The total yields and compositions of the identified monomers are summarized in Fig. 6-3 and Fig. 6-4, respectively, and the chemical structures and abbreviations of monomers are given in Table 6-1.

Under the pyrolysis conditions (no Pd/C in N₂), the product compositions varied greatly with solvent type. In the GPC profiles (Fig. 6-2), broad signals at retention times shorter than that of CA are clearly observed when water or methanol was used as a solvent. This indicates that coniferyl alcohol tended to condense in these protic solvents, resulting in relatively low monomer yields (27.2 mol% for water and 30.0 mol% for methanol, Fig. 6-3). As illustrated in Fig. 6-5, quinone methide (QM) intermediates would be produced from CA as precursors of condensation in water and methanol, where proton transfer from phenolic OH to C_β or C_γ-oxygen, which is required for the QM formation, occurs by solvation of these protic solvents.

Kotake et al. found that the QM formation from CA was effectively suppressed in diphenoxybenzene, an aprotic solvent, and when CA or lignin was pyrolyzed in this solvent, condensation was effectively inhibited to increase the monomer yield. In aprotic solvents, proton

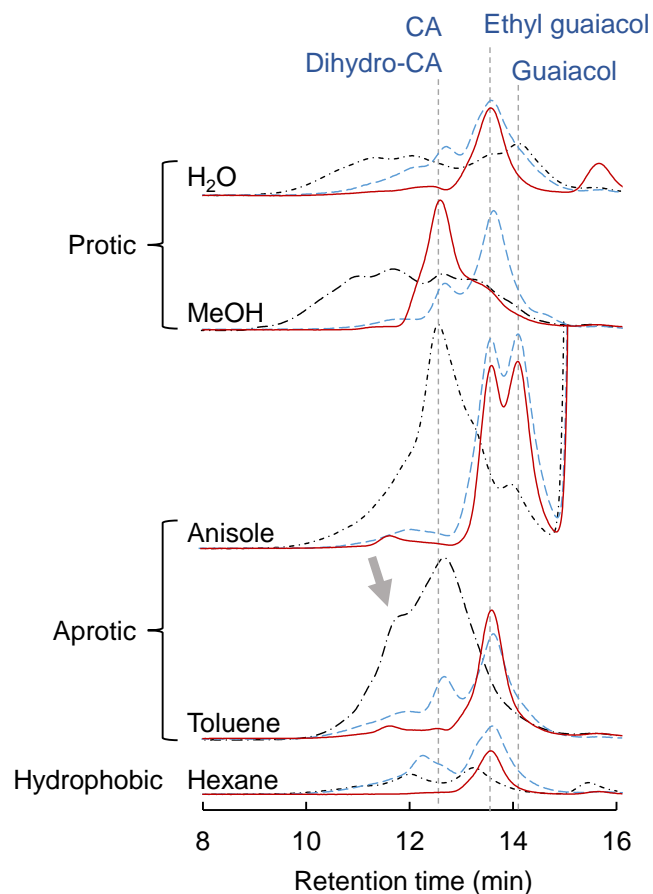


Fig. 6-2 Gel-permeation chromatograms of the reaction mixtures obtained from coniferyl alcohol (CA) after treatment at 350 °C for 1 h in different solvents. Dotted and dash black line: N₂; dash blue line: Pd/C, N₂; solid red line: Pd/C, H₂.

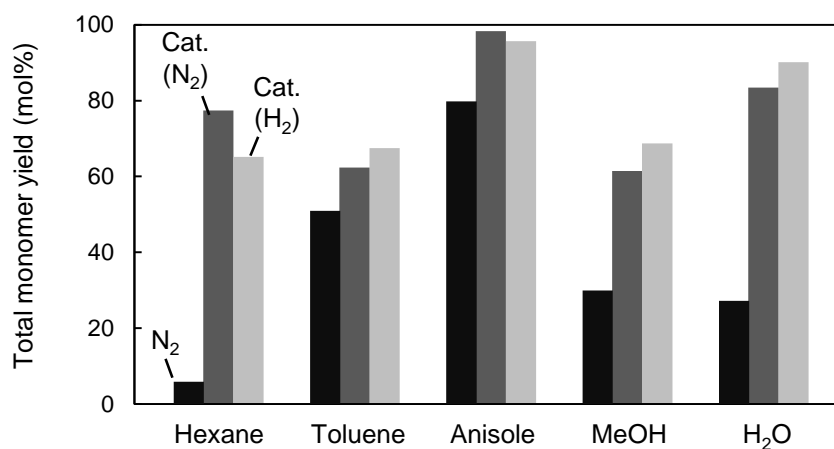
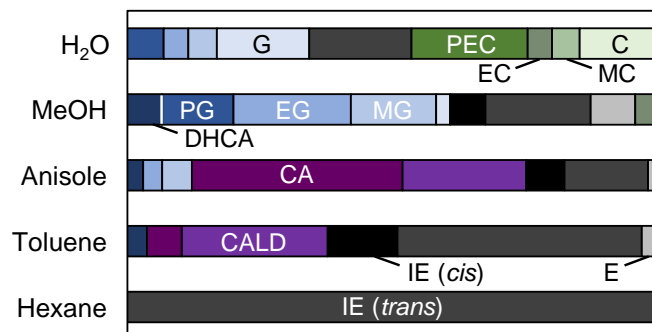
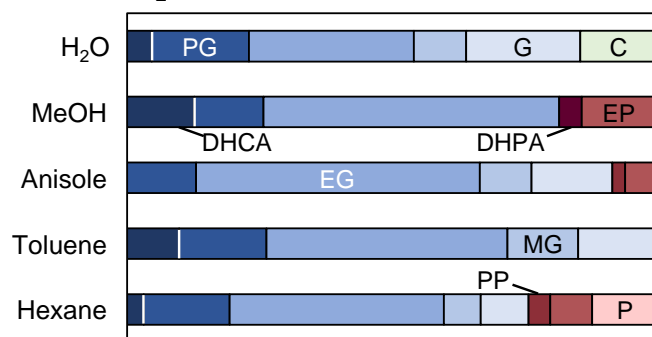


Fig. 6-3 Total monomer yield from coniferyl alcohol after treatment at 350 °C for 1 h in different solvents. Black column: N₂; dark grey column: Pd/C, N₂; light grey column: Pd/C, H₂.

A. No catalyst/ N₂



B. Pd/C/N₂



C. Pd/C/ H₂

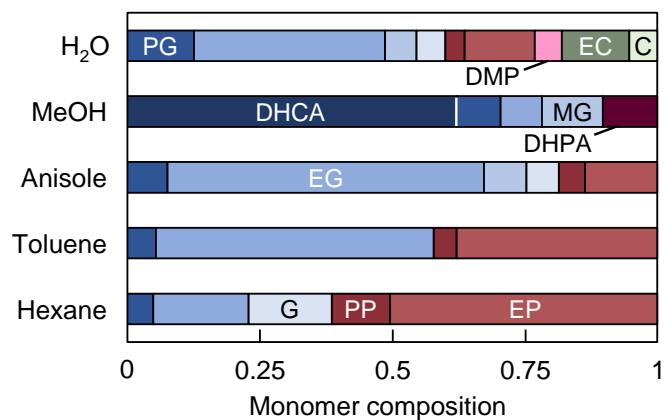
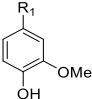
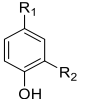
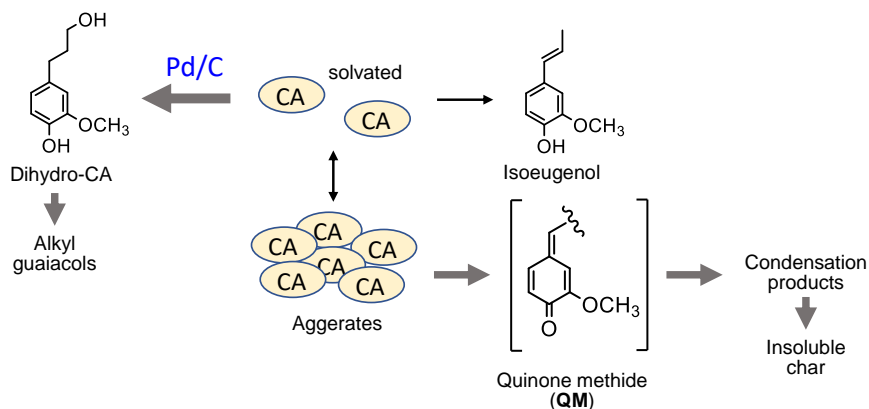


Fig. 6-4 Monomer composition in the products obtained from coniferyl alcohol after treatment at 350 °C for 1 h in different solvents. (a): N₂; (b): Pd/C, N₂; (c): Pd/C, H₂. See Table 1 for full names of all legends.

Table 6-1 Chemical structures and abbreviations for various monomeric products.

	Legends	R ₁		Legends	R ₂	R ₁
Coniferyl alcohol	CA	CHCH ₂ CH ₂ OH	<i>p</i> -Coumaryl alcohol	DHPA	H	CH ₂ CH ₂ CH ₂ OH
Coniferyl aldehyde	CALD	CHCHCHO	Propyl phenol	PP	H	CH ₂ CH ₂ CH ₃
Isoeugenol (<i>cis</i>)	IE (<i>cis</i>)	CHCHCH ₃	Ethyl phenol	EP	H	CH ₂ CH ₃
Isoeugenol (<i>trans</i>)	IE (<i>trans</i>)	CHCHCH ₃	Methyl phenol	MP	H	CH ₃
Eugenol	E	CH ₂ CHCH ₂	Phenol	P	H	H
Propiovanillone	PO	COCHCH ₃	<i>o</i> -Methyl phenol	<i>o</i>-MP	CH ₃	H
Acetovanillone	AO	COCH ₃	<i>m</i> -Methyl phenol	<i>m</i>-MP	H	H
Dihydroconiferyl alcohol	DHCA	CH ₂ CH ₂ CH ₂ OH	Dimethyl phenol	DMP	CH ₃	CH ₃
Propyl guaiacol	PG	CH ₂ CH ₂ CH ₃	Propenyl catechol	PEC	OH	CHCHCH ₃
Ethyl guaiacol	EG	CH ₂ CH ₃	Ethyl catechol	EC	OH	CH ₂ CH ₃
Methyl guaiacol	MG	CH ₃	Methyl catechol	MC	OH	CH ₃
Guaiacol	G	H	Catechol	C	OH	H

A. Hexane



B. Other solvents

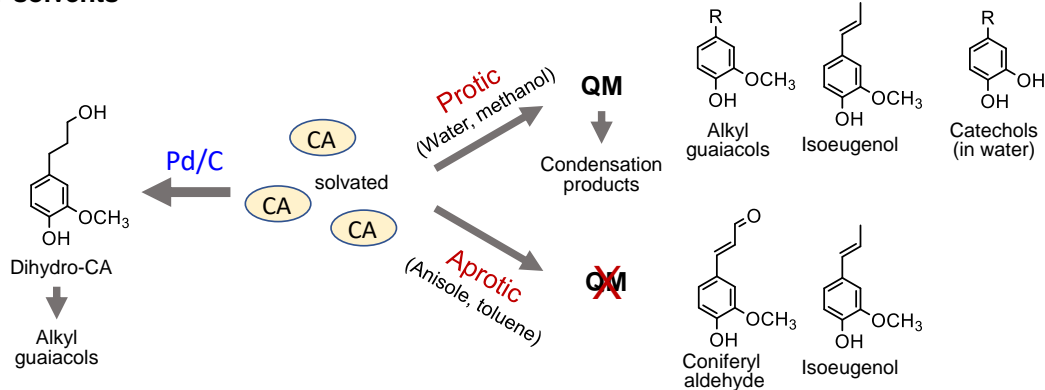


Fig. 6-5 Proposed conversion pathways of CA depended by the properties of the solvent at 350 °C.

transfer required for the QM formation is inhibited by solvation. The GPC profiles of the reaction mixtures obtained in anisole and toluene can be explained by this inhibitory effect. This is supported by the higher monomer yields with anisole (79.8 mol%) and toluene (50.9 mol%) than with water and methanol. The lower monomer yield obtained in toluene than in anisole is due to coupling of radical species formed from monomers with those from toluene as explained below. The radical coupling products would be observed as a shoulder with arrow at 11.7 min in the GPC profile (toluene).

In hexane, intensity of the GPC signals is comparatively small, and the monomer yield was limited to 5.9 mol%. Alternatively, a black residue (char) was generated in the pyrolyzates only when hexane was used as a solvent. This indicates that CA tended to condense and was converted into solid carbonized substances. As shown in Fig. 6-5, the solubility of CA is very limited in hydrophobic hexane, and hence CA molecules would aggregate, and the condensation via QM intermediates is expected to occur, as the proton transfer required for the QM formation is enabled by the interaction of CA molecules, like the action of protic solvents. Only a small portion of CA is soluble in hexane and converted to monomeric products.

Chemical structures of monomers also depended on the solvent type under the pyrolysis conditions (Fig. 6-4a). The side chain of CA is known to transform into oxidized and reduced structures, thus redox-type reactions occur during pyrolysis. The monomer compositions obtained in anisole and toluene are explainable with the redox-type reactions (Fig. 6-6). Some

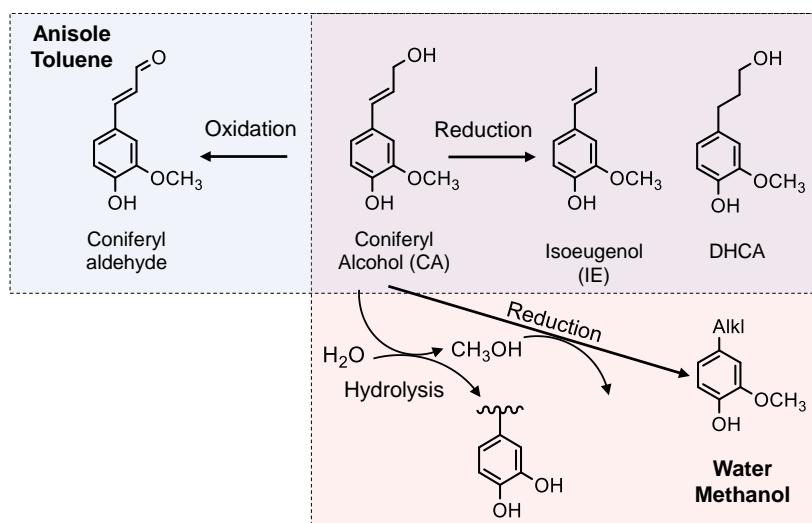


Fig. 6-6 Proposed solvent effects on the redox reactions of coniferyl alcohol in pyrolysis.

CA was oxidized to coniferyl aldehyde but some was reduced to isoeugenol, eugenol and dihydroconiferyl alcohol (DHCA). For anisole, the molar ratio of oxidation/reduction products was close to 1 (1.6 times). In hexane, only isoeugenol was detected as a monomer, but the yield was only 5.9 mol%. The reason is currently unknown, but this is likely due to the low solubility of CA and CA-derived products in hydrophobic hexane. Polar products would aggregate and be converted to char as described above.

The monomer compositions obtained in water and methanol were quite different from those obtained in other solvents. Hydrolysis products (catechol and methyl, ethyl and propenyl catechol) and a methanolysis product (methyl catechol) were detected in water and methanol in 46.7 mol% and 4.6 mol%, respectively.

Alkyl guaiacols are the major products formed under catalytic hydrogenolysis conditions with Pd/C (Fig. 6-4b and 4c). However, it is noted that any oxidation products of CA were not detected in water and methanol, but that all detectable monomers were reduction products including isoeugenol, eugenol, DHCA, and alkyl guaiacols (Fig. 6-4a). The yield of alkyl guaiacols reached 51.6 mol% in methanol, followed by in water (16.8 mol%) and in anisole (9.1 mol%). These results suggest that methanol has the ability to reduce CA and other intermediates (Fig. 6-6). In our previous study, the hydroxypropyl side chain of dihydroconiferyl alcohol was converted to ethyl group through deformylation, releasing reactive hydrogens that were utilized for catalytic hydrogenolysis. Based on this observation, methanol would be converted to formaldehyde and reactive hydrogens. Formaldehyde would further degrade into CO and reactive hydrogen, although further study is necessary to conclude this proposal. The methoxy groups of the guaiacyl units are hydrolyzed in water to form methanol, although it is not certain whether water has reducing ability. Anisole also has a methyl ether structure that serves as a source of methanol, but no evidence was available for the formation of methanol from anisole.

6.3.2 Catalytic hydrogenolysis of coniferyl alcohol (CA)

By using Pd/C, the monomer composition became similar regardless of the type of solvent. Ethyl guaiacol was the major component along with other hydrogenated products (DHCA, guaiacol and methyl, and propyl guaiacol). The reaction atmosphere (N₂ or H₂) had little effect on the monomer composition, with a few exceptions (DHCA in methanol, phenols, and propyl

guaiacol). These exceptions will be discussed below. These observations support previous proposal; hydrogen is not a required element as reactive hydrogen species are generated in situ.

The transformation pathways of the pyrolysis products in Fig. 6-4a to guaiacol and methyl, ethyl, and propyl guaiacol have already been reported in previous papers (isoeugenol and eugenol \rightarrow propyl guaiacol, CALD and DHCA \rightarrow ethyl guaiacol). On the other hand, saturated alkyl groups are very stable under the present reaction conditions. Therefore, the monomer compositions can be mostly explained by catalytic conversion of pyrolysis products in Fig. 6-4a.

Monomer yields in water, methanol, and hexane significantly improved by the addition of Pd/C (27.2 mol% \rightarrow 83 mol% for water, 30.0 mol% \rightarrow 61 mol% for methanol, and 5.9 mol% \rightarrow 77 mol% for hexane). These results can be explained by the competition between pyrolytic condensation and catalytic conversion. Catalytic conversions would occur more efficiently than the pyrolytic condensation. This was supported by the GPC chromatograms obtained in water and methanol (Fig. 6-2), which show almost no condensation product signal in the presence of Pd/C. The significant improvement in monomer yield in hexane is worth noting. Even in the poor solvent for CA, the Pd/C-mediated catalytic transformation proceeded very efficiently. In the case of anisole and toluene, the monomer yields did not change significantly due to the effective inhibition of pyrolytic condensation in these aromatic (aprotic) solvents.

By changing the reaction atmosphere from N₂ to H₂, the contribution of propyl guaiacol tended to decrease, which can also be argued in terms of competition between pyrolysis and catalytic conversion. As mentioned above, propyl guaiacol is mainly produced from isoeugenol and eugenol, pyrolysis products, while CA is directly converted to ethyl guaiacol via DHCA by catalytic process. The contributions of propyl guaiacol were reduced in all solvents by changing the atmosphere from N₂ to H₂. This can be explained because of the reaction conditions that favor catalytic hydrogenolysis.

As reported in the literature, the conversion of guaiacol to phenol by demethoxylation proceeded more efficiently under H₂ than N₂. Interestingly, the conversion rate from guaiacols to phenols were directly related to the polarity of solvent except water [phenols/guaiacols molar ratio: 1.6 (hexane) > 0.7 (toluene) > 0.2 (anisole) > 0.1 (methanol), Fig. 6-4c]. In water, phenols were produced more efficiently than in methanol, presumably through catechol formed by hydrolysis. In a model experiment using guaiacol or catechol under the similar reaction conditions in H₂ (Fig. 6-7), catechol was converted to phenol in 67 mol% yield. Interestingly,

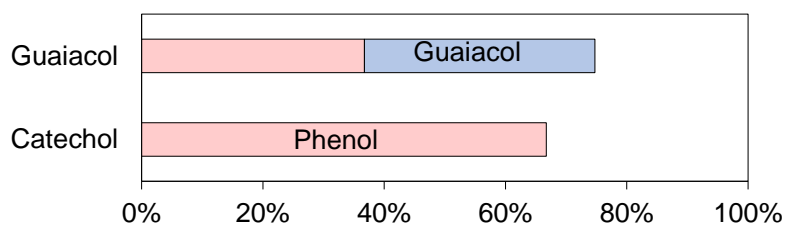


Fig. 6-7 Monomers obtained from pyrolysis assisted catalytic hydrogenolysis of guaiacol and catechol in water at 350 °C for 60 min. (reaction compound: 10 mg, Pd/C: 10 mg; water: 2 mL; H₂: 3mL/0.1 MPa).

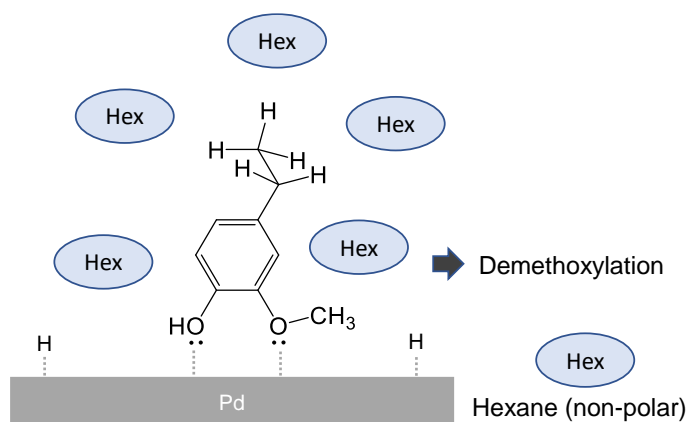


Fig. 6-8 Proposed effect of hexane on the adsorption manner of monomer products in pyrolysis-assisted hydrogenolysis process.

phenol was obtained from guaiacol in 36.7 mol% yield, but catechol was not produced. These results indicate that the conversion of catechol to phenol occurs very rapidly once catechol is formed.

There has been research activity on catalytic demethoxylation, and it has been proposed that the selectivity of ring saturation and demethoxylation is governed by the association type between the compound and the catalytic surface. As shown in Fig. 6-8, the association in which the aromatic compounds are arranged perpendicular to the catalyst surface is thought to work favorably for the demethoxylation reaction. In the non-polar solvent, the methyl, ethyl, and propyl side chains are more efficiently solvated, whereas polar hydroxyl and methoxyl groups are forced to face the polar Pd surface, facilitating such association.

Another important influence of the reaction atmosphere is the yield of DHCA in methanol.

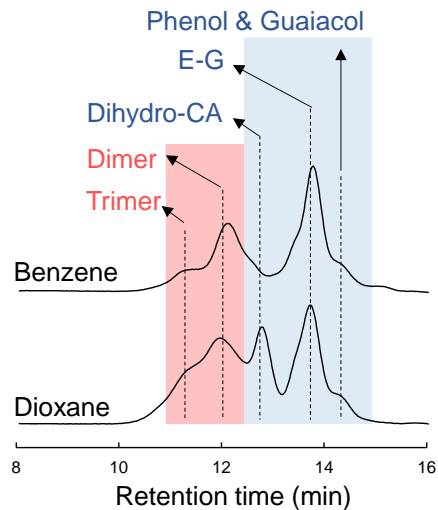


Fig. 6-9 GPC chromatograms of products obtained from pyrolysis-assisted catalytic hydrogenolysis of MWL after treatment at 350 °C for 30 min in benzene and dioxane.

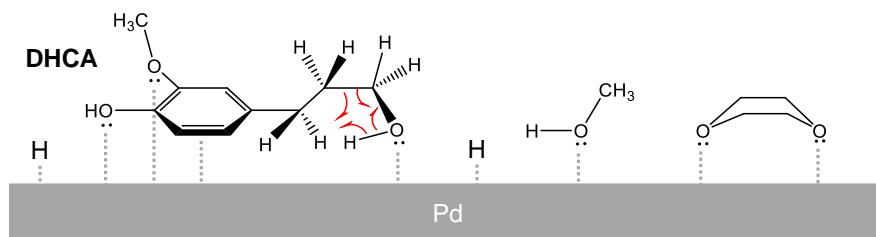


Fig. 6-10 Proposed association manners of DHCA, methanol, and dioxane on Pd surface during pyrolysis-assisted hydrogenolysis process.

Under catalytic hydrogenolysis conditions, DHCA is converted to ethyl guaiacol, whereas H_2 rather inhibited the conversion. Similar results were observed with dioxane (GPC chromatogram in Fig. 6-9 and Fig. 6-2). In other solvents, this reaction was promoted with H_2 and DHCA was not detected under H_2 . Therefore, solvents must be involved in these unexpected results. A rational explanation for the inhibition of DHCA hydrogenolysis in methanol and dioxane is currently elusive, but may involve association of DHCA, methanol, and dioxane on the Pd surface (Fig. 6-10). In our previous paper, it was proposed that the deformylation of DHCA proceeds via a four-center transition state on the Pd surface, even in the absence of H_2 . Methanol and dioxane may also bind to the Pd surface in a similar manner. H_2 effects on these association competitions may be involved, but further studies are needed to explain these unexpected results.

6.3.3 Monomer formation from MWL in different solvents

Other pyrolysis products such as vanillin are also produced from the pyrolysis of MWL along with CA. Radical species contribute more in the MWL reaction, as the pyrolytic cleavage of the ether bond occurs mainly through a homolysis mechanism, forming radical species as the primary pyrolysis products. These differences should be noted when discussing MWL reactivity with CA results. The monomer yields and compositions obtained from Japanese cedar MWL in different solvents at 350 °C for 30 and 60 min are summarized in Fig. 6-11. Yield (60 min)/yield (30 min) ratio is also included in this figure to understand the effect of treatment duration. The anisole results have been reported in our previous paper.

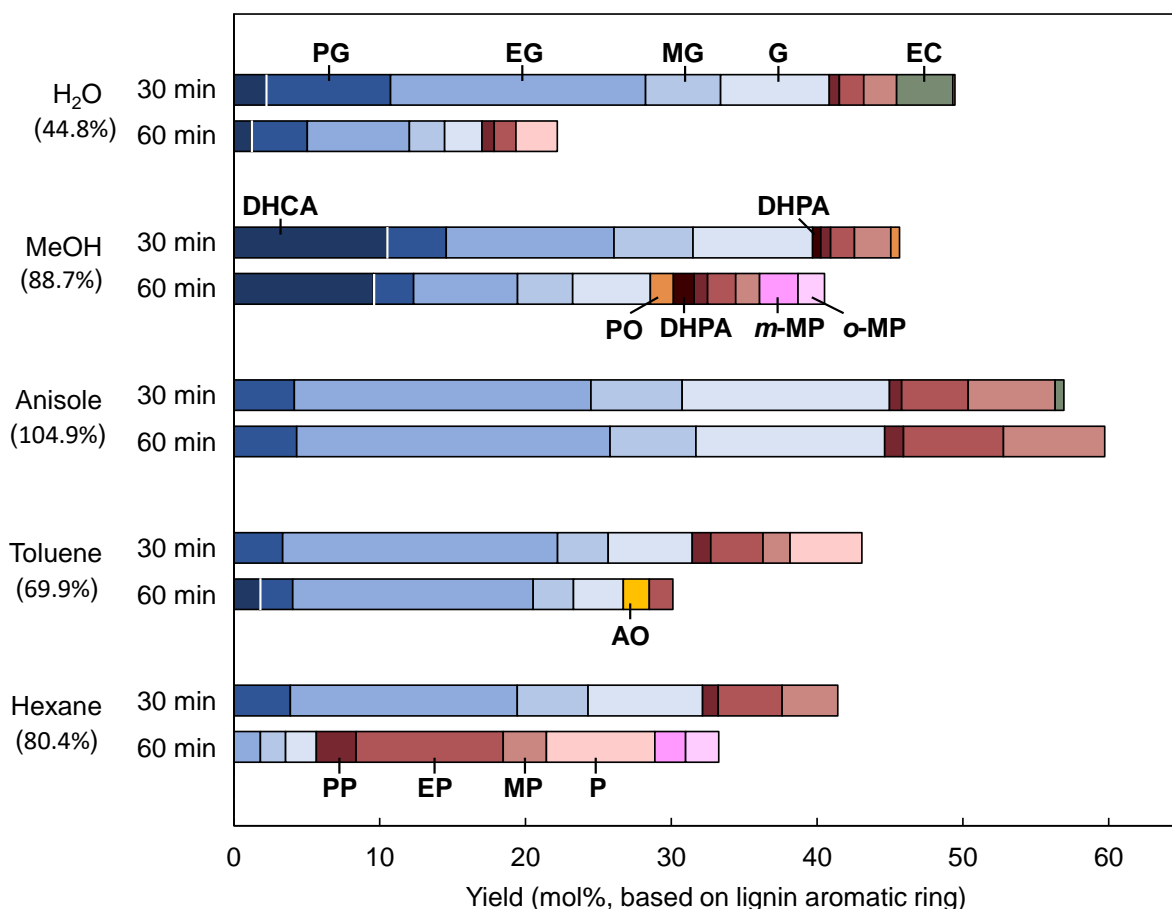


Fig. 6-11 Monomers obtained from pyrolysis-assisted catalytic hydrogenolysis of Japanese cedar MWL in different solvents at 350 °C. (MWL: 10 mg, Pd/C: 10 mg; solvent: 2 mL; H₂: 3mL/0.1 MPa). Percentage in parenthesis is the total monomer yield at 30 min as compared with that at 60 min.

The monomer yields at 30 min follow the same order as observed for CA (60 min) [anisole (56.9 mol%) > water (49.5 mol%) > methanol (45.7 mol%) > toluene (43.1 mol%) > hexane (41.4 mol%), value in parenthesis: monomer yield from MWL]. However, increasing the reaction time from 30 to 60 minutes decreased the yields for most solvents except anisole, while the yield increased slightly in anisole. In particular, the reduction rate in water was as high as 44.8%. This can be explained by hydrolysis of the methoxyl group of the guaiacyl unit. In a model experiment (Fig. 6-7), only 74.8 mol% and 66.7 mol% of aromatic monomers were recovered from guaiacol and catechol, respectively, producing phenol as the sole monomer product. These results indicate that the monomeric products formed from MWL in water undergo further degradation via catechol-type intermediates (Fig. 6-12a). In water, ethyl catechol was produced in 3.9 mol% at 30 min, but any catechol derivatives were not detected at 60 min.

Another type of side reaction was shown for methanol, toluene and hexane to explain the yield loss with extended reaction time. Careful analysis of the products from CA detected various radical coupling products formed by the addition of solvent-derived radicals to the side-chain C=C bonds of CA and its pyrolytic intermediates (Fig. 6-13, Fig. 6-12b). Methyl radical, benzyl radical, and hexyl radical would be produced from methanol, toluene, and hexane,

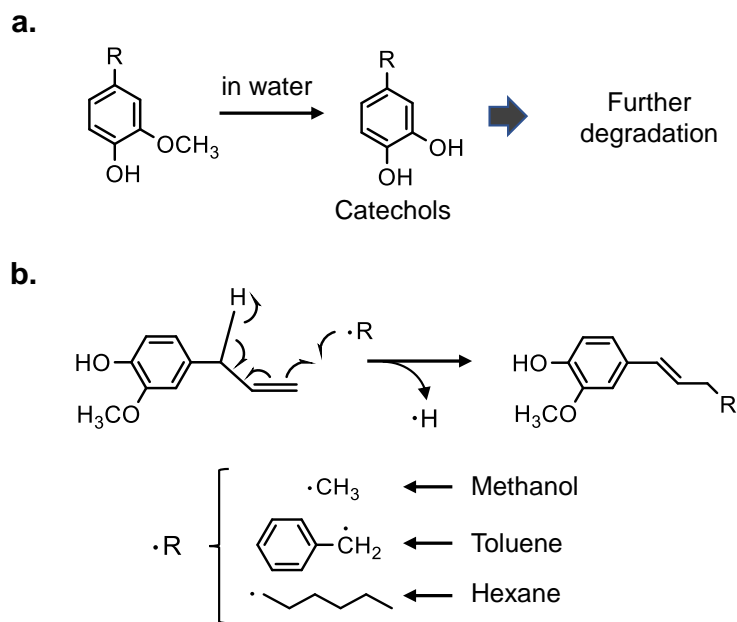


Fig. 6-12 Side reactions as expected to occur during pyrolysis-assisted catalytic hydrogenolysis of coniferyl alcohol.

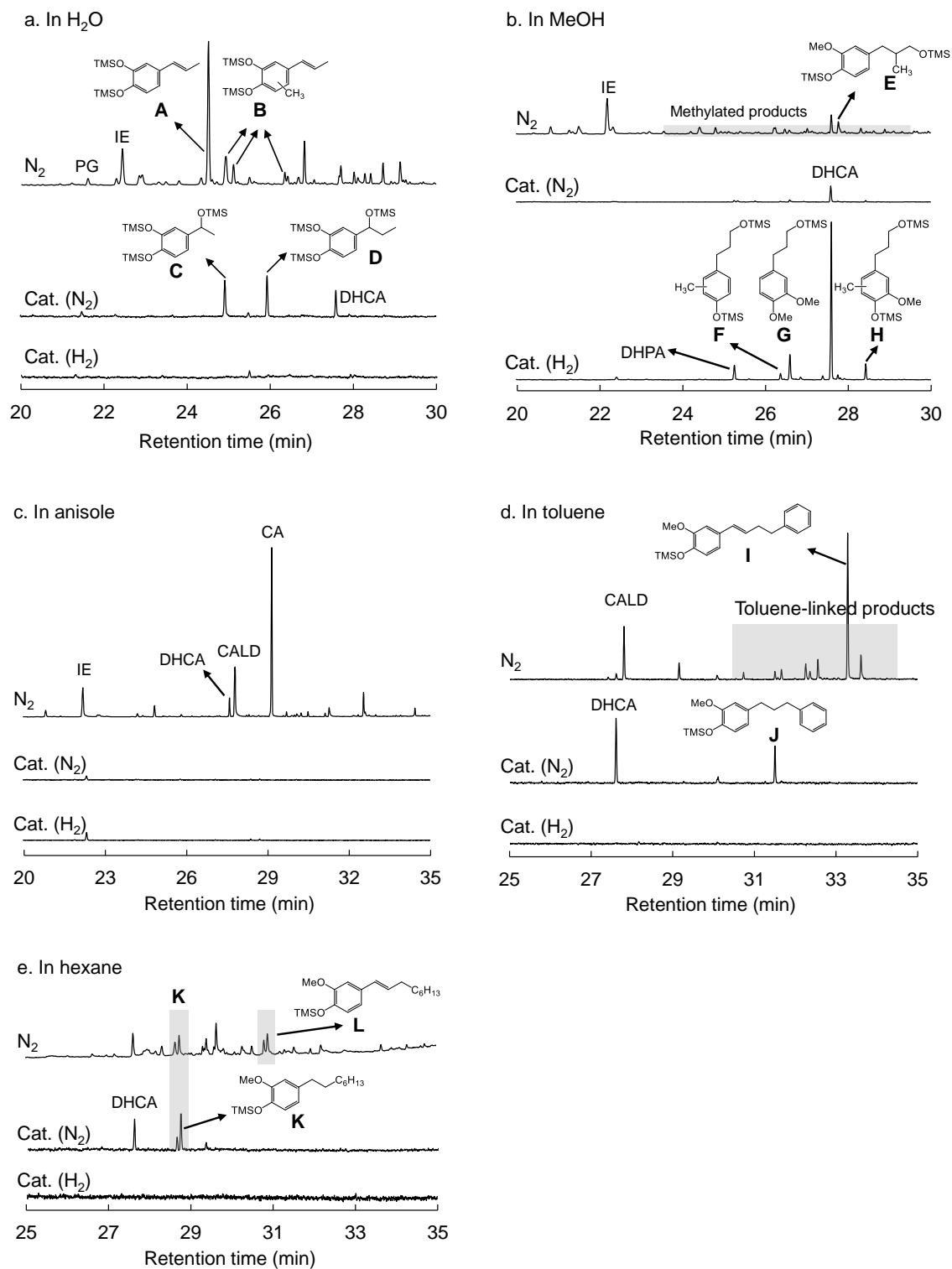


Fig. 6-13 GC/MS total ion chromatograms of the TMS-derivatives of reaction mixtures obtained from coniferyl alcohol through thermal treatment in (a) water, (b) methanol, (c) anisole, (d) toluene, (e) hexane at 350 °C after treatment with 60 min.

respectively, under the pyrolysis-assisted catalytic hydrogenolysis conditions. Ortho- and meta-methyl phenol detected from MWL in methanol (60 min, Fig. 6-11) would be formed by the coupling of methyl radicals to phenol. Interestingly, methylation products were also detected from CA in water and methanol (Fig. 6-13), indicating that methyl radical was formed via the methanol produced by the hydrolysis of the methoxyl group. These radical coupling reactions would occur favorably in MWL than in CA, because the lignin ether bonds in MWL are homolytically cleaved, resulting in a more radical state of the reaction medium.

Such undesired reactions were not detected in anisole, resulting in high monomer yield and high monomer stability. Therefore, anisole is the solvent of choice for monomer production from MWL. The monomer yield was the highest among the solvents used in this study, and prolonged treatment did not reduce the yield.

The characteristic feature of solvent for monomer composition observed in CA were also observed in MWL (Fig. 6-11). Dihydroconiferyl alcohol (DHCA) contributed more in methanol and could not be completely hydrogenated to ethyl guaiacol even at 60 min. The smaller contribution of DHCA in the monomers obtained from MWL than from CA may be due to less available H₂ for the MWL reactions. Hydrogen would be consumed for stabilization of radical species formed by homolysis of lignin ether bonds. Vanillin and other carbonyl compounds formed through other lignin pyrolysis reactions also consume hydrogen.

As observed for CA, the formation of phenols by demethoxylation was prominent in hexane, and the content of phenols in the monomer reached 61.500 mol% in hexane at 60 min. On the other hand, the yield of phenols in toluene was much lower than expected from the CA results. This is likely due to radical coupling of the product phenols with the benzyl radical formed from toluene. Unlike the CA reaction, the lignin ether bonds are homolytically cleaved, resulting in a more radical state of the reaction medium. Under such conditions, radical coupling reactions predominate. Phenols are more reactive for radical coupling than guaiacols because they have another ortho carbon as a coupling site. Easier radical formation from toluene than from hexane due to the formation of the more stable benzyl radical might explain the difference in the yields of phenols. Anyway, hexane is the best solvent for phenol production from lignin among the solvents used in this study. Phenols are the potential commodity chemicals in chemical industry.

6.4 Conclusion

Solvent effects on pyrolysis-assisted catalytic hydrogenolysis of CA (the major pyrolysis product of lignin) and MWL isolated from Japanese cedar were investigated at 350 °C by using Pd/C and various solvents. The following conclusions were obtained. Under the pyrolysis (no catalyst in N₂) conditions, CA condensed in protic solvents (water and methanol) but not in aprotic solvents (anisole and toluene). In hydrophobic hexane, solubility of CA was low and condensation occurred on insoluble aggregates to form char. Hydrolysis of the methoxyl group of CA took place in water. Redox reactions of CA occurred for in anisole and toluene, but no oxidation products were detected in methanol and water, probably due to the reducing ability of methanol.

These characteristic features of pyrolysis of CA almost disappeared by the addition of Pd/C, indicating that catalytic hydrogenolysis proceeded very efficiently even under N₂. Production of phenols by demethoxylation also occurred over Pd/C, particularly under H₂, and the efficiency from CA was inversely related to the solvent polarity. Unexpectedly, hydrogenolysis of DHCA to ethyl guaiacol was inhibited by changing the atmosphere from N₂ to H₂ only in methanol. The transformation of MWL were basically explained by the CA results except for some side reactions caused by the more radical state of the reaction medium of MWL, since the lignin ether bonds homolytically cleave. Degradation via catechols formed by hydrolysis (water) and radical coupling reactions with radicals formed from solvents (methanol, toluene, and hexane) reduced the monomer yield, especially in long treatments. Based on these results, anisole was the best solvent for monomer production from MWL, and hexane was the best solvent for the production of phenols from MWL.

Chapter 7

Concluding Remarks

7.1 Conclusions

The monomer production behavior from softwood lignin by the pyrolysis assisted catalytic hydrogenolysis were studied. Since the pyrolysis process is likely prior to the catalytic process, the author started the research with pyrolysis, followed by pyrolysis-assisted catalytic hydrogenolysis.

In *chapter 2*, the decomposed products from Japanese cedar pyrolysis at 270–380 °C in an aprotic solvent with a hydrogen donor were fractionated to four fractions, and the lignin-derived products were analyzed in detail. The yield of lignin-derived oligomer was limited to approximately 20 wt% (lignin basis) at 270 °C, and increased to 80% at > 300 °C. The α - and β -ether bonds in proto-lignin were cleaved to form γ -hydroxypropyl. A portion of β -ether structure was transformed to vinyl ether. In the contrast, condensed type β - β , β -aryl and 5-5' bonds remained, and the β -aryl type existed as stilbene in the oligomer. The obtained lignin-derived oligomer was rich in phenolic and alcohol OH groups.

In *chapter 3*, Pd/C was added to the pyrolysis of milled wood lignin with the aim to break the recalcitrant 4-*O*-5, and condensed bonds for monomer yield improvement. The monomer yield was increased from 27 to 60 mol% when temperature rising from 200 to 350 °C. In the meantime, the main monomer products changed from dihydroconiferyl alcohol to guaiacol and alkyl guaiacols. Dimer model studies revealed that 4-*O*-5-, α -aryl bonds were cleaved, while 5-5 bond was still not cleaved. The undesirable saturation of aromatic rings was also suppressed over Pd/C catalyst during pyrolysis-assisted catalytic hydrogenolysis of the lignin. This approach was also applicable to organosolv lignin, giving monomers in 43.5 mol% yield at 350 °C.

In *chapter 4*, the degradation behavior of pinoresinol (β - β structure) in pyrolysis-assisted catalytic hydrogenolysis was investigated. C-C bonds in β - β were hard to cleaved. Limited monomers were obtained along with naphthalene products, and the dimers were main products. THF- and tetralin-type side chains were formed at 250-300 °C, and phenylnaphthalene structures

were formed at 350 °C. these results provide one explanation for the polycyclic aromatic hydrocarbons formation during lignin pyrolysis.

In *chapter 5*, the reactivities of various intermediate products from lignin pyrolysis in pyrolysis-assisted catalytic hydrogenolysis using Pd/C and H₂ in anisole at 300 and 350 °C were investigated to understand the role of pyrolysis on monomer formation behavior. Saturated alkyl side chains (methyl, ethyl, and propyl) were very stable, and they were not reacted. Unsaturated C=C bonds were hydrogenated to saturated alkyls. Conjugated α -ketone changed to -CH₂-, while conjugated aldehydes underwent deformylation through α -scission. Deformylation also proceeded for side chains bearing OH groups. Lignin pyrolysis intermediates containing conjugated C=C and C=O groups had particularly high affinity for Pd/C, and their reaction could finish in 2 min. Therefore, the composition of side-chain alkyls of monomers, including unsubstituted ones, depends on the chemical composition of intermediates produced by pyrolysis

In *chapter 6*, the solvent effects on monomer formation behavior in the pyrolysis-assisted catalytic hydrogenolysis at 350 °C was investigated. Coniferyl alcohol, as the typical pyrolysis products of softwood, has different reactivities depended on the property of solvents. The lower the polarity of the solvent, the more favorable the production of phenols. Radical reaction occurred in all solvent as the side reaction, leading to the decrease in monomer yield. In methanol and dioxane, the conversion of dihydroconiferyl alcohol to ethyl guaiacol was unfavorable. Anisole was the best solvent for aromatic monomer production, while water is the worst solvent for prolonged treatments.

In summary, these studies show that catalytic hydrogenolysis in pyrolysis condition can be a feasible technology for the high monomer yield from softwood lignin, and technical lignin. The formations of final monomer products were highly depended on pyrolysis pathway.

7.2 Prospects for the future research

Chapter 2 shows that 5-5, 4-O-5, β - β , β -aryl were existed in the oligomer products from lignin pyrolysis. The reactivity of β -aryl was still unclear, and a model study would be necessary.

Chapter 3 and *chapter 4* shows the adsorption manners of dimers, and monomers on Pd surface. As the reactivities of these substrates were highly depended on the adsorption manner, it

could be interesting to reduce the size of Pd so that two aromatic rings of 5-5 could be associated with two different Pd particles for achieving C-C cleavage.

Chapter 4 shows that the monomer yield from pyrolysis-assisted catalytic hydrogenolysis of kraft lignin after treatment for 10 min at 350 °C only reached 14 mol%. This low yield is largely related to the sulfur in kraft lignin. It is particularly important to explore a method for efficiently converting kraft lignin. For instance, removing sulfur in kraft lignin before reaction, modifying catalyst to avoid the sulfur poisoning, or changing the mediate to avoid the contact between sulfur and catalyst during reaction.

Chapter 6 shows that monomer types were highly depended on solvent used. Hexane could be a good solvent for phenol production. Water could be a good solvent for catechol production, if the further degradation of catechol could be avoided. In addition, alkyl alcohols were produced from pyrolysis-assisted hydrogenolysis of milled wood lignin in methanol. This indicates the polymer effect could affect the degradation manner of lignin. Weighting of different pyrolysis pathways might be worth to study.

When the wood was used, the monomer yield was reduced a lot. Cell wall containing polysaccharides might affect the result much, and it is worth to study the role of cell wall.

References

- Asmadi, M., Kawamoto, H., Saka, S., 2012. The effects of combining guaiacol and syringol on their pyrolysis. *Holzforschung* 66, 323–330. <https://doi.org/10.1515/hf.2011.165>
- Asmadi, M., Kawamoto, H., Saka, S., 2011a. Gas- and solid/liquid-phase reactions during pyrolysis of softwood and hardwood lignins. *Journal of Analytical and Applied Pyrolysis* 92, 417–425. <https://doi.org/10.1016/j.jaap.2011.08.003>
- Asmadi, M., Kawamoto, H., Saka, S., 2011b. Thermal reactions of guaiacol and syringol as lignin model aromatic nuclei. *Journal of Analytical and Applied Pyrolysis* 92, 88–98. <https://doi.org/10.1016/j.jaap.2011.04.011>
- B.P. Statistical Review, 2020. Statistical Review of World Energy. *Statistical Review of World Energy* 67, 1–56.
- Belgacem, M.N., Gandini, A., 2008. Monomers, Polymers and Composites from renewable resources.
- Biswas, B., Singh, R., Kumar, J., Ali, A., Krishna, B.B., Bhaskar, T., 2016. Slow pyrolysis of prot, alkali and dealkaline lignins for production of chemicals. *Bioresource Technology* 213, 319–326. <https://doi.org/10.1016/j.biortech.2016.01.131>
- Björkman A, 1956. Studies on finely divided wood. Part 1. Extraction of lignin with neutral solvents. *Sven Papperstidn* 59, 477–485.
- Bouxin, F.P., McVeigh, A., Tran, F., Westwood, N.J., Jarvis, M.C., Jackson, S.D., 2015. Catalytic depolymerisation of isolated lignins to fine chemicals using a Pt/alumina catalyst: Part 1 - Impact of the lignin structure. *Green Chemistry* 17, 1235–1242. <https://doi.org/10.1039/c4gc01678e>
- Burke, M., Hsiang, S.M., Miguel, E., 2015. Global non-linear effect of temperature on economic production. *Nature* 527, 235–239. <https://doi.org/10.1038/nature15725>
- Buryan, P., 1991. Thermal decomposition of dimethylphenols. *Journal of Analytical and Applied Pyrolysis* 22, 83–93. [https://doi.org/10.1016/0165-2370\(91\)85008-U](https://doi.org/10.1016/0165-2370(91)85008-U)
- Carlos A. Leon y Leon, Vannice, M.A., 1991. Adsorption and catalytic properties of Pd/SiO₂, Cu/SiO₂, and Pd-Cu/SiO₂ systems: I. Hydrogen, carbon monoxide and oxygen adsorption on Pd/SiO₂ and Cu/SiO₂. *Applied Catalysis* 69, 269–290. [https://doi.org/10.1016/s0166-9834\(00\)83309-6](https://doi.org/10.1016/s0166-9834(00)83309-6)
- Cho, J., Chu, S., Dauenhauer, P.J., Huber, G.W., 2012. Kinetics and reaction chemistry for slow pyrolysis of enzymatic hydrolysis lignin and organosolv extracted lignin derived from maplewood. *Green Chemistry* 14, 428–439. <https://doi.org/10.1039/c1gc16222e>
- Church, J.A., White, N.J., 2011. Sea-Level Rise from the Late 19th to the Early 21st Century. *Surveys in Geophysics* 32, 585–602. <https://doi.org/10.1007/s10712-011-9119-1>
- Cooke, L.M., Mccarthy, J.L., Hibbert, H., 1941. Studies on Lignin and Related Compounds. LXI. Hydrogenation of Ethanolysis Fractions from Maple Wood (Part 2) 63, 3056–3061.
- Dessbesell, L., Paleologou, M., Leitch, M., Pulkki, R., Xu, C. (Charles), 2020. Global lignin supply overview and kraft lignin potential as an alternative for petroleum-based polymers. *Renewable and Sustainable Energy Reviews* 123, 109768. <https://doi.org/10.1016/j.rser.2020.109768>
- Dorrestijn, E., Kranenburg, M., Poinot, D., Mulder, P., 1999. Lignin depolymerization in hydrogen-donor solvents.

- Holzforschung 53, 611–616. <https://doi.org/10.1515/HF.1999.101>
- Egsgaard, H., Ahrenfeldt, J., Ambus, P., Schaumburg, K., Henriksen, U.B., 2014. Gas cleaning with hot char beds studied by stable isotopes. *Journal of Analytical and Applied Pyrolysis* 107, 174–182. <https://doi.org/10.1016/j.jaap.2014.02.019>
- Ehara, K., Saka, S., 2002. A comparative study on chemical conversion of cellulose between the batch-type and flow-type systems in supercritical water. *Cellulose* 9, 301–311. <https://doi.org/10.1023/A:1021192711007>
- Eliot Steinberg, G.A.C. and A.W.R.R., 1954. Aminoalkyl Esters of 1,2,3,10b-Tetrahydrofluoranthene-10b-carboxylic Acid. *Journal of the American Chemical Society* 76, 5445–54475.
- Feng, S., Wei, R., Leitch, M., Xu, C.C., 2018. Comparative study on lignocellulose liquefaction in water, ethanol, and water/ethanol mixture: Roles of ethanol and water. *Energy* 155, 234–241. <https://doi.org/10.1016/j.energy.2018.05.023>
- Fergus, B.J., Procter, A.R., Scott, J.A.N., Goring, D.A.I., 1969. The distribution of lignin in sprucewood as determined by ultraviolet microscopy. *Wood Science and Technology* 3, 117–138. <https://doi.org/10.1007/BF00639636>
- Galkin, M. V., Samec, J.S.M., 2014. Selective route to 2-propenyl aryls directly from wood by a tandem organosolv and palladium-catalysed transfer hydrogenolysis. *ChemSusChem* 7, 2154–2158. <https://doi.org/10.1002/cssc.201402017>
- Gao, J., Kim, J.S., Terziev, N., Allegretti, O., Daniel, G., 2014. Chemical and ultrastructural changes in compound middle lamella (CML) regions of softwoods thermally modified by the Termovuoto process. *Holzforschung* 68, 849–859. <https://doi.org/10.1515/hf-2013-0221>
- Gillet, S., Aguedo, M., Petitjean, L., Morais, A.R.C., Da Costa Lopes, A.M., Łukasik, R.M., Anastas, P.T., 2017. Lignin transformations for high value applications: Towards targeted modifications using green chemistry. *Green Chemistry* 19, 4200–4233. <https://doi.org/10.1039/c7gc01479a>
- Godard, H.P., McCarthy, J.L., Hibbert, H., 1941. Studies on Lignin and Related Compounds. LXII. High Pressure Hydrogenation of Wood Using Copper Chromite Catalyst (Part 1). *Journal of the American Chemical Society* 63, 3061–3066.
- Grein, F., 2002. Twist angles and rotational energy barriers of biphenyl and substituted biphenyls. *Journal of Physical Chemistry A* 106, 3823–3827. <https://doi.org/10.1021/jp0122124>
- Guo, Y., Zhou, J., Wen, J., Sun, G., Sun, Y., 2015. Structural transformations of triploid of *Populus tomentosa* Carr. lignin during auto-catalyzed ethanol organosolv pretreatment. *Industrial Crops and Products* 76, 522–529. <https://doi.org/10.1016/j.indcrop.2015.06.020>
- Harris, E.E., D'Ianni, J., Adkins, H., 1938. Reaction of Hardwood Lignin with Hydrogen. *Journal of the American Chemical Society* 60, 1467–1470. <https://doi.org/10.1021/ja01273a056>
- He, J., Zhao, C., Mei, D., Lercher, J.A., 2014. Mechanisms of selective cleavage of C-O bonds in di-aryl ethers in aqueous phase. *Journal of Catalysis* 309, 280–290. <https://doi.org/10.1016/j.jcat.2013.09.012>
- Heitner, C., Dimmel, D.R., Schmidt, J.A., 2016. Lignin and lignans: advances in chemistry, CRC press. <https://doi.org/10.1201/ebk1574444865>

- Héroguel, F., Nguyen, X.T., Luterbacher, J.S., 2019. Catalyst Support and Solvent Effects during Lignin Depolymerization and Hydrodeoxygenation. *ACS Sustainable Chemistry and Engineering* 7, 16952–16958. <https://doi.org/10.1021/acssuschemeng.9b03843>
- Higuchi, T., 2012. *Biosynthesis and biodegradation of wood components*. Elsevier.
- Holtman, K.M., Chang, H.M., Kadla, J.F., 2004. Solution-State Nuclear Magnetic Resonance Study of the Similarities between Milled Wood Lignin and Cellulolytic Enzyme Lignin. *Journal of Agricultural and Food Chemistry* 52, 720–726. <https://doi.org/10.1021/jf035084k>
- Hosoya, T., Kawamoto, H., Saka, S., 2007. Pyrolysis behaviors of wood and its constituent polymers at gasification temperature. *Journal of Analytical and Applied Pyrolysis* 78, 328–336. <https://doi.org/10.1016/j.jaap.2006.08.008>
- IEA, 2020. *World Energy Outlook 2020*.
- International Energy Agency, 2018. *The Future of Petrochemicals – Analysis*. International Energy Agency 11–25.
- IPCC, 2021. *Climate Change 2021 The Physical Science Basis Summary for Policymakers Working Group I Contribution to the Sixth Assessment Report of the Intergovernmental Panel on Climate Change, Climate Change 2021: The Physical Science Basis*.
- Jiang, W., Lyu, G., Liu, Y., Wang, C., Chen, J., Lucia, L.A., 2014. Quantitative analyses of lignin hydrothermolysates from subcritical water and water-ethanol systems. *Industrial and Engineering Chemistry Research* 53, 10328–10334. <https://doi.org/10.1021/ie5011178>
- Kawamoto, H., 2017. Lignin pyrolysis reactions. *Journal of Wood Science* 63, 117–132. <https://doi.org/10.1007/s10086-016-1606-z>
- Kawamoto, H., Horigoshi, S., Saka, S., 2007a. Pyrolysis reactions of various lignin model dimers. *Journal of Wood Science* 53, 168–174. <https://doi.org/10.1007/s10086-006-0834-z>
- Kawamoto, H., Horigoshi, S., Saka, S., 2007b. Effects of side-chain hydroxyl groups on pyrolytic β -ether cleavage of phenolic lignin model dimer. *Journal of Wood Science* 53, 268–271. <https://doi.org/10.1007/s10086-006-0839-7>
- Kawamoto, H., Nakamura, T., Saka, S., 2008a. Pyrolytic cleavage mechanisms of lignin-ether linkages: A study on p-substituted dimers and trimers. *Holzforschung* 62, 50–56. <https://doi.org/10.1515/HF.2008.007>
- Kawamoto, H., Ryoritani, M., Saka, S., 2008b. Different pyrolytic cleavage mechanisms of β -ether bond depending on the side-chain structure of lignin dimers. *Journal of Analytical and Applied Pyrolysis* 81, 88–94. <https://doi.org/10.1016/j.jaap.2007.09.006>
- Kawamoto, H., Saka, S., 2007. Role of side-chain hydroxyl groups in pyrolytic reaction of phenolic β -Ether type of lignin dimer. *Journal of Wood Chemistry and Technology* 27, 113–120. <https://doi.org/10.1080/02773810701515119>
- Kim, J.Y., Heo, S., Choi, J.W., 2018. Effects of phenolic hydroxyl functionality on lignin pyrolysis over zeolite catalyst. *Fuel* 232, 81–89. <https://doi.org/10.1016/j.fuel.2018.05.133>
- Kim, J.Y., Moon, J., Lee, J.H., Jin, X., Choi, J.W., 2020. Conversion of phenol intermediates into aromatic hydrocarbons over various zeolites during lignin pyrolysis. *Fuel* 279, 118484.

<https://doi.org/10.1016/j.fuel.2020.118484>

- Klein, M.T., Virk, P.S., 1983. Model pathways in lignin thermolysis. 1. Phenethyl phenyl ether. *Industrial & Engineering Chemistry Fundamentals* 22, 35–45.
- Klein, M.T., Virk, P.S., 1981. Model Pathways in Lignin Thermolysis. American Chemical Society, Division of Petroleum Chemistry, Preprints 26, 1082.
- Kotake, T., Kawamoto, H., Saka, S., 2015. Pyrolytic formation of monomers from hardwood lignin as studied from the reactivities of the primary products. *Journal of Analytical and Applied Pyrolysis* 113, 57–64. <https://doi.org/10.1016/j.jaap.2014.09.029>
- Kotake, T., Kawamoto, H., Saka, S., 2014. Mechanisms for the formation of monomers and oligomers during the pyrolysis of a softwood lignin. *Journal of Analytical and Applied Pyrolysis* 105, 309–316. <https://doi.org/10.1016/j.jaap.2013.11.018>
- Kotake, T., Kawamoto, H., Saka, S., 2013. Pyrolysis reactions of coniferyl alcohol as a model of the primary structure formed during lignin pyrolysis. *Journal of Analytical and Applied Pyrolysis* 104, 573–584. <https://doi.org/10.1016/j.jaap.2013.05.011>
- Krashen, S.D., 1982. Evaluation of the Quantitative Assay of Lignin Distribution by SEM-EDXA-Technique S. 46, 55.
- Kratzl, K., Vierhapper, F.W., 1971. Synthese von ¹⁴C-kernmarkierten Vanillinen und Bikreosolen (Spezifisch ¹⁴C-kernmarkierte Phenolderivate, 2. Mitt.). *Monatshefte für Chemie* 102, 425–430.
- Labidi, J., 2016. Depolymerization of Different Organosolv Lignins in Supercritical Methanol, Ethanol, and Acetone To Produce Phenolic Monomers. <https://doi.org/10.1021/acssuschemeng.5b01377>
- Lancefield, C.S., Westwood, N.J., 2015. The synthesis and analysis of advanced lignin model polymers. *Green Chemistry* 17, 4980–4990. <https://doi.org/10.1039/c5gc01334h>
- Lancefield, C.S., Wienk, H.J., Boelens, R., Weckhuysen, B.M., Bruijninx, P.C.A., 2018. Identification of a diagnostic structural motif reveals a new reaction intermediate and condensation pathway in kraft lignin formation. *Chemical Science* 9, 6348–6360. <https://doi.org/10.1039/c8sc02000k>
- Lange, W., Schweers, W., 1980. The carboxymethylation of organosolv and kraft lignins. *Wood Science and Technology* 14, 1–7. <https://doi.org/10.1007/BF00353458>
- Li, C., Zhao, X., Wang, A., Huber, G.W., Zhang, T., 2015. Catalytic Transformation of Lignin for the Production of Chemicals and Fuels. *Chemical Reviews* 115, 11559–11624. <https://doi.org/10.1021/acs.chemrev.5b00155>
- Li, S., Shi, L., Wang, C., Yue, F., Lu, F., 2020. Naphthalene Structures Derived from Lignins During Phenolation. *ChemSusChem* 13, 5549–5555. <https://doi.org/10.1002/cssc.202001693>
- Lieth, Helmut, and R.H.W., 2012. Primary Productivity of the Biosphere. Springer Science & Business Media.
- Lin, S.Y., Dence, C.W., 1992. Methods in lignin chemistry. Springer-Verlag. <https://doi.org/10.1007/978-3-642-74065-7>
- Ludmila, H., Michal, J., Andrea, Š., Aleš, H., 2015. Lignin, potential products and their market value. *Wood Research* 60, 973–986.
- Luo, X., Gong, Z., Yang, G., Huang, L., Chen, L., Shuai, L., 2022. In-situ oxidation/reduction facilitates one-pot

- conversion of lignocellulosic biomass to bulk chemicals in alkaline solution. *Chemical Engineering Journal* 429, 132365. <https://doi.org/10.1016/j.cej.2021.132365>
- Ma, R., Xu, Y., Zhang, X., 2015. Catalytic oxidation of biorefinery lignin to value-added chemicals to support sustainable biofuel production. *ChemSusChem* 8, 24–51. <https://doi.org/10.1002/cssc.201402503>
- Matsuoka, S., Kawamoto, H., Saka, S., 2014. What is active cellulose in pyrolysis? An approach based on reactivity of cellulose reducing end. *Journal of Analytical and Applied Pyrolysis* 106, 138–146. <https://doi.org/10.1016/j.jaap.2014.01.011>
- Matsushita, Y., 2015. Conversion of technical lignins to functional materials with retained polymeric properties. *Journal of Wood Science* 61, 230–250. <https://doi.org/10.1007/s10086-015-1470-2>
- Mellerowicz, E.J., Baucher, M., Sundberg, B., Boerjan, W., 2001. Unravelling cell wall formation in the woody dicot stem. *Plant Molecular Biology* 47, 239–274. <https://doi.org/10.1023/A:1010699919325>
- Mellerowicz, E.J., Sundberg, B., 2008. Wood cell walls: biosynthesis, developmental dynamics and their implications for wood properties. *Current Opinion in Plant Biology* 11, 293–300. <https://doi.org/10.1016/j.pbi.2008.03.003>
- Microscopy, E., Rothbard, D.R., Sheehan, J.G., Paint, T., Manual, C.T., 2002. Institute of Paper Science and Technology.
- Minami, E., Kawamoto, H., Saka, S., 2003. Reaction behavior of lignin in supercritical methanol as studied with lignin model compounds. *Journal of Wood Science* 49, 158–165. <https://doi.org/10.1007/s100860300025>
- Minami, E., Saka, S., 2003. Comparison of the decomposition behaviors of hardwood and softwood in supercritical methanol. *Journal of Wood Science* 49, 73–78. <https://doi.org/10.1007/s100860300012>
- Miyamoto, K., Kawamoto, H., 2019. Influence of vinyl ether intermediate over formation of CB=O and CA=CB monomers during pyrolysis of lignin model dimers. *Journal of Analytical and Applied Pyrolysis* 137, 54–60. <https://doi.org/10.1016/j.jaap.2018.11.009>
- Moon, R.J., Martini, A., Nairn, J., Simonsen, J., Youngblood, J., 2011. Cellulose nanomaterials review: Structure, properties and nanocomposites, *Chemical Society Reviews*. <https://doi.org/10.1039/c0cs00108b>
- Nakamura, T., Kawamoto, H., Saka, S., 2008. Pyrolysis behavior of Japanese cedar wood lignin studied with various model dimers. *Journal of Analytical and Applied Pyrolysis* 81, 173–182. <https://doi.org/10.1016/j.jaap.2007.11.002>
- Nakamura, T., Kawamoto, H., Saka, S., 2007. Condensation reactions of some lignin related compounds at relatively low pyrolysis temperature. *Journal of Wood Chemistry and Technology* 27, 121–133. <https://doi.org/10.1080/02773810701515143>
- Nomura, T., Kawamoto, H., Saka, S., 2017. Pyrolysis of cellulose in aromatic solvents: Reactivity, product yield, and char morphology. *Journal of Analytical and Applied Pyrolysis* 126, 209–217. <https://doi.org/10.1016/j.jaap.2017.06.006>
- Oasmaa, A., Johansson, A., 1993. Catalytic Hydrotreating of Lignin with Water-Soluble Molybdenum Catalyst. *Energy & Fuels* 7, 426–429.
- Obst, J.R., Landucci, L.L., 1986. Quantitative ¹³C NMR of lignins–Methoxyl: aryl ratio. *Holzforschung* 40, 87–92.

- Pan, X., Gilkes, N., Kadla, J., Pye, K., Saka, S., Gregg, D., Ehara, K., Xie, D., Lam, D., Saddler, J., 2006. Bioconversion of hybrid poplar to ethanol and co-products using an organosolv fractionation process: Optimization of process yields. *Biotechnology and Bioengineering* 94, 851–861. <https://doi.org/10.1002/bit.20905>
- Parmesan, C., 2006. Ecological and evolutionary responses to recent climate change. *Annual Review of Ecology, Evolution, and Systematics* 37, 637–669. <https://doi.org/10.1146/annurev.ecolsys.37.091305.110100>
- Peng, S., Huang, J., Sheehy, J.E., Laza, R.C., Visperas, R.M., Zhong, X., Centeno, G.S., Khush, G.S., Cassman, K.G., 2004. Rice yields decline with higher night temperature from global warming. *Proceedings of the National Academy of Sciences of the United States of America* 101, 9971–9975. <https://doi.org/10.1073/pnas.0403720101>
- PEPPER, J.M., 1972. Lignin Chemistry. *Nature* 237, 54–54. <https://doi.org/10.1038/237054a0>
- Phaiboonsilpa, N., Yamauchi, K., Lu, X., Saka, S., 2010. Two-step hydrolysis of Japanese cedar as treated by semi-flow hot-compressed water. *Journal of Wood Science* 56, 331–338. <https://doi.org/10.1007/s10086-009-1099-0>
- Plomion, C., Leprovost, G., Stokes, A., 2001. Wood Formation in Trees. *Am Soc Plant Biol* 127, 1513–1523. <https://doi.org/10.1104/pp.010816.1>
- Rabemanolontsoa, H., Ayada, S., Saka, S., 2011. Quantitative method applicable for various biomass species to determine their chemical composition. *Biomass and Bioenergy* 35, 4630–4635. <https://doi.org/10.1016/j.biombioe.2011.09.014>
- Rabemanolontsoa, H., Saka, S., 2013. Comparative study on chemical composition of various biomass species. *RSC Advances* 3, 3946–3956. <https://doi.org/10.1039/c3ra22958k>
- Ralph, S.A., Ralph, J., Landucci, L., Landucci, L., 2004. NMR Database of Lignin and Cell Wall Model Compounds [WWW Document]. US Forest Prod. Lab., Madison, WI.
- Saiz-Jimenez, C., De Leeuw, J.W., 1986. Lignin pyrolysis products: Their structures and their significance as biomarkers. *Organic Geochemistry* 10, 869–876. [https://doi.org/10.1016/S0146-6380\(86\)80024-9](https://doi.org/10.1016/S0146-6380(86)80024-9)
- Saka, S., Thomas, R.J., Science, P., Carolina, N., 1982. A Study of Lignification in Loblolly Pine Tracheids by the SEM-EDXA Technique. *Wood Science and Technology* 179, 167–179.
- Sax, K.J., Saari, W.S., Mahoney, C.L., Gordon, J.M., 1960. Preparation and Infrared Absorption Spectra of Some Phenyl Ethers I. *Journal of Organic Chemistry* 25, 1590–1595. <https://doi.org/10.1021/jo01079a029>
- Schutyser, W., Renders, T., Van Den Bosch, S., Koelewijn, S.F., Beckham, G.T., Sels, B.F., 2018. Chemicals from lignin: An interplay of lignocellulose fractionation, depolymerisation, and upgrading. *Chemical Society Reviews* 47, 852–908. <https://doi.org/10.1039/c7cs00566k>
- Schutyser, W., Van Den Bosch, S., Renders, T., De Boe, T., Koelewijn, S.F., Dewaele, A., Ennaert, T., Verkinderen, O., Goderis, B., Courtin, C.M., Sels, B.F., 2015. Influence of bio-based solvents on the catalytic reductive fractionation of birch wood. *Green Chemistry* 17, 5035–5045. <https://doi.org/10.1039/c5gc01442e>
- Setter, C., Sanchez Costa, K.L., Pires de Oliveira, T.J., Farinassi Mendes, R., 2020. The effects of kraft lignin on the physicochemical quality of briquettes produced with sugarcane bagasse and on the characteristics of the bio-

- oil obtained via slow pyrolysis. *Fuel Processing Technology* 210, 106561. <https://doi.org/10.1016/j.fuproc.2020.106561>
- Sharma, R.K., Hajaligol, M.R., 2003. Effect of pyrolysis conditions on the formation of polycyclic aromatic hydrocarbons (PAHs) from polyphenolic compounds. *Journal of Analytical and Applied Pyrolysis* 66, 123–144. [https://doi.org/10.1016/S0165-2370\(02\)00109-2](https://doi.org/10.1016/S0165-2370(02)00109-2)
- Shen, D., Zhao, J., Xiao, R., 2016. Catalytic transformation of lignin to aromatic hydrocarbons over solid-acid catalyst: Effect of lignin sources and catalyst species. *Energy Conversion and Management* 124, 61–72. <https://doi.org/10.1016/j.enconman.2016.06.067>
- Shuai, L., Sitison, J., Sadula, S., Ding, J., Thies, M.C., Saha, B., 2018. Selective C–C Bond Cleavage of Methylene-Linked Lignin Models and Kraft Lignin. *ACS Catalysis* 8, 6507–6512. <https://doi.org/10.1021/acscatal.8b00200>
- Singh, R., Prakash, A., Dhiman, S.K., Balagurumurthy, B., Arora, A.K., Puri, S.K., Bhaskar, T., 2014. Hydrothermal conversion of lignin to substituted phenols and aromatic ethers. *Bioresource Technology* 165, 319–322. <https://doi.org/10.1016/j.biortech.2014.02.076>
- Song, Q., Wang, F., Cai, J., Wang, Y., Zhang, J., Yu, W., Xu, J., 2013. Lignin depolymerization (LDP) in alcohol over nickel-based catalysts via a fragmentation-hydrogenolysis process. *Energy and Environmental Science* 6, 994–1007. <https://doi.org/10.1039/c2ee23741e>
- statista [WWW Document], 2022. . Statista. URL <https://www.statista.com/markets/410/topic/445/chemical-industry/#overview>
- Sun, Z., Fridrich, B., De Santi, A., Elangovan, S., Barta, K., 2018. Bright Side of Lignin Depolymerization: Toward New Platform Chemicals. *Chemical Reviews* 118, 614–678. <https://doi.org/10.1021/acs.chemrev.7b00588>
- Sy, L.K., Brown, G.D., 1998. Novel phenylpropanoids and lignans from *Illicium verum*. *Journal of Natural Products* 61, 987–992. <https://doi.org/10.1021/np9800553>
- Takada, M., 2017. DECOMPOSITION BEHAVIORS OF LIGNIN IN HYDROTHERMAL TREATMENT OF LIGNOCELLULOSICS.
- Tang, D., Huang, X., Tang, W., Jin, Y., 2021. Lignin-to-chemicals: Application of catalytic hydrogenolysis of lignin to produce phenols and terephthalic acid via metal-based catalysts. *International Journal of Biological Macromolecules* 190, 72–85. <https://doi.org/10.1016/j.ijbiomac.2021.08.188>
- Terashima, N., Fukushima, K., Tsuchiya, S., Takabe, K., 1986. Heterogeneity in formation of lignin. VII. An autoradiographic study on the formation of guaiacyl and syringyl lignin in poplar. *Journal of Wood Chemistry and Technology* 6, 495–504. <https://doi.org/10.1080/02773818608085241>
- Terashima, N., Kitano, K., Kojima, M., Yoshida, M., Yamamoto, H., Westermarck, U., 2009. Nanostructural assembly of cellulose, hemicellulose, and lignin in the middle layer of secondary wall of ginkgo tracheid. *Journal of Wood Science* 55, 409–416. <https://doi.org/10.1007/s10086-009-1049-x>
- Timell, T.E., Syracuse, N.Y., 1967. Recent progress in the chemistry of wood hemicelluloses. *Wood Science and Technology* 1, 45–70. <https://doi.org/10.1007/BF00592255>
- Torr, K.M., van de Pas, D.J., Cazeils, E., Suckling, I.D., 2011. Mild hydrogenolysis of in-situ and isolated *Pinus*

- radiata lignins. *Bioresource Technology* 102, 7608–7611. <https://doi.org/10.1016/j.biortech.2011.05.040>
- Tyminski, A., Timell, T.E., 1960. The Constitution of a Glucomannan from White Spruce (*Picea glauca*). *Journal of the American Chemical Society* 82, 2823–2827. <https://doi.org/10.1021/ja01496a038>
- Van Aelst, K., Van Sinay, E., Vangeel, T., Cooreman, E., Van Den Bossche, G., Renders, T., Van Aelst, J., Van Den Bosch, S., Sels, B.F., 2020. Reductive catalytic fractionation of pine wood: Elucidating and quantifying the molecular structures in the lignin oil. *Chemical Science* 11, 11498–11508. <https://doi.org/10.1039/d0sc04182c>
- Van Den Bosch, S., Schutyser, W., Vanholme, R., Driessen, T., Koelewijn, S.F., Renders, T., De Meester, B., Huijgen, W.J.J., Dehaen, W., Courtin, C.M., Lagrain, B., Boerjan, W., Sels, B.F., 2015. Reductive lignocellulose fractionation into soluble lignin-derived phenolic monomers and dimers and processable carbohydrate pulps. *Energy and Environmental Science* 8, 1748–1763. <https://doi.org/10.1039/c5ee00204d>
- Wang, J., 2021. THERMAL DEGRADATION REACTIVITY OF CELLULOSE AND HEMICELLULOSE IN JAPANESE CEDAR AND JAPANESE BEECH JIAWEI WANG.
- Wang, J., Minami, E., Kawamoto, H., 2023. Pyrolysis-assisted catalytic hydrogenolysis of softwood lignin at elevated temperatures for the high yield production of monomers. *Green Chemistry*. <https://doi.org/10.1039/D2GC03719J>
- Wang, J., Minami, E., Kawamoto, H., 2022. Stable oligomer formation from lignin by pyrolysis of softwood in an aprotic solvent with a hydrogen donor. *ChemistryOpen* 11, e202200104. <https://doi.org/10.1002/open.202200104>.
- Wang, S., Ru, B., Dai, G., Shi, Z., Zhou, J., Luo, Z., Ni, M., Cen, K., 2017. Mechanism study on the pyrolysis of a synthetic β -O-4 dimer as lignin model compound. *Proceedings of the Combustion Institute* 36, 2225–2233. <https://doi.org/10.1016/j.proci.2016.07.129>
- Wang, W., Wang, M., Li, X., Cai, L., Shi, S.Q., Duan, C., Ni, Y., 2020. Microwave-Assisted Catalytic Cleavage of C-C Bond in Lignin Models by Bifunctional Pt/CDC-SiC. *ACS Sustainable Chemistry and Engineering* 8, 38–43. <https://doi.org/10.1021/acssuschemeng.9b06606>
- Watanabe, T., Kawamoto, H., Saka, S., 2015. Pyrolytic reactivities of deuterated β -ether-type lignin model dimers. *Journal of Analytical and Applied Pyrolysis* 112, 23–28. <https://doi.org/10.1016/j.jaap.2015.02.028>
- Watanabe, T., Kawamoto, H., Saka, S., 2009. Radical chain reactions in pyrolytic cleavage of the ether linkages of lignin model dimers and a trimer. *Holzforschung* 63, 424–430. <https://doi.org/10.1515/HF.2009.076>
- Wen, J.L., Sun, S.L., Xue, B.L., Sun, R.C., 2013. Recent advances in characterization of lignin polymer by solution-state nuclear magnetic resonance (NMR) methodology. *Materials* 6, 359–391. <https://doi.org/10.3390/ma6010359>
- Wong, S.S., Shu, R., Zhang, J., Liu, H., Yan, N., 2020. Downstream processing of lignin derived feedstock into end products. *Chemical Society Reviews* 49, 5510–5560. <https://doi.org/10.1039/d0cs00134a>
- Yamaguchi, A., Mimura, N., Shirai, M., Sato, O., 2017. Bond cleavage of lignin model compounds into aromatic monomers using supported metal catalysts in supercritical water. *Scientific Reports* 7, 1–7. <https://doi.org/10.1038/srep46172>
- Yang, T., Wu, K., Li, B., Du, C., Wang, J., Li, R., 2021. Conversion of lignin into phenolic-rich oil by two-step

- liquefaction in sub-supercritical ethanol system assisted by carbon dioxide. *Journal of the Energy Institute* 94, 329–336. <https://doi.org/10.1016/j.joei.2020.10.001>
- Zakzeski, J., Bruijninx, P.C.A., Jongerius, A.L., Weckhuysen, B.M., 2010. The catalytic valorization of lignin for the production of renewable chemicals. *Chemical Reviews* 110, 3552–3599. <https://doi.org/10.1021/cr900354u>
- Zhang, J., Sun, J., Wang, Y., 2020. Recent advances in the selective catalytic hydrodeoxygenation of lignin-derived oxygenates to arenes. *Green Chemistry* 22, 1072–1098. <https://doi.org/10.1039/c9gc02762a>
- Zhao, C., Hu, Z., Shi, L., Wang, C., Yue, F., Li, S., Zhang, H., Lu, F., 2020. Profiling of the formation of lignin-derived monomers and dimers from: Eucalyptus alkali lignin. *Green Chemistry* 22, 7366–7375. <https://doi.org/10.1039/d0gc01658f>
- Zhao, C., Huang, J., Yang, L., Yue, F., Lu, F., 2019. Revealing Structural Differences between Alkaline and Kraft Lignins by HSQC NMR. *Industrial and Engineering Chemistry Research* 58, 5707–5714. <https://doi.org/10.1021/acs.iecr.9b00499>
- Zhou, G., Jensen, P.A., Le, D.M., Knudsen, N.O., Jensen, A.D., 2016. Direct upgrading of fast pyrolysis lignin vapor over the HZSM-5 catalyst. *Green Chemistry* 18, 1965–1975. <https://doi.org/10.1039/c5gc01976a>
- Zhou, X., Li, W., Mabon, R., Broadbelt, L.J., 2017. A Critical Review on Hemicellulose Pyrolysis 08801, 52–79. <https://doi.org/10.1002/ente.201600327>

Acknowledgments

First, the author would like to express his greatest gratitude to Professor Haruo Kawamoto, Department of Socio-Environment Energy Science, Graduate School of Energy Science, Kyoto University, for his supervision and encouragement for this research. His extensive knowledge and seasoned experience enlightened and benefited the author in each conversation. His patient guidance and meticulous support enabled the author to overcome the countless difficulties. His enthusiasm and conscientiousness for scientific research deeply inspired the author to explore the unknown. It is the author's luck and honor to be his apprentice.

The author would like to express his great gratitude to Professor Toshiyuki Takano, Division of Forest and Biomaterials Science, Graduate School of Agriculture, Kyoto University, for his careful reading of the manuscript and his valuable advice on future research. The advices he provided at the graduation defense made author's oral presentation more professional and logically coherent.

The author would like to express his great gratitude to Professor Takayuki Kameda, Graduate School of Energy Science, Department of Socio-Environmental Energy Science, for his valuable suggestions on author's graduation defense. These valuable suggestions make the author's public defense much easier to be understandable to researchers in other fields.

The author would like to express the sincere gratitude to Associate Professor Eiji Minami, Department of Socio-Environmental Energy Science, Graduate School of Energy Science, for his unwavering support and willingness to share his experience and research ideas. His technical support in the experimental apparatus provides great confidence to the author to complete this research.

The author would like to express the great appreciation to Specific Assist. Prof. Chen Qu, International Advanced Energy Science Research and Education Center Graduate School of Energy Science, for her kind, patient and intelligent suggestions and advices.

The author would also like to express the appreciation to Prof. Baoguo Lu, National Institute of Clean-and-Low-Carbon Energy, for his in-depth explanation of some catalyst-related knowledge.

The author is grateful to Assistant Prof. Masatsugu Takada, Graduate School of Bio-Applications and Systems Engineering, Tokyo University of Agriculture and Technology, for his support on equipment utilization, and kind explanation on wood cells wall.

The author is grateful to the secretary of Laboratory of Energy Ecosystem, Kyoto University, Ms. Rie Nakanishi, for her kindly help and support to the daily troubles encountered in the laboratory.

The author would also like to express the great appreciation to all the members in the laboratory for their continuous support and impressive friendship. Especially, I would like to express my gratitude to Dr. Jiawei Wang, Dr. Takashi Nomura, Dr. Yuanyuan Zhao, Dr. Latifa Seniorita, Ms. Yilin Yao, Mr. Qiming Jin, Mr. Yu Wang, Mr. Ikeda Francisco Alex for their kind help, useful advices and pleasant leisure time.

The author also like to thank Chinese Scholarship Council (CSC) for providing the financial support for the past three years.

Last but not least, the author would like to thank his parents for their support and understanding at every important moment in his life. They gave the author the most powerful support and enough confidence and courage to face the most difficult moment.

List of Publications

Original papers

1. J. Wang, E. Minai, H. Kawamoto (2022) Stable Oligomer Formation from Lignin by Pyrolysis of Softwood in an Aprotic Solvent with a Hydrogen Donor. *ChemistryOpen*, 11(9), e202200104 (Highlight)
2. J. Wang, E. Minami and H. Kawamoto (2023) Pyrolysis-assisted hydrogenolysis of softwood lignin at elevated temperatures for the high yield production of monomers. *Green Chemistry*, 2023, DOI: 10.1039/D2GC03719J. (Front cover)
3. J. Wang, E. Minami and H. Kawamoto (2023) Role of pyrolysis in pyrolysis-assisted catalytic hydrogenolysis of lignin and mechanistic insights into catalytic conversion. *Journal of Analytic and Applied Pyrolysis*. (in press)
4. J. Wang, E. Minami and H. Kawamoto (2023) Effects of solvent on pyrolysis-assisted catalytic hydrogenolysis of softwood lignin for high-yield production of monomers and phenols. *ChemSusChem*. (under review)
5. J. Wang, E. Minami and H. Kawamoto (2023) Naphthalene formation behavior from pinoresinol in the pyrolysis-assisted hydrogenolysis. (in preparation)

Conferences and symposiums

1. J. Wang, H. Kawamoto. (2018) Pyrolytic degradation of lignin in wood in the presence of hydrogen donor and aromatic solvent. Oral, *The 63rd Lignin Symposium*. Nov 1-2, Koganei, Tokyo.
2. J. Wang, H. Kawamoto. (2019) Influences of pyrolysis temperature on formation of lignin- and polysaccharide-derived products from softwood in the presence of H-donor and aromatic solvent. Oral, *The 69th Annual Meeting of the japan wood research society*. March 14-16, Hakodate.
3. J. Wang, E. Minami, H. Kawamoto. (2020) Pyrolysis of Japanese cedar wood in toluene and ethylbenzene. Oral, *The 70th Annual Meeting of the japan wood research society*. March 16-18, Tottori.
4. J. Wang, E. Minami, H. Kawamoto. (2021) Cell Wall Effects in Pyrolysis of Lignin in Cedar Wood. Oral, *The 71st Annual Meeting of the japan wood research society*. March 19-21, Tokyo. Online

5. J. Wang, E. Minami, H. (2021) Kawamoto. Catalytic pyrolysis of softwood lignin in solvent at elevated temperatures to cleave condensed linkages for high-yield monomer preparation. Oral, *the 66th Lignin Symposium*. Nov 4-5, Online.
6. J. Wang, E. Minami, H. Kawamoto. (2022) Thermocatalytic Hydrogenolysis of Japanese Cedar Lignin to Monomers. Poster, *The 21st International Symposium on Wood, Fiber and Pulping Chemistry*. March 7-10, Raleigh, USA. (canceled)
7. J. Wang, E. Minami, H. Kawamoto. (2022) Role of pyrolysis in thermocatalytical hydrogenolysis of lignin. Oral, *The 72th Annual Meeting of the Japan Wood Research Society*. March 15-17, Nagoya. Online
8. J. Wang, E. Minami, H. Kawamoto. (2022) Role of pyrolysis on the product composition in thermocatalytic hydrogenolysis of lignin. Oral, *The 67th Lignin Symposium*. Nov 10-11, Online.

Awards

1. Best Student Oral Presentation Award. *71st Annual Meeting of the Japan Wood Research Society*. March 19-21 (2021), Tokyo (online)